ELASTO-PLASTIC FINITE ELEMENT ANALYSIS OF RECTANGULAR HOLLOW SECTION T-JOINT

by

Laila El-hifnawy, B.Eng. (Civil Engineering)

A Thesis
Submitted to the School of Graduate Studies
in Partial Fulfilment of the Requirements
for the Degree
Master of Engineering

McMaster University

December 1980

To my parents

MASTER OF ENGINEERING (1980)
(Civil Engineering and Engineering Mechanics)

McMASTER UNIVERSITY
Hamilton, Ontario

TITLE: ELASTO-PLASTIC FINITE ELEMENT ANALYSIS OF RECTANGULAR HOLLOW SECTION T-JOINT

AUTHOR: Laila El-hifnawy, B.Sc. (Civil Engineering)
(Alexandria University)

SUPERVISORS: Dr. R. M. Korol and Dr. F. A. Mirza

NUMBER OF PAGES: viii, 108

ABSTRACT

A research program is presented to analyze the behaviour of rectangular hollow section (RHS) T-joints in the elasto-plastic range of loading. An attempt was made to obtain the joint ultimate and working strengths. The study includes the determination of both rotational and punching shear stiffnesses of the RHS T-joint due to applied moment and branch member axial loads respectively.

Two different joint types were analyzed, the unreinforced T-joint and the haunch reinforcement type. In both cases, the chord top flange was considered as a thin plate loaded on the perimeter of the rigid inclusion, and supported by coupled springs along its longitudinal edges, thus simulating the action of the side walls and connecting bottom flanges. Transverse edges, some distance from the joint, were taken as simply supported.

The finite element formulation that is proposed incorporates rectangular plate and boundary elements with springs. The model is then used to study elastic connections. The joint stiffness values are shown to be in good agreement with the experimental results available in the literature.

Finally, a study of the RHS T-joint behaviour under both axial load and applied moment, in the elastic-plastic range of loading, is presented. The sensitivity of joints to different geometric parameters of width ratio, λ, haunch size, λ_1, and chord thickness,

t, for the entire range of loading is included. A prediction of the ultimate and working loads and moments that can be resisted by RHS T-joints, is given.

ACKNOWLEDGEMENTS

In presenting this thesis, I wish to express my thanks and graditude to the following individuals:

- My supervisors, Dr. R. M. Korol and Dr. F. A. Mirza for their guidance and support throughout this thesis.
- Linda Hunter, Secretary, Department of Electrical and Computer Engineering, McMaster University, for her time in typing the thesis.

Finally, a special thank you to my husband for his encouragement toward my education at McMaster University.

TABLE OF CONTENTS

LIST OF SYMBOLS

Symbols used throughout are generally defined when introduced. The more common symbols are listed below:

a	general finite element length
b	chord width, general finite element width
b_1	branch member width
C	punching shear stiffness
E	Young's modulus
h	chord member depth
h_1	branch depth
H_1	inclusion length
J	rotational stiffness
k_v	vertical spring constant
k_r	rotational spring constant
k_{vr}	coupled spring constant
L	plate length
M	moment applied through branch member
M_{ult}	ultimate moment applied through branch member
M^*_{ult}	ultimate moment obtained by limit analysis
$M_{working}$	working moment applied through branch member
P	axial load applied through branch member

P_{ult}	ultimate axial load
P^*_{ult}	ultimate axial load calculated by limit analysis
$P_{working}$	working axial load
r	chord corner radius
t_o	reference chord thickness
U	strain energy
w	work done by external loads
x, y, z	dimensional co-ordinates
ξ, η, ζ	nondimensional co-ordinates
λ	width ratio $(b_1/b = b_1/h)$
λ_1	haunch size ratio (H_1/h_1)
ϕ	chord member rotation about y axis
δ	deflection of chord member at the perimeter of the inclusion
π	potential energy
ν	Poisson's ratio
$\bar{\sigma}$	effective stress
$\bar{\sigma}_o$	yield stress
$\Delta\bar{\sigma}$	effective stress increment
$\bar{\varepsilon}$	effective strain
$\Delta\bar{\varepsilon}$	effective strain increment
$\{A\}$	vector of twelve unknown constants appearing in selected displacement field
$[B]$	strain matrix relating nodal displacements to strains
$[C]$	matrix relating effective strain increment to the total strain increments

$[D]$	elasticity matrix of material constants
$[D_{ep}]$	elastic-plastic $[D]$ matrix
$[K^e]$	finite element stiffness matrix
$[k_s]$	spring constants matrix
$[K_B]$	finite element matrix due to springs on the element boundary
$\{N\}$	shape function
$\{P^e\}$	element nodal force vector
$[T]$, $[T]^{-1}$	the transformation matrix and its inverse relating element displacement vector to the $\{A\}$ vector of constants
$\{w^e\}$	element displacement vector
$\{\varepsilon\}$	strain vector
$\{\sigma\}$	stress vector

CHAPTER 1

HOLLOW STRUCTURAL SECTIONS (HSS)

1.1 Introduction

Hollow structural sections (HSS) have played an increasingly important role in steel structural applications during the last twenty years, particularly in Europe, Japan and Canada. They have been found to offer a wide range of advantages. Some of these are listed below.

(i) Their geometrical shape effectively resists torsion and out-of-plane forces; the exposed surface area is less than that of conventional wide flange shapes, thus facilitating the application of protective coatings; their clean lines and smooth surfaces permit architects to satisfy the required aesthetic objectives.

(ii) Maintenance of HSS members is easier and cheaper than that of the more traditional sections.

(iii) Simple end cuts of square and rectangular HSS are sufficient for weld-connecting members together.

HSS are used in buildings, bridges, piles, tunnel supports, and electrical transmission towers, ..., etc.

One of the most common types of construction is the Vierendeel

truss. It is comprised of rectangular panels without diagonal members and hence its connections are of the so called T-type.

The main purpose of this study is the analysis of welded T-type joints fabricated from HSS.

1.2 Literature Review

A considerable amount of research work has been conducted on single chord RHS T-joints. For example, experimental results have been reported by Redwood (1), Brady (2), Mee (3), El-Zanaly (4), Korol et al (5), while Redwood (6), Mee (3) and Korol and Mansour (7) have undertaken analytical and numerical modelling investigations. Jubb and Redwood (1) indicated that, from experimental tests, an unreinforced equal width joint would behave in an approximately rigid manner. They also stated that for unequal width connections, there is a considerable reduction in joint stiffness and hence the assumption of using rigid joints in the design of Vierendeel trusses is inappropriate. Redwood (6) analysed the unreinforced joint with $\lambda < 1$ by considering the top flange plate of the chord as a thin plate loaded through a symmetrically located inclusion. The plate problem was solved numerically in the elastic range, using the finite difference method, and gave reasonable agreement with the results obtained from the unreinforced joint tests. Blockley and Eastwood (8), used the same basic analysis for this type of joint taking into account the rounded corners of the chord member. Consequently, the longitudinal edges of the top chord plate were presumed to deflect as well as

rotate during the loading process. They established an empirical formula to calculate the stiffness of the plate edge vertical support, while Jubb et al (1) estimated the rotational stiffness. Mansour and Korol (9) did a similar analysis considering the plate resting on elastic springs along its longitudinal edges for both unreinforced and haunch joints. Their results compared best with experimental results (5), (3), (6) when the vertical spring constant $\rightarrow \infty$, with the rotational spring constant > 0. They concluded that the unreinforced unequal width joints were very weak. Their theoretical results and El-Zanaty's experimental results (4) indicated that the haunch type connection is an excellent strengthening device. Brady (2) also undertook to study the effect of using different reinforcing devices of unequal width connections under applied moment.

Mouty (10) worked out theoretical formulas for the calculation of the strength of welded joints. His tests were carried out up to the point of plastic failure. Based on certain experimental results, he proposed a simple yield line model. He assumed that the area under the inclusion is infinitely rigid and is subjected to either translation (axial rigidity) or rotation only (rotational rigidity). Using the upper bound limit theorem, he obtained a failure mechanism for both cases and calculated the ultimate load and moment as a function of the dimensions of the chord and the inclusion for a prescribed yield stress.

1.3 Classification of Connections

The HSS connections can be classified into two categories and two basic types. The unreinforced, equal width ($\lambda = b_1/b = 1.0$) and unequal width ($\lambda < 1.0$) connections are shown in figure (1.1). The parameters b_1 and $h = b$, are the widths of the branch and chord members, respectively. In the case of unreinforced equal width connections, most of the load from the branch member is directly transferred from the web plates of the branch to the web plates of the chord member as they are connected in the same plane by weldment. For the unreinforced unequal width connections, the behaviour of the joint can be analysed as a plate problem with the loading resisted by bending of the top flange. Thus, the stiffness of this connection is greatly reduced. In order to increase the efficiency of this joint, a number of stiffening devices have been proposed. The type which is analysed in this work is known as the haunch connection. The haunch consists of HSS wedges cut at 45° to mate the corner of the branch and chord members. Figure (1.2) shows this type of connection where $\lambda_1 = H_1/h_1$ is the size of the haunch, in which H_1 is the composite length. The advantage of the haunch type, of course, is its ability to efficiently spread the load over a larger area, thus improving the joint stiffness and strength.

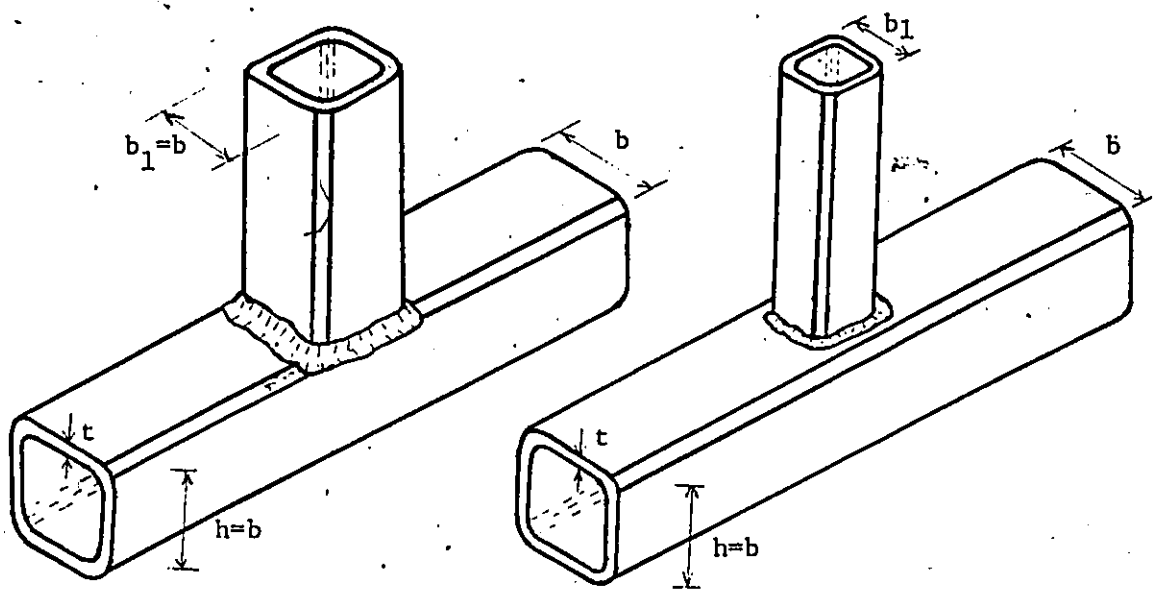

a) Equal width ($\lambda=b_1/b=1$) b) Unequal width ($\lambda<1$)

Fig. 1.1 Unreinforced Connection

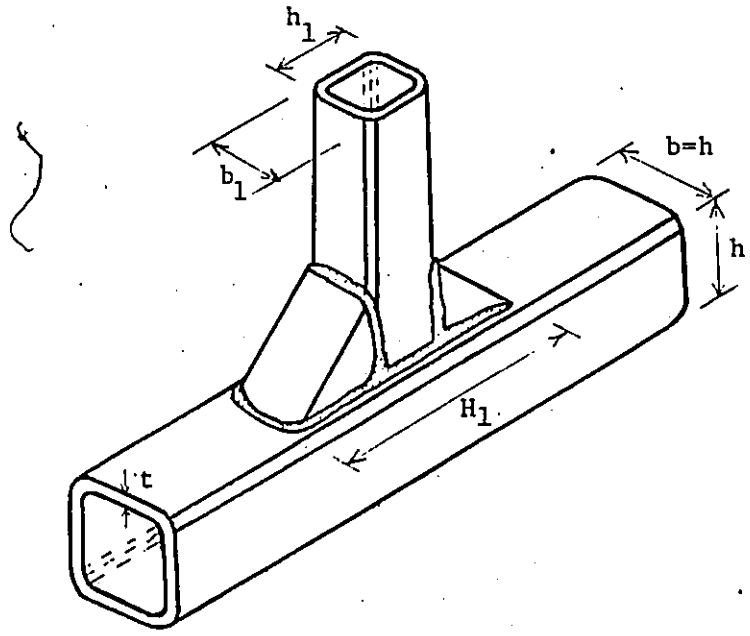

Fig. 1.2 Haunch Connection

1.4 Summary of Objectives

The objective of this thesis, then is to undertake the following study

A theoretical model is developed for the T-joint by considering the top chord flange as a thin plate with transverse bending. The effect of the remaining section on the top plate is incorporated through coupled translational and rotational springs along the longitudinal edges which form the so-called boundary elements with springs. A computer program capable of determining the elastic-plastic behaviour of the RHS T-joint is developed and employed to solve the problem.

Two types of T-joints are analysed in this work, the unreinforced unequal width connection and the haunch joint. Two loading types are considered, branch member axial load and branch member bending moment. In each case, the major geometrical parameters that influence joint behaviour, namely, λ, λ_1 and t are studied.

The results are presented both in the elastic and plastic range of loading. The former results are compared with the few available experimental test results (5). Finally, comparisons are made between predicted ultimate strengths using the elastic-plastic model with those from the rigid plastic analysis given by Mouty (10).

CHAPTER 2

THEORETICAL MODEL OF RECTANGULAR HOLLOW SECTION (RHS) T-JOINT

2.1 Modelling of the Joint

Clearly an exact analysis for determining the stiffness characteristics of a rectangular hollow section T-joint, shown in figure 2.1, would involve a three-dimensional analysis necessitating a large storage requirement and a major allocation of computer time. In this study, the behaviour of the single RHS joint is simulated by a two-dimensional model. The top flange of the chord member is treated as a thin plate supported by coupled springs along the edges as shown in figure 2.2. The effect of the rest of the hollow section, excluding the top plate, is incorporated through the transverse stiffness of the frame of unit width indicated in figure 2.3. It should be noted that only one-half of the chord needs to be analysed because of symmetry. The effect of overall bending of the chord member along the longitudinal direction is neglected in order to focus on the joint behaviour itself. This is accomplished by placing two rollers at points A and B of the frame in figure 2.3 which are at the transition of the rounded corner portion to the flat plate.

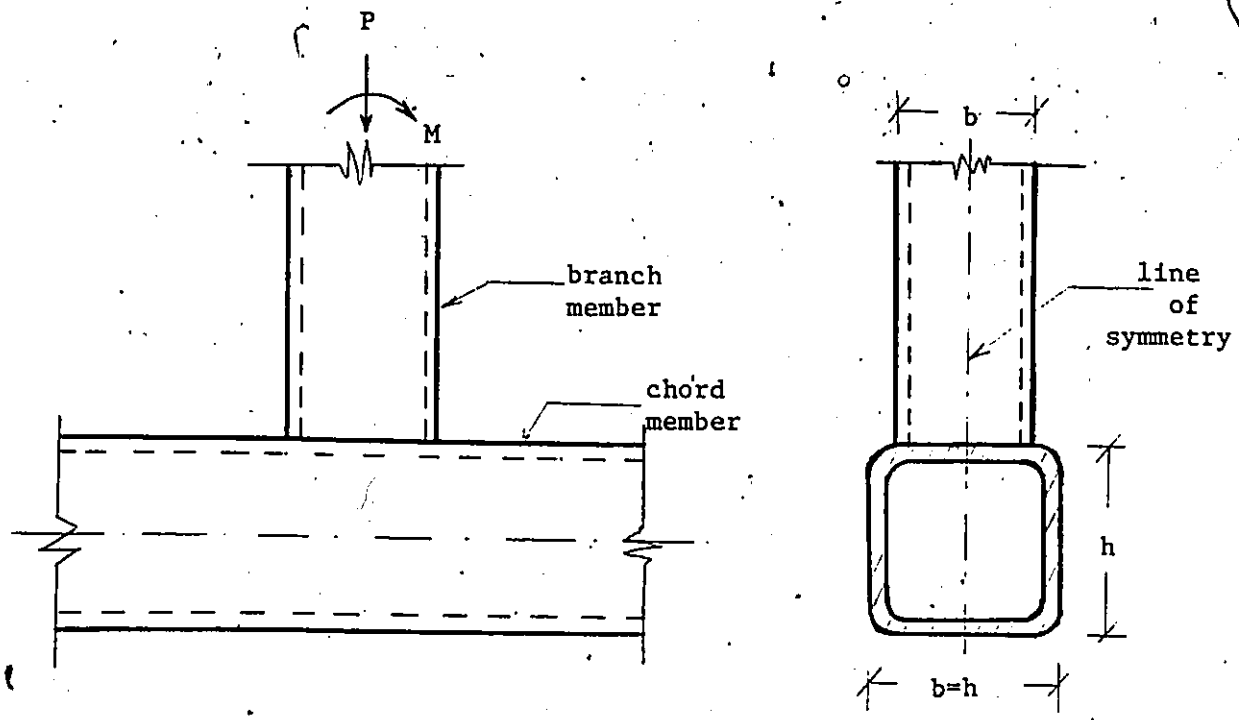

Figure 2.1 Detail of the Rectangular Hollow Structural T-Joint

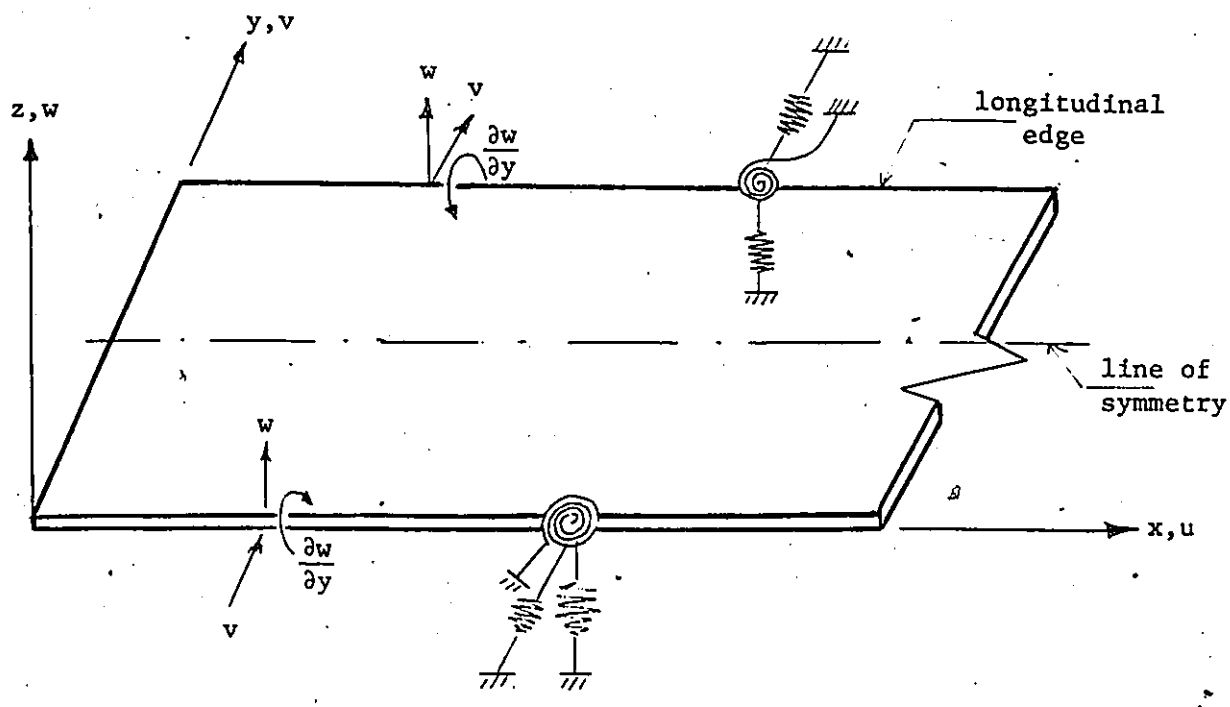

Figure 2.2 Top Flange of the Chord Member as a Thin Plate

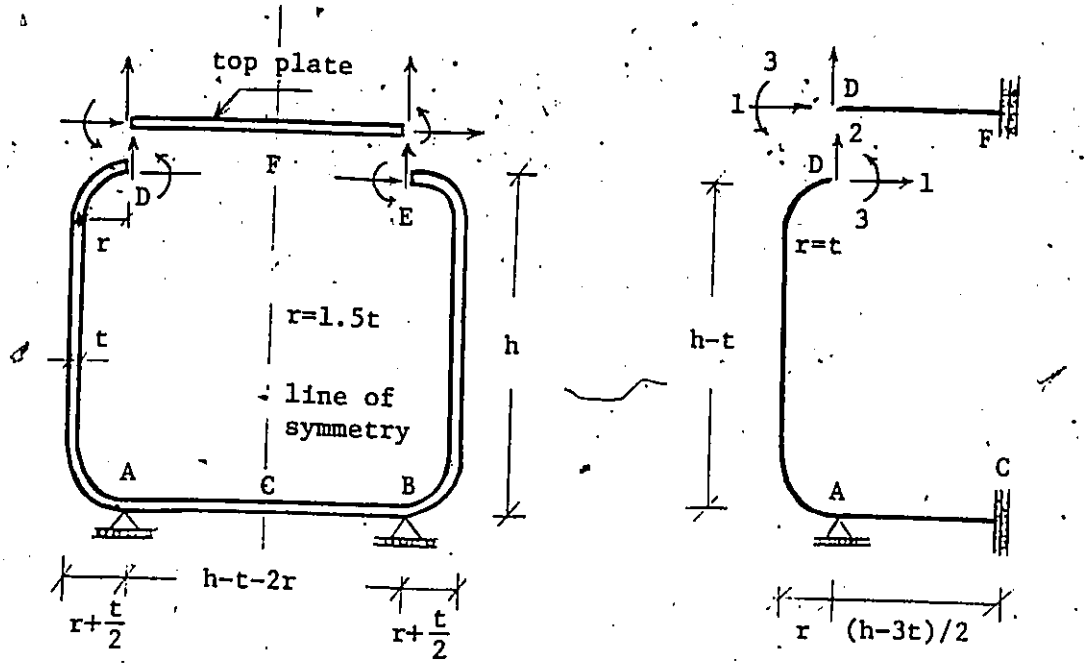

(a) Full Chord

(b) One Half the Chord

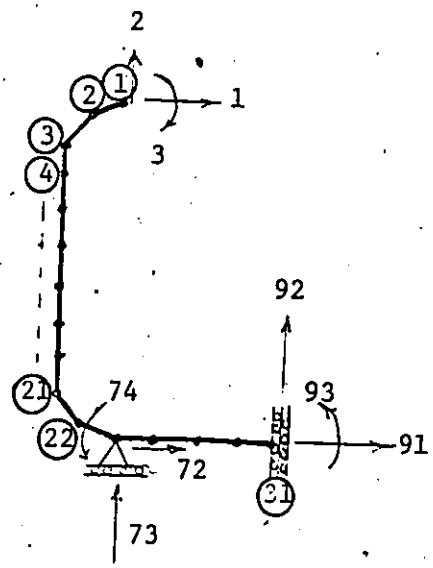

(c) Idealization for the Plane Frame Stiffness Analysis

Figure 2.3 Cross Sectional Model of the Chord Member

2.2 Spring Constants

The stiffness coefficients per unit length for the coupled springs are determined by stiffness analysis of the frame CAD in figure 2.3b. The frame is divided into 31 elements with 93 degrees of freedom as shown in figure 2.3c. The three-by-three frame stiffness matrix is determined in terms of geometric and elastic (or elastic-plastic) properties of the hollow section and degrees of freedom (DOF's) 1, 2, 3. Thus, by incorporating the proper boundary conditions, the frame will appropriately model the transverse influence of the remaining section on the top plate. The spring coefficient matrix (3 x 3), for one-half of the chord, can be obtained from the overall stiffness matrix for the frame in the following manner:

(i) Set the displacement at degrees of freedom (DOF's) number 73 (roller at A) and 91 (from symmetry) and 93 (rotation at c) equal to zero (figure 2.3c);

(ii) Set DOF 1 equal to unity and DOF's 2 and 3 to zero;

(iii) Solve for the holding forces corresponding to DOF's 1, 2, 3. These forces represent the first column in the required matrix of spring coefficients.

(iv) Repeat steps (i) and (iii) for DOF's 2 and 3, set equal to unity one at a time while maintaining the other two at zero as done for DOF 1 in step (ii).

To account for the plate action, the member flexural rigidity, EI per unit length, is replaced by the plate bending rigidity $D = \frac{Et^3}{12(1-\nu^2)}$ where t is the thickness of the chord, E is the modulus of elasticity and ν, is Poisson's ratio. The spring stiffness matrix $\frac{Et^3}{12(1-\nu^2)}$ is obtained twice for each joint, one for the elastic case and the other for the elastic-strain hardening case according to the stress-strain curve chosen for the material used and indicated in figure 2.4. A strong coupling exists among the spring constants which points out that it is inappropriate to use uncoupled springs as was done for simplified models with uncoupled flexibility coefficients used by Redwood (1) and Korol and Mansour (8).

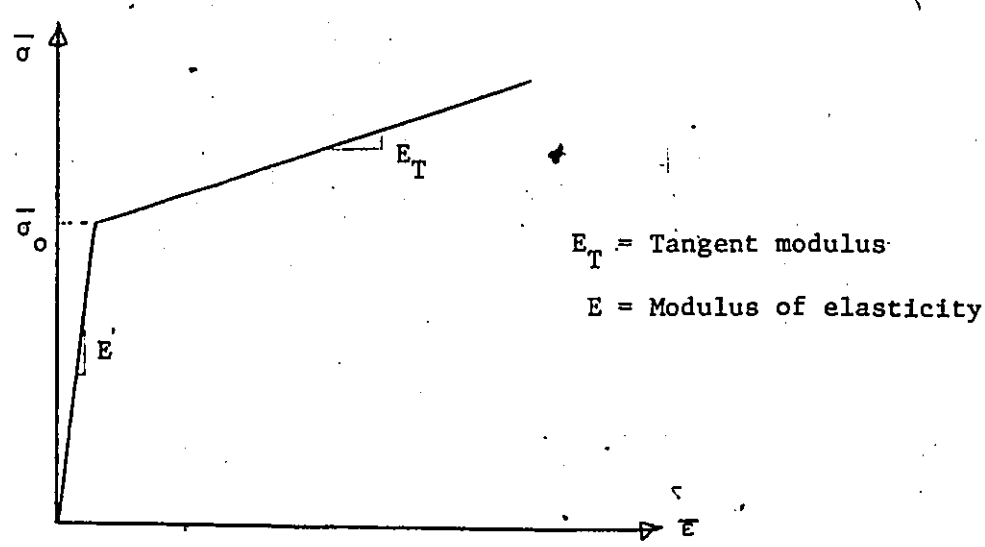

Figure 2.4 Effective stress-effective strain curve for steel

The boundary spring matrix $[\overline{k_s}]$ is a symmetric matrix and relates the generalized edge forces $\{\overline{F}\}$ to the edge displacements $\{\overline{W}\}$ through equation 2.2.1.

$$\{\overline{F}\} = [\overline{k_s}]\ \{\overline{W}\} = [\overline{k}]\ \begin{Bmatrix} v \\ w \\ \frac{\partial w}{\partial y} \end{Bmatrix} \qquad (2.2.1)$$

where v, w and $\frac{\partial w}{\partial y}$ are in-plane displacement in y, out-of-plane displacement and edge rotation about x (see figure 2.2). Since the thin plate analysis pertinent to this work does not incorporate in-plane action, equation 2.2.1 reduces to

$$\{F\} = [k_s]\ \{W\} = [k_s] \begin{Bmatrix} w \\ \frac{\partial w}{\partial y} \end{Bmatrix} \qquad (2.2.2)$$

and

$$[k_s] = \begin{bmatrix} k_v & k_{vr} \\ k_{rv} & k_r \end{bmatrix} \qquad (2.2.3)$$

where k_v is the vertical spring constant; k_r is the rotational spring constant, and $k_{vr} = k_{rv}$ is the coupling term.

A typical $[k_s]$ matrix is calculated for a 254 x 254 x 9.5 mm chord, using the modulus of elasticity E = 199.955 x 10^3 MPa and the Poisson's ratio ν = 0.3.

$$[k_s]^e = \begin{bmatrix} 62 & -730 \\ -730 & 13290 \end{bmatrix} \qquad (2.2.4)$$

The elastic-plastic $[k_s]$ matrix for the same chord is obtained by using E_T (in figure 2.4) = 0.025 E, for the top rounded corner elements of the model in figure 2.3c, and is given by

$$[k_s]^{ep} = \begin{bmatrix} 15 & -125 \\ -125 & 1350 \end{bmatrix} \qquad (2.2.5)$$

One can observe, from equations 2.2.4 and 2.2.5, that the off-diagonal terms are either of the same order or larger than the corresponding diagonal terms. This, of course, confirms the existence of strong coupling among the vertical and rotational spring stiffness.

2.3 Load Transfer System

In the analysis of the T-joint it is assumed that the branch member behaves as a beam column. Furthermore, the top flange plate within the inclusion is presumed to undergo only rigid body type translation δ or rotation ϕ because of the stiffening effect provided by the periphery of the branch member. The load transfer from the branch member edges to the chord member is assumed to occur along the branch member edges as a line load and is distributed according to the beam column theory.

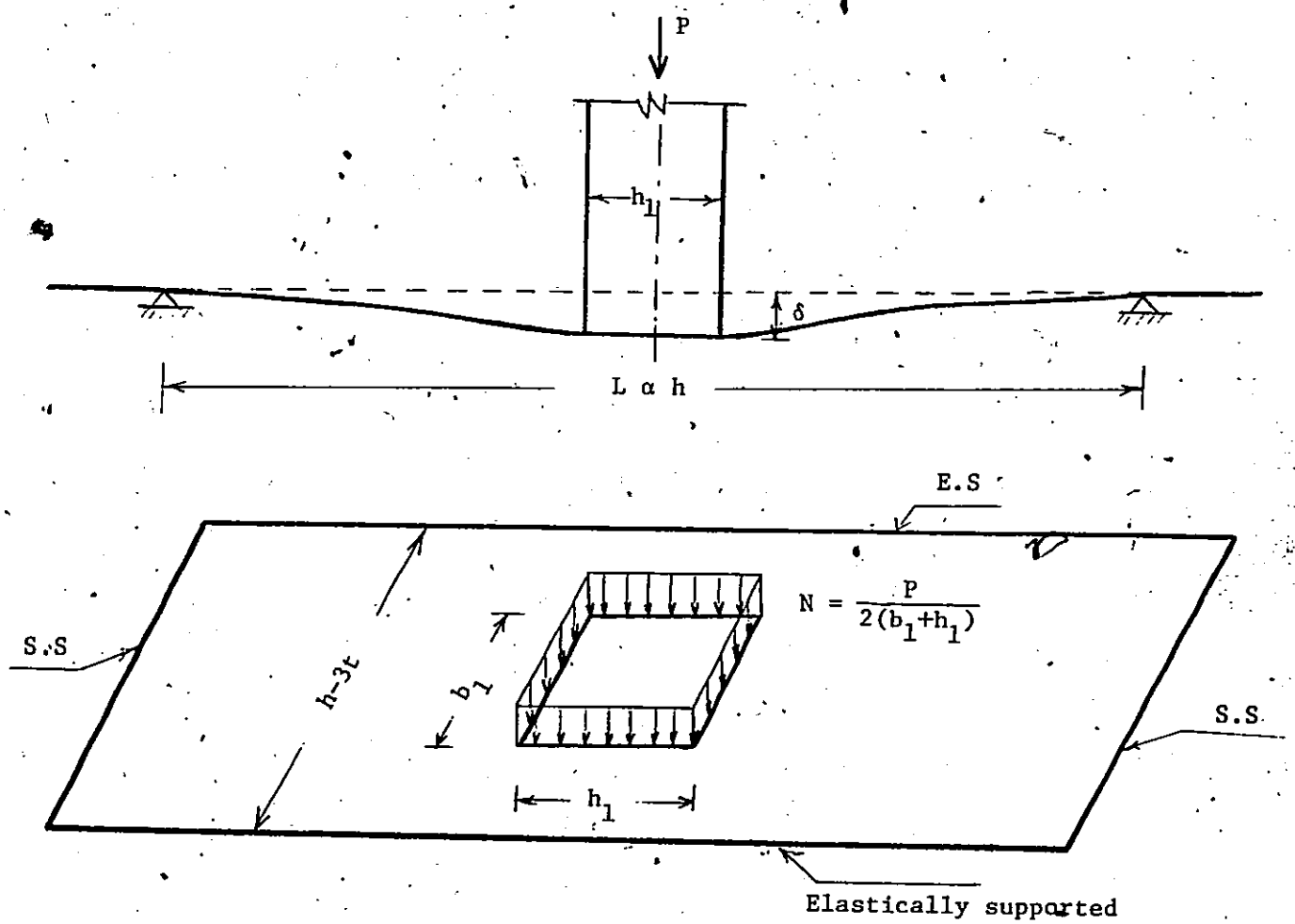

Figure 2.5a Model of Branch Axial Loading of Chord Flange Plate

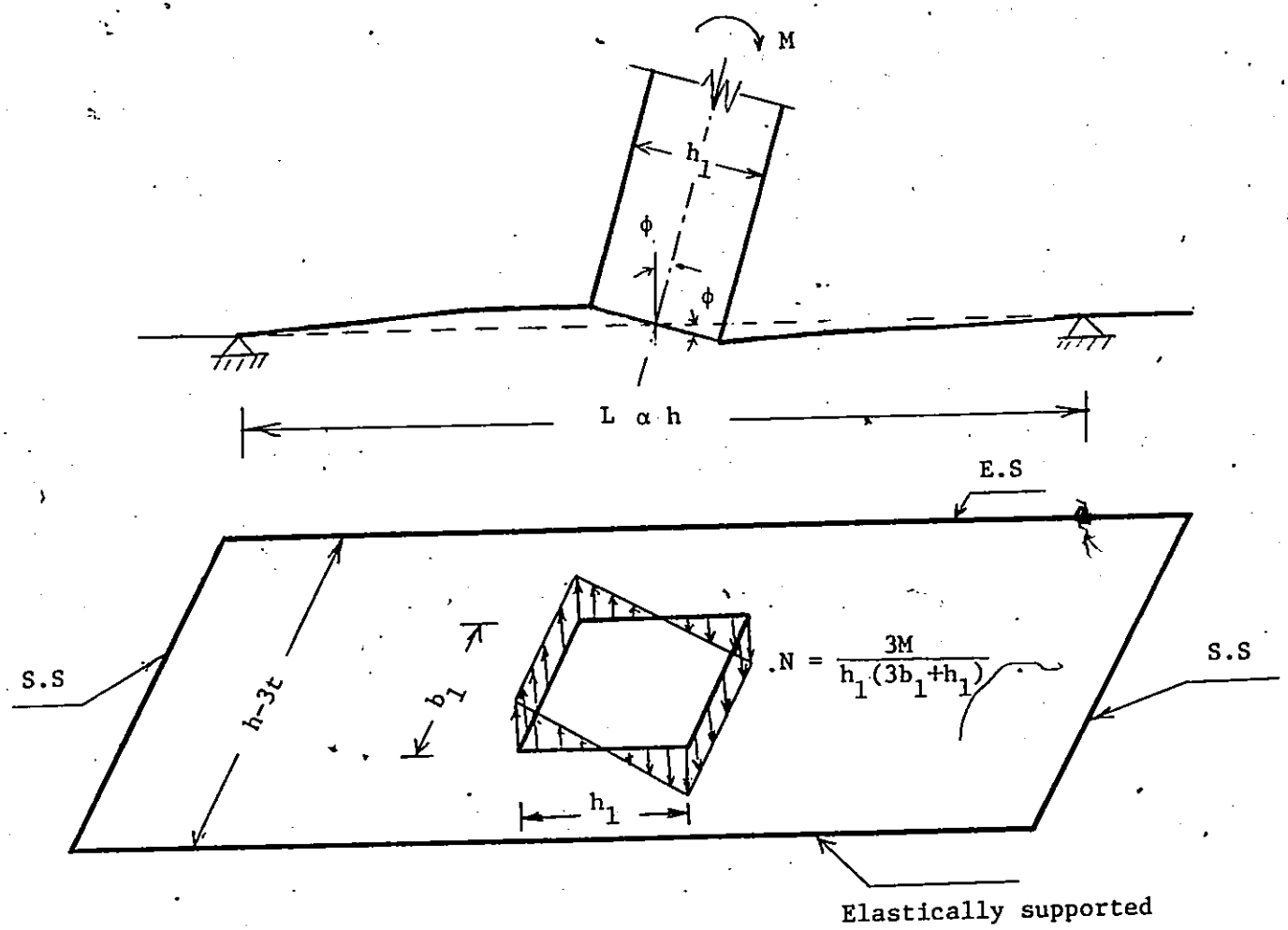

Figure 2.5b Model of Branch Member Bending of Chord Flange Plate

Figure 2.5 shows typical axial and moment transfer systems and rigid body type displacement of the part of the plate within the inclusion. The punching shear and the rotational stiffnesses are then defined by the equations

$$C = \frac{P}{\delta} \quad , \quad J = \frac{M}{\phi} \quad . \qquad (2.3.1)$$

2.4 Boundary Conditions

The top flange plate is assumed to be elastically supported along its two longitudinal edges. The plate length was selected on the basis of proportionality with the width and sufficiently long to ensure end boundary conditions would not have an appreciable effect on plate behaviour.

Boundaries at the ends are assumed to be simply supported (S.S) edges (see figure 2.5).

2.5 Top Flange of Chord as a Thin Elastic Plate

2.5.1 Assumptions

1. The material of the plate is elastic, homogeneous and isotropic.
2. The deflections are small compared to the plate thickness.
3. The deformations are such that straight lines, initially normal to the middle surface, remain straight lines normal to the deformed middle surface.

4. The stresses normal to the middle surface are negligible (i.e. $\sigma_z = 0$).
5. The strains in the middle surface produced by in-plane stresses are neglected in comparison with strains due to bending, i.e., transverse shear deformations are neglected.

Small and large-scale tests have proved the validity of these assumptions (12).

2.5.2 Governing Equations

The co-ordinate system and deflections are shown in figure 2.6a.

a) Deflections

An arbitrary point p in figure 2.6b experiences transverse displacement w and also in-plane displacements u and v because of rotation of the plate element. Accordingly, the displacements of p to p' are

$$u = -z \frac{\partial w}{\partial x}$$

and (2.5.1)

$$v = -z \frac{\partial w}{\partial y}$$

b) Strains

These are given by

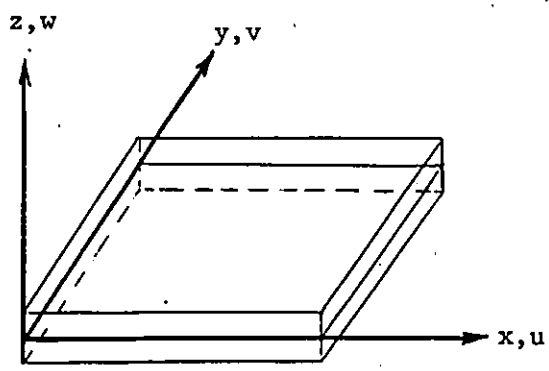

Figure 2.6A

Directions of Axes and Deflections

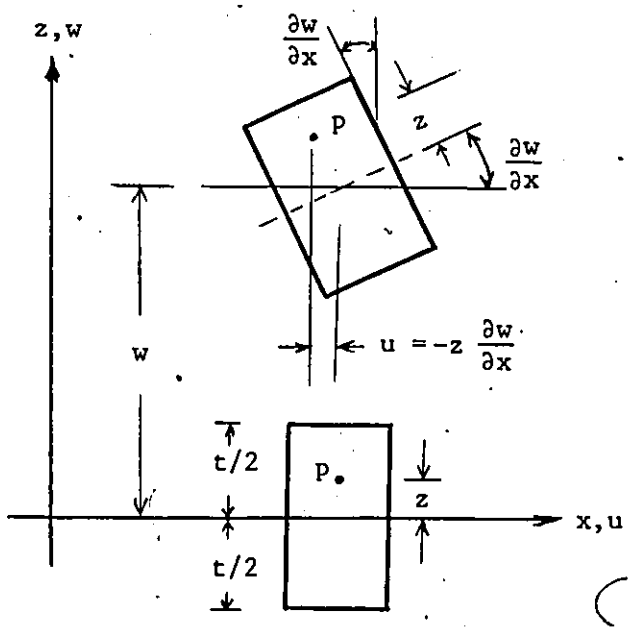

Figure 2.6b

Deflection of a Small Plate Element

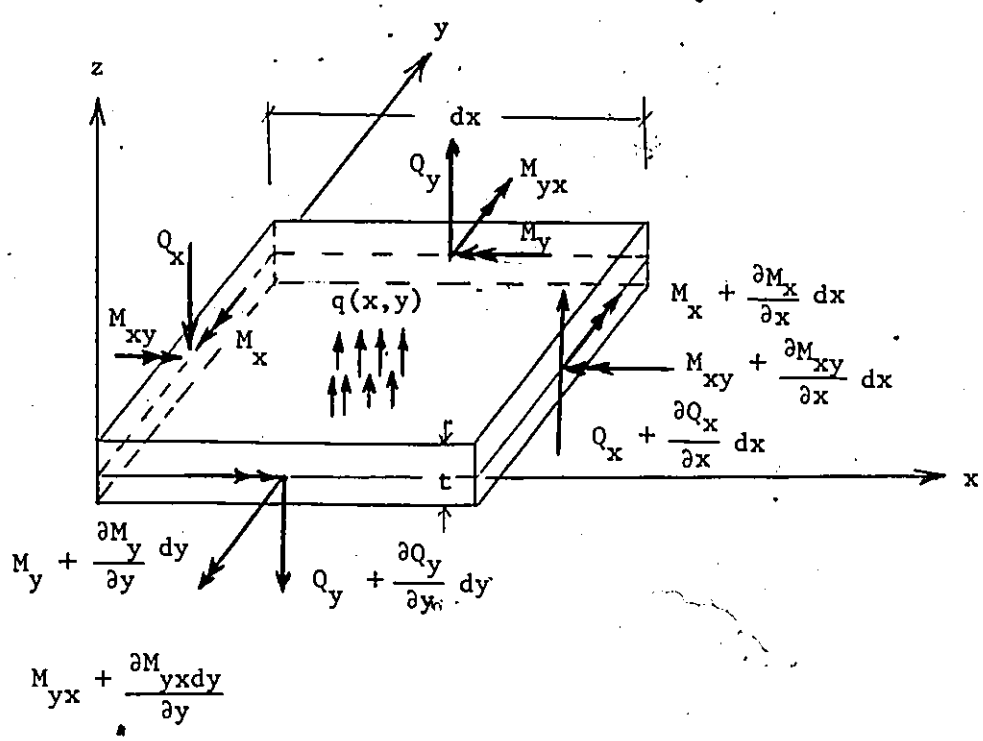

Figure 2.7

External and Internal Forces

$$\varepsilon_x = \frac{\partial u}{\partial x} = -z \frac{\partial^2 w}{\partial x^2}$$

$$\varepsilon_y = \frac{\partial v}{\partial y} = -z \frac{\partial^2 w}{\partial y^2} \qquad (2.5.2)$$

$$\gamma_{xy} = \frac{\partial u}{\partial y} + \frac{\partial v}{\partial x} = -2z \frac{\partial^2 w}{\partial x \partial y}$$

where γ_{xy} is the engineering shear strain.

c) <u>Stresses</u>

Using Hooke's law for isotropic plane stress ($\sigma z = 0$) condition

$$\varepsilon_x = \frac{\sigma_x - \nu\sigma_y}{E}$$

$$\varepsilon_y = \frac{\sigma_y - \nu\sigma_x}{E} \qquad (2.5.3)$$

$$\gamma_{xy} = \frac{\tau_{xy}}{G} = 2(1 + \nu) \frac{\tau_{xy}}{E}$$

Substituting equations 2.5.2 into equations 2.5.3, yields the stresses in the plate;

$$\sigma_x = \frac{E}{1-\nu^2}(\varepsilon_x + \nu\varepsilon_y) = \frac{-Ez}{1-\nu^2}\left(\frac{\partial^2 w}{\partial x^2} + \nu\frac{\partial^2 w}{\partial y^2}\right)$$

$$\sigma_y = \frac{E}{1-\nu^2}(\nu\varepsilon_x + \varepsilon_y) = \frac{-Ez}{1-\nu^2}\left(\nu\frac{\partial^2 w}{\partial x^2} + \frac{\partial^2 w}{\partial y^2}\right) \qquad (2.5.4)$$

$$\tau_{xy} = G\gamma_{xy} = \frac{E}{2(1+\nu)}\gamma_{xy} = \frac{-Ez}{1+\nu}\left(\frac{\partial^2 w}{\partial x \partial y}\right)$$

Finally the moments of these stresses about the neutral plane give

$$M_x = -D\left(\frac{\partial^2 w}{\partial x^2} + \nu\frac{\partial^2 w}{\partial y^2}\right)$$

$$M_y = -D\left(\nu\frac{\partial^2 w}{\partial x^2} + \frac{\partial^2 w}{\partial y^2}\right) \qquad (2.5.5)$$

$$M_{xy} = -D\,(1-\nu)\frac{\partial^2 w}{\partial x \partial y} = -M_{yx}$$

where $D = \dfrac{Et^3}{12(1-\nu^2)}$ is the flexural rigidity of the plate; and M_x, M_y are the bending moments per unit length about y and x axes, respectively; M_{xy} and M_{yx} are the twisting moments per unit length about x and y axes, respectively. These forces are shown on the

infinitesimal plate element in figure 2.7.

d) Differential Equation for Plate Bending

The equilibrium equation of an isotropic elastic thin plate is given by

$$\frac{\partial^4 w}{\partial x^4} + \frac{\partial^4 w}{\partial x^2 \partial y^2} + \frac{\partial^4 w}{\partial y^4} = \frac{q(x, y)}{D}$$

or $$\nabla^4 w = \frac{q(x, y)}{D} \qquad (2.5.3)$$

where $\nabla^4 = \frac{\partial^4}{\partial x^4} + \frac{\partial^4}{\partial x^2 \partial y^2} + \frac{\partial^4}{\partial y^4}$ is the

biharmonic operator ($\nabla^4 = (\nabla^2)^2$) and q(x, y) is the distributed transverse load on the plate.

Detailed derivation of this equation can be found in reference (11).

e) Boundary Conditions

To solve equation 2.5.3, certain boundary conditions have to be imposed and satisfied on each edge. In this study two types of edge supportsare encountered. These are:

i) Simply supported edge along the y-axis (transverse edges).

$$w = \frac{\partial w}{\partial y} = 0$$

ii) Elastically support edge along the x-axis.

The vertical deflection w and edge rotation $\frac{\partial w}{\partial y}$ along the longitudinal edges are equated to those of connecting, boundary springs (figure 2.2).

f) <u>Potential Energy and Strain Energy</u>

If the plate is subjected to a transverse load q(x, y), the potential energy Π is given by

$$\Pi = U - W \tag{2.5.4}$$

where W is the potential energy of the applied loading and U is the strain energy of the plate.

$$U = U_{PB}$$

$$= \frac{D}{2} \iint_A \left[\left(\frac{\partial^2 w}{\partial x^2}\right)^2 + \left(\frac{\partial^2 w}{\partial y^2}\right)^2 + 2\nu \left(\frac{\partial^2 w}{\partial x^2}\right)\left(\frac{\partial^2 w}{\partial y^2}\right) \right. \tag{2.5.5}$$

$$\left. + 2(1 - \nu) \left(\frac{\partial^2 w}{\partial x \partial y}\right)^2 \right] dxdy$$

If the plate is supported elastically along one or more edges, then the strain energy expression becomes

$$U = U_{PB} + U_B \quad . \tag{2.5.6}$$

U_{PB} is given by equation 2.5.5 and U_B is the strain energy of the elastic support (edge springs) and is given by

$$U_B = \frac{1}{2} \int_{S_o} \{W\}^T [k_s] \{W\} \, d\, S \tag{2.5.7}$$

where $[k_s]$ and $\{W\}$ have been defined in equation 2.2.2 and S_o is the length of the elastic support.

CHAPTER 3

FINITE ELEMENT FORMULATION OF RHS T-JOINT UNDER ELASTIC LOADS

3.1 Introduction

In the analysis of RHS T-joints, the top flange of the chord member is modelled as a thin plate supported on edge springs (figure 2.2). The finite element method has been adopted in order to obtain a solution for the biharmonic plate bending differential equation with complicated boundary conditions due to modelling of the rest of the section.

A description of the method, the type of element, and a brief outline of the basic concepts relevent to the RHS T-connection will be presented in this chapter.

3.2 Brief Description of the Finite Element Method

Briefly, the basis of the finite element method is the representation of the domain by an assemblage of subdivisions called finite elements. Element properties are formulated using a simple polynomial interpolation scheme that gives displacements at any point within an element in terms of the nodal displacements of the element, i.e., the displacement finite element method.

A variational principle, such as the principle of minimum potential energy, is employed to obtain a set of equilibrium equations for each element. These sets of equilibrium equations are then assembled by interconnecting the finite elements at the nodes so as to maintain the equilibrium of nodal forces and maintain a certain continuity requirement. See references (13, 14, 15) for details.

3.2.1 Advantages of Finite Element Method

Following are the advantages of using the finite element method;

-- flexibility to use various shapes of elements to model a structure of arbitrary geometry;

-- ability to accommodate complicated boundary conditions with relative ease;

-- versatility to model composite materials with varying elastic properties;

-- representation of the actual structure in a physical sense instead as approach to an abstract model that is hard to visualize;

-- rapid convergence of the displacements with decreasing element sizes.

3.3 Non-Conforming Rectangular Plate Bending Finite Element

3.3.1 Description of 12 DOF Non-Conforming Plate Bending Element

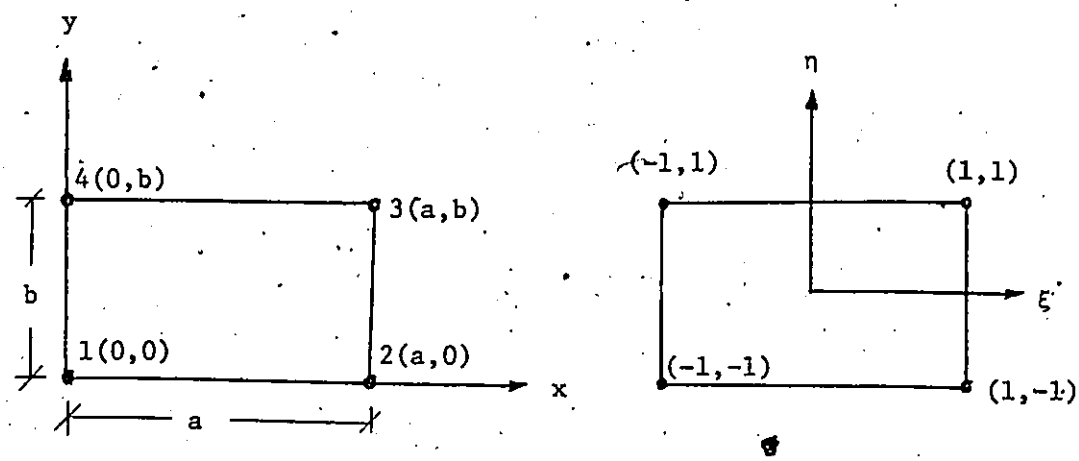

(I) x and y co-ordinates (II) Normalized Co-ordinates

Figure 3.1 Rectangular Element Geometry and Co-ordinate Systems

The twelve degrees of freedom (DOF), non-conforming rectangular plate bending element with three DOF (w, $\frac{\partial w}{\partial x}$ and $\frac{\partial w}{\partial y}$) at each node is used for the plate bending analysis of the top chord, Fig. 3.1. This element has been shown to perform and converge reasonably well, see Zienkiewicz (15).

A complete cubic plus x^3y and xy^3 terms are used to approximate displacement $w(x,y)$ within the element, i.e.,

$$w(x,y) = a_1 + a_2x + a_3y + a_4x^2 + a_5xy + a_6y^2 + a_7x^3$$

$$+ a_8x^2y + a_9xy^2 + a_{10}y^3 + a_{11}x^3y + a_{12}xy^3 . \qquad (3.3.1)$$

The generalized parameters $a_1, a_2, \ldots, a_{12}$ are then related to the nodal degrees of freedom through the transformation matrix [T].

$$\{w^e\} = [T]\{A\} \tag{3.3.2}$$

where $$\{w^e\}^T = \langle w_{x_1}, w_{y_1}, w_1, \ldots\ldots, w_4 \rangle \tag{3.3.3}$$

and $$\{A\}^T = \langle a_1, a_2, a_3, \ldots\ldots\ldots, a_{12} \rangle \tag{3.3.4}$$

and $\underset{12\times12}{[T]}$ matrix and its inverse appear in Appendix A. From equation 3.3.2

$$\{A\} = [T]^{-1}\{w^e\} \tag{3.3.5}$$

After substitution of equation 3.3.5 into equation 3.3.1, one can obtain the shape functions in equation 3.3.6 expressed in terms of normalized co-ordinates ξ, η shown in figure 3.1(II).

$$
w(\xi,\eta)=\{w^e\}\left\{\begin{array}{c}
a\left(\frac{1-\xi}{2}\right)\left(\frac{1+\xi}{2}\right)\left(\frac{1-\eta}{2}\right) \\
b\left(\frac{1-\xi}{2}\right)\left(\frac{1+\eta}{2}\right)\left(\frac{1-\eta}{2}\right) \\
\left[1-\left(\frac{1+\xi}{2}\right)\left(\frac{1+\eta}{2}\right)-(2-\xi)\left(\frac{1+\xi}{2}\right)^2\left(\frac{1-\eta}{2}\right)-\left(\frac{1-\xi}{2}\right)(2-\eta)\left(\frac{1+\eta}{2}\right)^2\right] \\
-a\left(\frac{1-\xi}{2}\right)\left(\frac{1+\xi}{2}\right)^2\left(\frac{1-\eta}{2}\right) \\
-b\left(\frac{1-\eta}{2}\right)^2\left(\frac{1+\xi}{2}\right)\left(\frac{1+\eta}{2}\right) \\
\left[(2-\eta)\left(\frac{1+\xi}{2}\right)^2\left(\frac{1-\eta}{2}\right)-\left(\frac{1+\xi}{2}\right)\left(\frac{1+\eta}{2}\right)\left(\frac{1-\eta}{2}\right)\eta\right] \\
-a\left(\frac{1-\xi}{2}\right)\left(\frac{1+\xi}{2}\right)^2\left(\frac{1+\eta}{2}\right) \\
-b\left(\frac{1-\eta}{2}\right)\left(\frac{1+\xi}{2}\right)\left(\frac{1+\eta}{2}\right)^2 \\
\left[(2-\xi)\left(\frac{1+\xi}{2}\right)^2\left(\frac{1+\eta}{2}\right)+\left(\frac{1+\xi}{2}\right)\left(\frac{1+\eta}{2}\right)\left(\frac{1-\eta}{2}\right)\eta\right] \\
a\left(\frac{1-\xi}{2}\right)^2\left(\frac{1+\xi}{2}\right)\left(\frac{1+\eta}{2}\right) \\
-b\left(\frac{1-\xi}{2}\right)\left(\frac{1-\eta}{2}\right)\left(\frac{1+\eta}{2}\right)^2 \\
\left[\left(\frac{1-\xi}{2}\right)(2-\eta)\left(\frac{1+\eta}{2}\right)^2-\left(\frac{1+\xi}{2}\right)\left(\frac{1-\xi}{2}\right)\left(\frac{1+\eta}{2}\right)\xi\right]
\end{array}\right\} \qquad (3.3.6)
$$

where $\xi = \frac{2x}{a} - 1$ and $\eta = \frac{2y}{b} - 1$ (3.3.7)

Each row in the above vector, represents a shape function N_i and equation 3.3.6 can be written as

$$w(\xi,\eta) = \sum_{i=1}^{12} N_i(\xi,\eta) \quad w_i = \{N\}\{w^e\} \tag{3.3.8}$$

where $w_1^e = w_{x_1}$, $w_2^e = w_{y_2}$, $w_3^e = w_1$,

$w_4^e = w_{x_2}$, ... , $w_1^e = w_4$ ... etc.

3.3.2 Stiffness Matrix

Before deriving the stiffness matrix, expressions for approximate strains are derived within an element. Using equations 2.5.2 and 3.3.8, we obtain

$$\underset{3\times1}{\{\varepsilon\}} = \begin{Bmatrix} \varepsilon_x \\ \varepsilon_y \\ \gamma_{xy} \end{Bmatrix} = \underset{3\times12}{\begin{Bmatrix} -z\dfrac{\partial^2 w}{\partial x^2} \\ -z\dfrac{\partial^2 w}{\partial y^2} \\ -2z\dfrac{\partial^2 w}{\partial x \partial y} \end{Bmatrix}} = \underset{3\times12}{\begin{Bmatrix} -z\dfrac{\partial^2 N}{\partial x^2} \\ -z\dfrac{\partial^2 N}{\partial y^2} \\ -2z\dfrac{\partial^2 N}{\partial x \partial y} \end{Bmatrix}} \underset{12\times1}{\{w^e\}} = \underset{3\times12}{[B]} \underset{12\times1}{\{w^e\}} \tag{3.3.9}$$

The matrix [B] is called the strain matrix relating displacements to strains.

The stresses are then given by equation 2.5.4 as

$$\{\sigma\} = \begin{Bmatrix} \sigma_x \\ \sigma_y \\ \tau_{xy} \end{Bmatrix}_{3x1} = \frac{E}{1-\nu^2} \begin{bmatrix} 1 & \nu & 0 \\ \nu & 1 & 0 \\ 0 & 0 & \frac{1-\nu}{2} \end{bmatrix} \begin{Bmatrix} \varepsilon_x \\ \varepsilon_y \\ \gamma_{xy} \end{Bmatrix} = \underset{3x3}{[D]} \; \underset{3x1}{\{\varepsilon\}} \qquad (3.3.10)$$

where [D] is the plane stress elasticity matrix for an isotropic material.

The potential energy of an element can be computed by

$$\Pi_e = \int_{vol} \frac{1}{2} \{\varepsilon\}^T [D] \{\varepsilon\} \, dV + U_B - \int_{surface} \{w\}^T \{F^e\} \, ds \qquad (3.3.11)$$

The first integral represents the strain energy. The second integral represents work done (loss in potential), U_B is the strain energy of boundary springs if present. Substituting equation 3.3.9 into equation 3.3.11 yields;

$$\Pi_e = \frac{1}{2} \{w^e\}^T \left(\int_{vol} [B]^T [D] [B] \, dV\right) \{w^e\} + U_B - \{w^e\}^T \int_{surface} \{N\}^T \{F^e\} \, ds \qquad (3.3.12)$$

The total potential energy of a structure combined of m elements is then the sum of the potential energies of all elements, i.e.

$$\Pi = \sum_{i=1}^{m} \Pi_e \tag{3.3.13}$$

The static equilibrium equations of an element are then obtained by minimizing Π_e

$$\frac{\partial \Pi_e}{\partial w_i^e} = 0 \qquad i = 1, 2, \ldots, 12 \tag{3.3.14}$$

or (excluding the boundary springs)

$$\left(\int_{vol} [B]^T [D][B]\, dV\right) \{w^e\} = \left(\int_{surface} \{N\}^T \{F^e\}\, ds\right) \tag{3.3.15}$$

From inspection of equation 3.3.15, the element stiffness matrix is recognized as

$$[K^e] = \int_{vol} [B]^T [D] [B]\, dV \tag{3.3.16}$$

and the consistent load vector as

$$\{P^e\} = \int_{surface} \{N\}^T \{F^e\}\, ds \tag{3.3.17}$$

In the presence of boundary springs, its contribution to the stiffness matrix in equation 3.3.16 must be accounted for.

The element stiffness matrices and the load vectors are then assembled to obtain the global equilibrium equations [Zienkiewicz (15)].

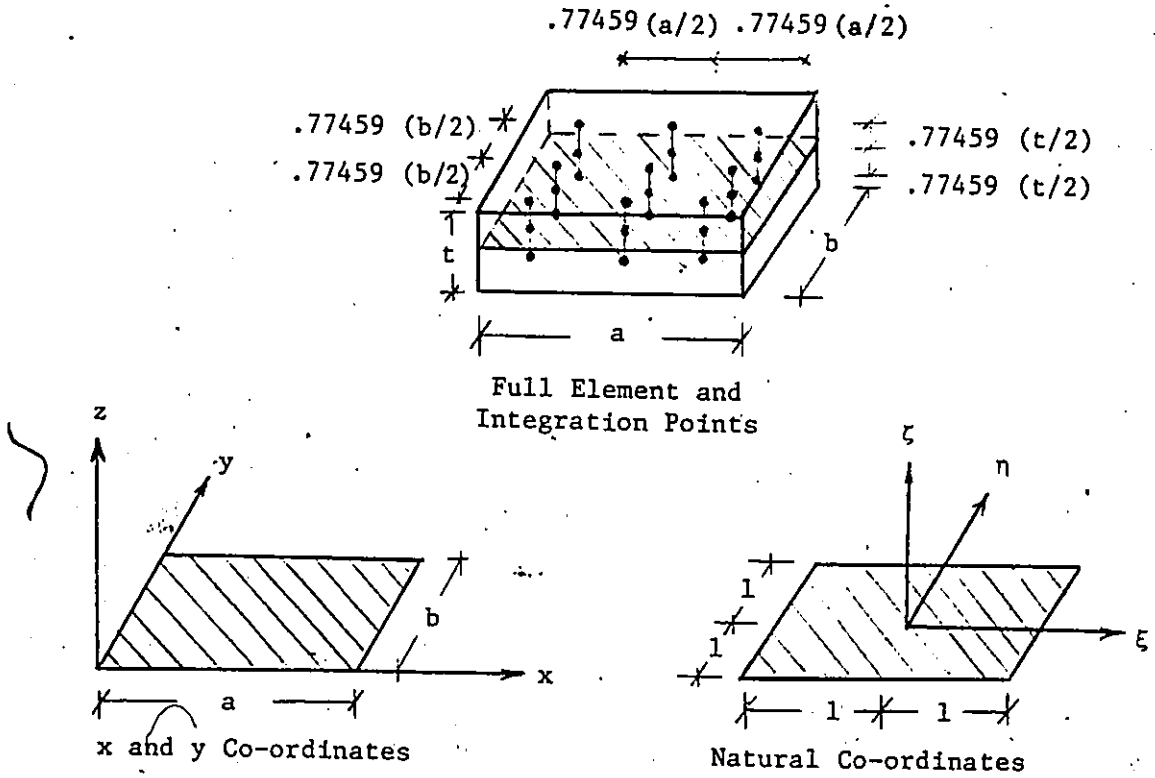

Fig. 3.2

To obtain the element stiffness matrix $[K^e]$, equation 3.3.16 may be written as (Figure 3.2).

$$[K^e] = \int_0^a \int_0^b \int_{-t/2}^{t/2} [B]^T [D] [B] \; dxdydz \qquad (3.3.18)$$

$$\text{or } [K^e] = \frac{a \cdot b \cdot t}{8} \int_{-1}^{+1} \int_{-1}^{+1} \int_{-1}^{+1} [B]^T [D] [B] \; d\xi d\eta d\zeta \qquad (3.3.19)$$

Clearly, the [B] matrix as indicated from equations 3.3.6, 3.3.8, 3.3.9 is a function of ξ, η, ζ and is given in Appendix (B).

In general, equation 3.3.19 is difficult to integrate exactly because of the complexity of the expressions. Hence, Gaussian numerical integration is employed. (See References (21) and (22).)

A general and simple form of Gauss integration of a function is

$$I = \int_{-1}^{+1} f(\xi)\, d\xi = \sum_{i=1}^{n} v_i f(\xi_i) \qquad (3.3.20)$$

where n is the number of integration points in ξ direction.

To numerically approximate the integral, the function is evaluated at several sampling points, then multiply the integral at each sampling point with the appropriate "weight factor", v_i, and add. Gauss' method uses the sampling points which have been optimized to yield minimum error. A greater accuracy is achieved by using more sampling point. In general, Gaussian quadrature using n points is exact if the integrand is a polynomial of degree 2n-1 or less. Thus the error is of order $\sigma(\Delta^{2n})$ where Δ is the spacing of sampling points. It is also of interest (15), (21) to determine (a) the minimum integration requirement permitting convergence, and (b) the integration requirements necessary to preserve the rate of convergence which would result if exact integration were used. Let p be the degree of the complete polynomial and m be the order of derivatives as occurring in the strain energy expression. Provided, the integration is exact to the order of 2(p-m) or shows an error of $\sigma(\Delta^{2(p-m)+1})$ or less, then no loss of convergence rate will occur. For the polynomial given in equation 3.3.1 p = 3 and from the strain energy expressions (equations 3.3.10 and 3.3.15) m = 2, i.e. the largest derivative is 2.

$$\therefore \quad 2n-1 \geq 2(3-2) = 2$$

$$2n \geq 3 \quad \text{or } n \geq \frac{3}{2} \qquad (3.3.21)$$

This means that an exact integration for formulation of the stiffness matrix is obtained with the use of three integration points in each direction. Of course, in the inelastic range, the material properties will vary as well and may yield an integrand of degree higher than 3.

Extension of equation 3.3.20 to three dimensions is straight forward and yields

$$I = \int_{-1}^{+1}\int_{-1}^{+1}\int_{-1}^{+1} f(\xi,\eta,\zeta)\, d\xi d\eta d\zeta$$

$$= \sum_i \sum_j \sum_k v_i\, v_j\, v_k\, f(\xi_i, \eta_j, \zeta_k)$$

Table 3.3.1 gives the appropriate coefficients (24) of the first three orders.

Number of Points	Locations, ξ_i	Associated Weights, v_i
1	$\xi_1 = 0.0000$	2.0
2	$\xi_1, \xi_2 = \pm 0.57735026918962$	1.0
3	$\xi_1, \xi_3 = \pm 0.77459666924148$	5/9
	$\xi_2 = 0.00000$	8/9

Table 3.3.1 Gauss Quadrature Coefficients

Next, consider the elements along the longitudinal boundary which are supported by the elastic springs.

3.3.3 Derivation of Boundary Elements with Springs

The total elastic strain energy for an element on the boundary can be expressed as

$$U_T^{\,e} = \frac{1}{2} \{w^e\}^T \{K^e\} \{w^e\} + U_B. \tag{3.3.23}$$

The first term on the right hand side of equation 3.3.23 is the strain energy due to bending of the plate element and the second term, U_B, is the strain energy of boundary springs due to edge displacements. Thus

$$\begin{aligned} U_B &= \frac{1}{2} \int_{a_e} \{W^e\}^T [k_s] \{W^e\} \, dx \\ &= \frac{1}{2} \{w^e\}^T [K_B] \{w^e\} \end{aligned} \tag{3.3.24}$$

where a_e is the length of the element edge resting on springs,

$$\{w^e\}^T = < w_{x1}, w_{y1}, w, w_{x2}, w_{y2}, \ldots\ldots, w_4 > ,$$

$[K_B]$ is the required stiffness matrix due to springs along one edge of the element, and $[k_s]$ is the boundary spring matrix, as defined in equation 2.2.3.

The strain energy given by equation 3.3.24 can be written as

$$U_B = U_v + U_r + U_w \tag{3.3.25}$$

where $U_v = \frac{1}{2} \int_{a_e} k_v \cdot w^2 \, dx$, the strain energy due to vertical springs

$U_r = \frac{1}{2} \int_{a_e} k_r \left(\frac{\partial w}{\partial y}\right)^2 dx$, the strain energy due to rotational springs and

$U_{vr} = \frac{1}{2} \int_{a_e} k_{vr} \cdot w \cdot \frac{\partial w}{\partial y} dx$, the strain energy due to coupling between vertical and rotational springs

(3.3.26)

From equation (3.3.1) the displacement can be written as

$$w(x,y) = \sum_{i=1}^{12} a_i \cdot x^{m_i} \cdot y^{n_i} \tag{3.3.27}$$

where $\{m\}^T = < 0, 1, 0, 2, 1, 0, 3, 2, 1, 0, 3, 1 >$

$\{n\}^T = < 0, 0, 1, 0, 1, 2, 0, 1, 2, 3, 1, 3 >$ (3.3.28)

$$\therefore (w)^2 = \sum_{i=1}^{12} \sum_{j=1}^{12} x^{m_i+m_j} \; y^{n_i+n_j} \; a_i \, a_j$$

$$\left(\frac{\partial w}{\partial y}\right)^2 = \sum_{i=1}^{12} \sum_{j=1}^{12} n_i \, n_j \; x^{m_i+m_j} \; y^{n_i+n_j-2} \; a_i \, a_j \tag{3.3.29}$$

$$w \cdot \frac{\partial w}{\partial y} = \sum_{i=1}^{12} \sum_{i=1}^{12} (n_i+n_j) \; x^{m_i+m_j} \; y^{n_i+n_j-1} \; a_i a_j$$

Using $\bar{\xi} = \frac{x}{a}$, $\bar{\eta} = \frac{y}{b}$

$$\therefore \int_0^1 w^2\, dx = a \sum_{i=1}^{12} \sum_{j=1}^{12} \bar{\eta}^{\,n_i+n_j}/(m_i+m_j+1)\; a_i\, a_j$$

$$\int_0^1 \left(\frac{\partial w}{\partial y}\right)^2 dx = \frac{a}{b^2} \sum_{i=1}^{12} \sum_{j=1}^{12} n_i n_j\, \bar{\eta}^{\,n_i+n_j-2}/(m_i+m_j+1)\; a_i\, a_j \qquad (3.3.30)$$

$$\int_0^1 w \cdot \frac{\partial w}{\partial y}\, dx = \frac{a}{b} \sum_{i=1}^{12} \sum_{j=1}^{12} (n_i+n_j)\, \bar{\eta}^{\,n_i+n_j-1}/(m_i+m_j+1)\; a_i\, a_j$$

From equation 3.3.27 the strain energy components U_v, U_r and U_{vr} can be determined so that equation 3.3.25 gives

$$U_B = \frac{1}{2} \{A\}^T \{\tilde{K}\} \{A\} \qquad (3.3.31)$$

where $\{A\}^T$ and $\{A\}$ are determined by equations 3.3.2 and 3.3.4 and the i, jth component of the matrix $[\tilde{K}]$ is given by

$$\tilde{K}_{ij} = [a \cdot k_v \cdot \bar{\eta}^{\,n_i+n_j} + \frac{a}{b^2} \cdot k_r\, n_i\, n_j\, \bar{\eta}^{\,n_i+n_j-2} + \frac{a}{b} k_{vr}\, (n_i+n_j)$$

$$\bar{\eta}^{\,n_i+n_j-1}] \,/\, (m_i+m_j+1) \qquad (3.3.32)$$

from equation 3.3.5 and 3.3.31

$$U_B = \frac{1}{2} \{w^e\}^T [T^{-1}]^T \{\tilde{K}\} [T]^{-1} \{w^e\} \,. \qquad (3.3.33)$$

Comparison of equation 3.3.31 with 3.3.24 yields the contribution, $[K_B]$ to the boundary element stiffness matrix and

$$[K_B] = [T^{-1}]^T [\tilde{K}] [T]^{-1} \qquad (3.3.34)$$

3.3.4 Load Vector

A consistent load vector is used in the finite element analysis. Since only the line loads along various edges of an element are considered, a brief derivation of the consistent load vector for such loads is presented here.

For line load, q_1, applied along edge 1-2 of an element (Figure 3.1), the work done, W_e, by the load is given by

$$W_e = \int_{a_e} q_1 \, w \, d\xi = \frac{a}{2} \int_{-1}^{+1} q_1 \, w(\xi,\eta) \, d\xi = \{\overline{P}\} \{w^e\} \qquad (3.3.35)$$

On integration, the load vector for the element is

$$\{\overline{P}\}^T = \frac{a}{2} q_1 < \frac{a}{6}, 0.0, 1.0, -\frac{a}{6}, 0,0, 1, 0.0, 0.0, 0.0, 0.0, 0,0, 0.0 > \qquad (3.3.36)$$

Similarly, if the load, q_2, is applied along edge 2-3 of an element (Figure 3.1), the following load vector is obtained

$$\{\overline{P}\}^T = \frac{b}{2} q_2 < 0.0, 0.0, 0.0, -\frac{b}{6}, 1.0, 0.0, \frac{b}{6}, 1.0, 0.0, 0.0, 0.0 > \qquad (3.3.37)$$

Of course, if the load is applied along edge 1-2 and 2-3 the load vector of an element will be equal to the sum of the $\{\overline{P}\}$ given by equations 3.3.36 and 3.3.37.

A similar procedure can be performed for edges 3-4 and 4-1.

3.4 Computer Program

In this section a brief presentation of the features of the computer program developed to solve the RHS T-joint using the finite element method is given. The program can also solve problems of rectangular plates subjected to various types of transverse loads, and for a variety of boundary conditions (simply supported, clamped, free and elastically supported).

Program Steps

1. Define the number of nodes, elements, variable per nodes and number of nodes per element.
2. Define the global co-ordinates of each node and local element node numbers, and define at each node whether the displacement is allowed or not (boundary conditions).
3. Define the material properties.
4. Construct the element stiffness matrix.
5. Construct the boundary stiffness matrix if the element lies on a boundary resting on springs.
6. Calculate the element load vector if the element is subjected to any type of loading.
7. Place element stiffness matrix and element load vector into the global stiffness matrix and load vector, respectively.
8. Solve the system of linear simultaneous equations.
9. Calculate strains, stresses and moments at required points.
10. Print the results.

A complete listing of the computer program appears in Appendix C.

Test Example

In order to check the formulations and computer program developed, as well as to gain confidence in the accuracy of the results obtained, the program was used to solve a plate problem for which an exact solution exists. A simple example considered here is that of a simply supported square plate subjected to either a concentrated load P or a uniformly distributed load of intensity q. The results are given in table 3.4.1 and are compared with Timoshenko's results.

Mesh	Total Number of Nodes	Uniform Load		Concentrated Load	
		W centre	Mx centre	W centre	Mx centre
2 x 2	9	0.005016	0.063169	0.013784	0.22824
4 x 4	25	0.004317	0.050053	0.012327	0.2045
exact (Timoshenko)		0.004062	0.049347	0.011600	0.18281
Multiplier		qL^4/D	qL^2	PL^2/D	PL

Table 3.4.1 Computed Central Deflections and Moments of Simply Supported Square Plate

The results given in Table 3.4.1 are identical to those given by Zienkiewicz (15) as expected. Test examples were also run in asymptotic cases in which $k_r \to 0$ (5.5), $k_r \to \infty$ (clamped); k_r and k_v both approaching ∞ (clamped). With only springs on the boundary and with thickness t or modulus $E \to \infty$ the result yielded rigid body plate displacements, i.e. only springs deflecting. The examples above indicated the correctness of the FEM program developed.

CHAPTER 4

Elastic-Plastic Finite Element Analysis of Thin Plates

4.1 Introduction

A general finite element displacement analysis capable of determining the complete elastic-plastic behaviour as well as a measure of the ultimate load carrying capacity of transversely loaded plates with any type of boundary conditions is presented in this Chapter. The approach is presented in an incremental form and is based on the tangent stiffness concept. The nonconforming rectangular plate bending element derived in section 3.3 , with the twenty-seven sampling points within the element has been used to aid in the description of the elastic-plastic behaviour of the plate, since the process of plastification is difficult to describe mathematically. The method has been developed for an elastic, linearly strain hardening material, but could be easily extended to treat a more general material behaviour.

A test example is given, demonstrating the validity of the proposed numerical technique.

4.2 Plasticity Relations

According to the Von Mises criterion, for the plane stress case, yielding begins under any state of stress when the effective stress $\bar{\sigma}$ exceeds a certain limit, where

$$\bar{\sigma} = \sqrt{\sigma_x^2 + \sigma_y^2 - \sigma_x\sigma_y + 3\tau_{xy}^2}. \tag{4.2.1}$$

An effective plastic strain increment $d\bar{\varepsilon}^p$ is defined as a combination of the separate plastic strain increments.

$$d\bar{\varepsilon}^p = \frac{2}{3}\sqrt{(d\varepsilon^p{}_x)^2 + (d\varepsilon^p{}_y)^2 - (d\varepsilon_x{}^p)\ (d\varepsilon_y{}^p) + \frac{3}{4}\ (d\gamma_{xy}{}^p)^2} \tag{4.2.2}$$

where γ_{xy} is the engineering shear strain, $\gamma_{xy} = \frac{\partial u}{\partial y} + \frac{\partial v}{\partial x}$.

The relation between effective stress and effective strain may be established by a uniaxial tension test and is shown in figure 4.1. This figure shows the elastic component $\bar{\varepsilon}^e$ of effective strain, and the relation between the slope H', the elastic modulus E and tangent modulus E_T. The total strain increment $d\bar{\varepsilon}$ is given by

$$d\bar{\varepsilon} = d\bar{\varepsilon}^{\,e} + d\bar{\varepsilon}^{\,p}$$

where $d\bar{\varepsilon}^{\,e} = \frac{d\bar{\sigma}}{E}$ and $d\bar{\varepsilon} = \frac{d\bar{\sigma}}{E_T}$. Substitution of $d\bar{\varepsilon}^{\,e}$ and $d\bar{\varepsilon}$ into the equation above leads to

$$d\bar{\varepsilon} = \frac{d\bar{\sigma}}{E_T} = \frac{d\bar{\sigma}}{E} + d\bar{\varepsilon}^p$$

Therefore $d\bar{\varepsilon}^{\,p} = (\frac{1}{E_T} - \frac{1}{E})\ d\bar{\sigma} = (\frac{E-E_T}{E\cdot E_T})\ d\bar{\sigma} = \frac{d\bar{\sigma}}{H'}$

and $$H' = \frac{d\bar{\sigma}}{d\bar{\varepsilon}^p} = \frac{E.E_T}{E-E_T}, \tag{4.2.3}$$

where H' is the slope of the tangent to the stress-plastic strain curve.

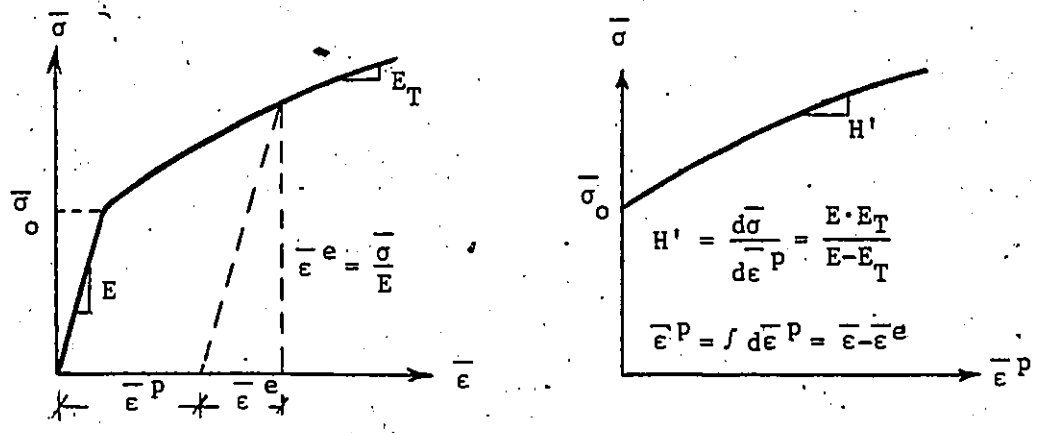

Figure 4.1 Effective Stress-Effective Strain Relations

Yielding first begins when $\bar{\sigma}$ exceeds $\bar{\sigma}_o$. As $\bar{\varepsilon}^p$ grows, the value of $\bar{\sigma}$ which must be exceeded to produce further yield also increases. This is, of course, the strain hardening phenomenon. If unloading occurs, one may assume that no matter what the subsequent state of stress, yielding resumes only when $\bar{\sigma}$ exceeds its previous maximum value. This is the assumption of isotropic hardening and ignores the Bauchinger effect.

Differentiation of both sides of equation 4.2.1 with respect to the stresses $\sigma_x, \sigma_y, \tau_{xy}$, and the substitution of the deviatoric stress σ_x', σ'_y, where

$$\sigma'_x = \frac{1}{3}(2\sigma_x - \sigma_y) \quad , \quad \sigma'_y = \frac{1}{3}(2\sigma_y - \sigma_x)$$

one obtains

$$d\bar{\sigma} = \{\frac{\partial\bar{\sigma}}{\partial\sigma}\}^T < d\sigma_x \quad d\sigma_y \quad d\tau_{xy} > \quad = \{\frac{\partial\bar{\sigma}}{\partial\sigma}\}^T < d\sigma > \qquad (4.2.4)$$

where

$$\underset{1x3}{\{\frac{\partial\bar{\sigma}}{\partial\sigma}\}^T} = < \frac{3\sigma'_x}{2\bar{\sigma}} \quad \frac{3\sigma'_y}{2\bar{\sigma}} \quad \frac{3\tau_{xy}}{\bar{\sigma}} > \qquad (4.2.5)$$

The Prandtl-Reuss flow rule states that

$$\underset{3x1}{\{d\varepsilon^p\}^T} = < d\varepsilon_x^p \quad d\varepsilon_y^p \quad d\gamma_{xy}^p > = \underset{3x1}{\{\frac{\partial\bar{\sigma}}{\partial\sigma}\}} \cdot d\bar{\varepsilon}^p \tag{4.2.6}$$

This equation defines the three plastic strain increments that result when the effective plastic strain increment $d\bar{\varepsilon}^p$ occurs under a known state of stress.

Since the strain increment $\{d\varepsilon\}$ is the sum of its elastic strain components $\{d\varepsilon^e\}$ and plastic strain components $\{d\varepsilon^p\}$, one can apply the Hooke's law to obtain

$$\underset{3x1}{\{d\sigma\}} = \underset{3x3}{[D]} \underset{3x1}{\{d\varepsilon^e\}} = [D][\{d\varepsilon\} - \{d\varepsilon^p\}] \tag{4.2.7}$$

where $[D]$ is the conventional isotropic elasticity matrix presented in equation 3.3.10.

A relation that yields $d\bar{\varepsilon}^p$ from the total strain increment $\{d\varepsilon\}$ is obtained from equations 4.2.3 and 4.2.4 in the following manner

$$d\bar{\sigma} = \{\frac{\partial\bar{\sigma}}{\partial\sigma}\}^T \{d\sigma\} = H' d\bar{\varepsilon}^p \tag{4.2.8}$$

Substitute equation 4.2.6 into equation 4.2.7

$$\underset{3x1}{\{d\sigma\}} = [D][\underset{3x1}{\{d\varepsilon\}} - \underset{3x1}{\{\frac{\partial\bar{\sigma}}{\partial\sigma}\}} d\bar{\varepsilon}^p] .$$

Premultiply both sides of this equation with $\{\frac{\partial\bar{\sigma}}{\partial\sigma}\}^T$ to obtain

$$d\bar{\sigma} = \{\frac{\partial\bar{\sigma}}{\partial\sigma}\}^T \{d\sigma\} = \{\frac{\partial\bar{\sigma}}{\partial\sigma}\}^T [D][\{d\varepsilon\} - \{\frac{d\bar{\sigma}}{\partial\sigma}\} d\bar{\varepsilon}^p]$$

From this equation and equation 4.2.8, one obtains

$$\left(H' + \left\{\frac{\partial\bar{\sigma}}{\partial\sigma}\right\}^T [D] \left\{\frac{\partial\bar{\sigma}}{\partial\sigma}\right\}\right) \; d\bar{\varepsilon}^P = \left\{\frac{\partial\bar{\sigma}}{\partial\sigma}\right\}^T [D] \{d\varepsilon\}$$

Hence

$$d\bar{\varepsilon}^P = \frac{\left\{\frac{\partial\bar{\sigma}}{\partial\sigma}\right\}^T [D]}{H' + \left\{\frac{\partial\bar{\sigma}}{\partial\sigma}\right\}^T [D] \left\{\frac{\partial\bar{\sigma}}{\partial\sigma}\right\}} \; \underset{1\times3}{\{d\varepsilon\}} \; \underset{3\times1}{} = [C] \{d\varepsilon\} \; . \tag{4.2.9}$$

An incremental stress-strain relation, analogous to Hooke's law, but valid beyond the proportional limit, is obtained by substitution of equation 4.2.9 into equation 4.2.6 and the result into equation 4.2.7. This relation is given by

$$\underset{3\times1}{\{d\sigma\}} = \left(\underset{3\times3}{[D]} - \underset{3\times3}{[D]} \underset{3\times1}{\left\{\frac{\partial\bar{\sigma}}{\partial\sigma}\right\}} \underset{1\times3}{[C]}\right) \{d\varepsilon\} = \underset{3\times3}{[D_{ep}]} \; \underset{3\times1}{\{d\varepsilon\}} \tag{4.2.10}$$

For plane stress problem $[D_{ep}]$ is (13,27)

$$\frac{E}{Q}\begin{bmatrix} \sigma'^2_y + 2p & & \text{symmetric} \\ -\sigma'_x \cdot \sigma'_y + 2\nu p & \sigma'^2_x + 2p & \\ -\frac{\sigma'_x + \nu\sigma'_y}{1+\nu}\tau_{xy} & -\frac{\sigma'_y + \nu\sigma'_x}{1+\nu}\tau_{xy} & \frac{R}{2(1+\nu)} + \frac{2H'}{9E}(1-\nu)\bar{\sigma}^2 \end{bmatrix} \tag{4.2.11}$$

where $p = \frac{2H'}{9E}\bar{\sigma}^2 + \frac{\tau_{xy}^2}{1+\nu}$

$$Q = R + 2(1-\nu^2)\,p \tag{4.2.12}$$

$$R = \sigma'^2_x + 2\nu\sigma'_x \cdot \sigma'_y + \sigma'^2_y$$

and ν = Poisson's ratio, E = elastic modulus.

See References (13, 15, 21, 26-31) for more details.

4.3 Incremental Method Using Tangent Stiffness

By applying load in increments and following plastic action as it develops, one can properly account for the path-dependent nature of plasticity. A typical step of the solution is described with the aid of figure 4.2, which is a single d.o.f. representation of an actual multi-d.o.f. problem. Suppose that under load $\{p\}_A$, the correct displacements $\{w\}_A$ and the structure tangent stiffness $[K]_A$ are known. Displacement increment $\{\Delta w\}_{AB}$ produced under the next load increment is computed in the following manner

$$[K]_A \{\Delta w\}_{AB} = \{\Delta P\}_{AB} = \{p\}_B - \{p\}_A$$

$$\{w\}_B = \{w\}_A + \{\Delta w\}_{AB} \tag{4.3.1}$$

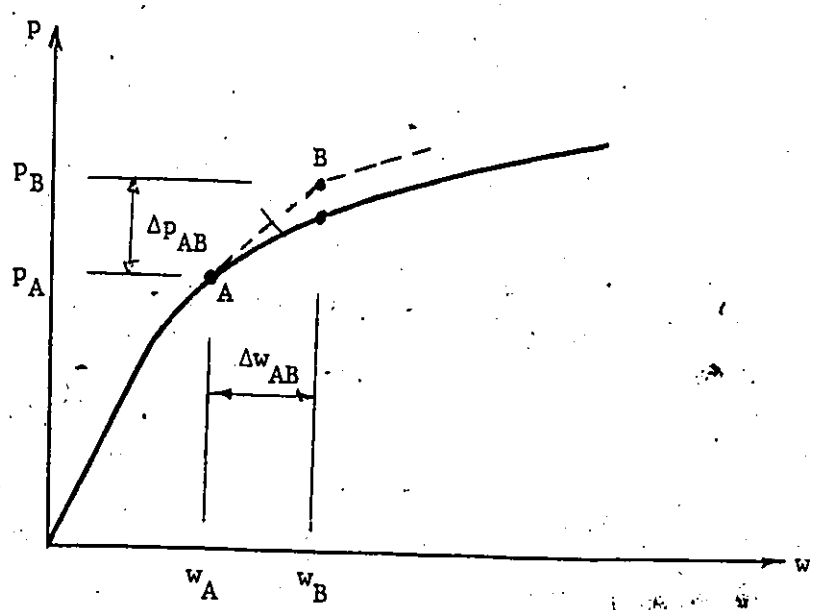

Figure 4.2 Load Versus Displacement Curve for Incremental Loads

Stresses, strains and tangent stiffness must now be updated. Displacement increment $\{\Delta w\}^e$ of an element is extracted from the global displacement increment $\{\Delta w\}_{AB}$. Then for each integration point within an element, one can proceed as follows.

Evaluate strains $\{\Delta\varepsilon\} = [B]\ \{\Delta w\}^e$ at any desired point within an element, where $\{\Delta\varepsilon\}$ in general contains both elastic and plastic parts. Next, by using equations 4.2.1 to 4.2.12, calculate the following quantities;

equation 4.2.9 $\quad \Delta\bar{\varepsilon}^P = [C]_A\ \{\Delta\varepsilon\}$

equation 4.2.6 $\quad \{\Delta\varepsilon^P\} = \{\frac{\partial\bar{\sigma}}{\partial\sigma}\}_A\ \Delta\bar{\varepsilon}^P$

equation 4.2.7 $\quad \{\Delta\sigma\} = [D](\{\Delta\varepsilon\} - \{\Delta\varepsilon^P\})$ $\qquad$ (4.3.2)

equation 4.2.8 $\quad \overline{\Delta\sigma} = H'_A\ \Delta\bar{\varepsilon}^P$

The updated quantities are $(\bar{\varepsilon}^P)_B = (\bar{\varepsilon}^P)_A + \Delta\bar{\varepsilon}^P$, $\{\varepsilon^P\}_B = \{\varepsilon^P\}_A + \{\Delta\varepsilon^P\}$. Next calculate H'_B corresponding to $\{\bar{\varepsilon}^P\}_B$ from figure 4.2.3. Evaluate appropriate $\{D_{ep}\}_B$ from equations 4.2.5 and 4.2.10. Using the appropriate $[D_{ep}]_B$ for each integration point, the elastic-plastic tangent stiffness matrix of an element can be evaluated following the procedure outlined in section 3.3.2

$$[K]^e = \int_{vol} [B]^T\ [D_{ep}]\ [B]\ dv$$

$$= \frac{a \cdot b \cdot t}{8} \int_{-1}^{+1}\int_{-1}^{+1}\int_{-1}^{+1} [B]^T\ [D_{ep}]\ [B]\ dv \qquad (4.3.3)$$

where a, b and t are the dimensions of an element and [B] is the strain matrix given by equation 3.3.9. Of course, the integration of equation 4.3.3 is carried out numerically. Thus, the updated tangent stiffness matrix has been calculated, and the next load increment ΔP is applied and the procedure repeated to determine the next displacement increment.

Some additional details deserve comment. Yielding begins when $\bar{\sigma}$ exceeds a value that will be called $\bar{\sigma}_o$ (figure 4.3). Some integration points will be elastic prior to application of the load increment and elastic-plastic afterwards. One way to account for this is as follows (29)

$$[D_{ep}] = m[D] + (1 - m)\,[D_{ep}] \qquad (4.3.4)$$

$$\text{where} \quad m = \frac{\bar{\sigma}_A}{\bar{\sigma}_o}$$

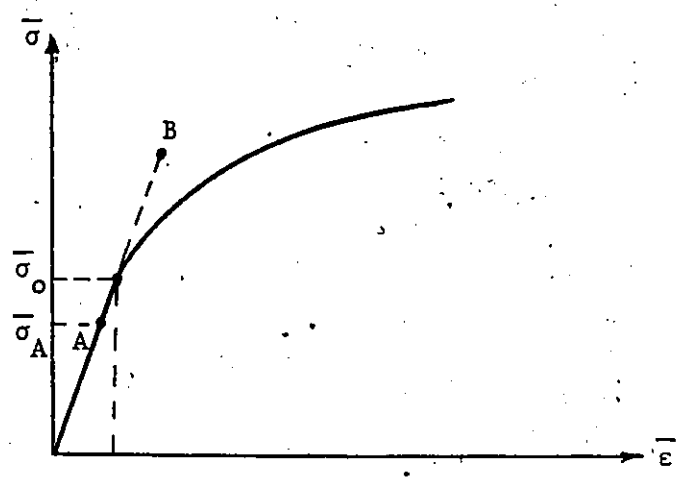

Figure 4.3 Elastic-Plastic Transition

If $\Delta\bar{\varepsilon}^p < 0$ at an integration point in a load step, elastic unloading is indicated. When this happens, $\Delta\bar{\varepsilon}^p$ is set equal to zero in equation 4.3.2, and in the next step stiffness is based on the elasticity matrix [D] instead of on $[D_{ep}]$. If isotropic hardening is assumed, plastic action is represented only if $\bar{\sigma}$ exceeds its previous maximum magnitude. If during loading $\Delta\bar{\varepsilon}^p < 0$ at many integration points, plastic collapse may be indicated (13, 27, 36), since at this stage the plastic region extends to such an extent that large plastic strains are possible without any increase in loading.

4.4 Computer Program

The computer program developed in section 3.4 to implement the elastic plate theory using finite element method is modified to account for the elastic-plastic behaviour of thin plates with different boundary conditions. The flow sequence for the computer program for solving an elastic-plastic problem using the present approach is summarized below.

1. Calculate elastic stresses, strains and displacements for a unit load.
2. Scale up all elastic values in order to cause yield at the point of maximum equivalent stress. Let P represent the load at this level.
3. Choose an increment of load (say 0.1 P), solve the equilibrium equations for the next displacement increment.
4. Calculate strain increment caused by 0.1 P.
5. Calculate $\Delta\bar{\varepsilon}^p$ for points exceeding yielding from previous loading.

6. Calculate stress increments and add to previous stresses.
7. Check that $\Delta\bar{\varepsilon}^p$ is positive or zero. If negative, stop computation. If not, proceed to step 8.
8. Calculate $[D_{ep}]$ for each integration point within each element after deciding whether a point is elastic, elastic-plastic or in the transition region.
9. Update element stiffness matrices, generate the overall stiffness matrix.
10. Return to 3 for the next increment of load.

4.3 Test Example

To verify the numerical technique presented, a simply supported plate is loaded well into the plastic range. Load deflection comparison with those presented in References (26, 31) is shown in figure 4.4. The plate is 254 mm x 254 mm and 10.2 mm thick, with $E = 69.95 \times 10^3$ MPa, , $E_T = 0.1E$ for $\bar{\sigma} > \bar{\sigma}_o$ and $\bar{\sigma}_o = 207.0$ MPa. As can be observed, there is very good agreement between the analytical solution given in Reference (31) which was based on the deformation theory, and the finite element method herein. An excellent agreement is also obtained, between the present finite element solution and the finite element solution given in Reference (26) using Hermite displacement functions, for the effective stress $\bar{\sigma}$ at the centre of the plate at a load of 1.724 MPa for the same plate problem

$$\bar{\sigma}_{centre} = 223 \text{ MPa} \quad \text{(Present Solution)}$$

$$= 216 \text{ MPa} \quad \text{(Reference (26))}$$

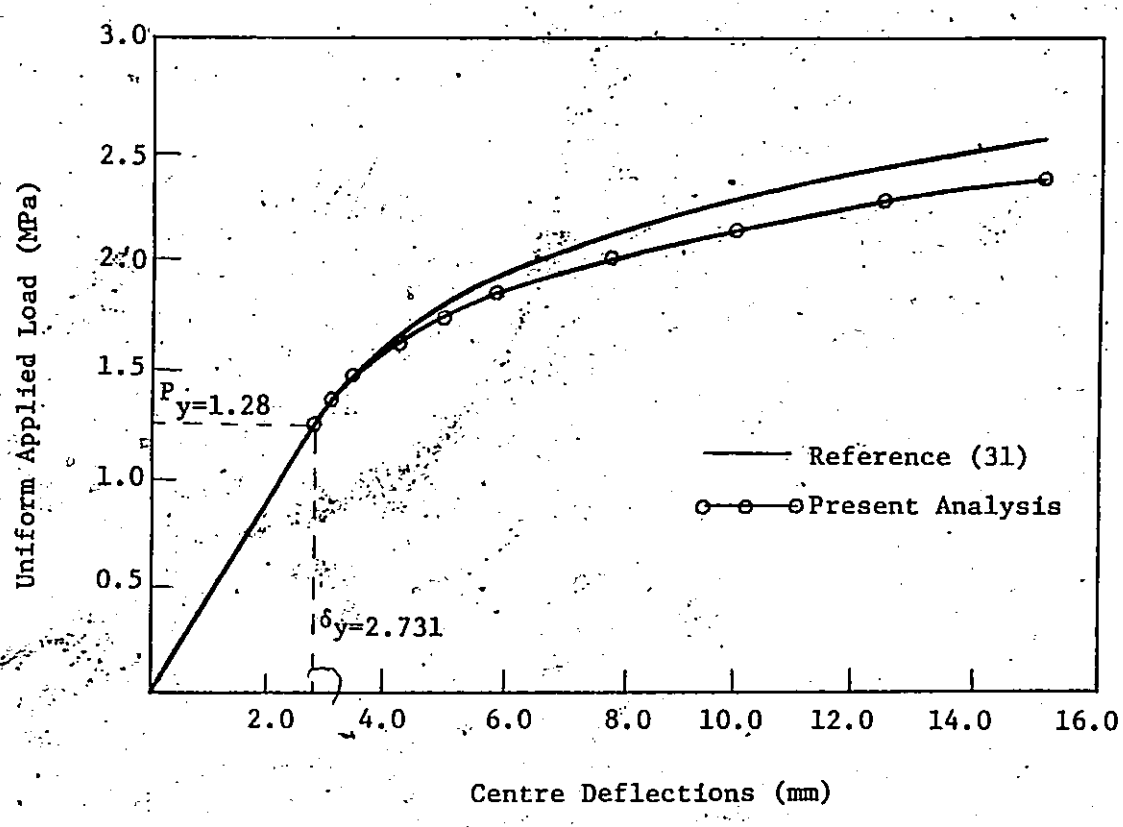

Figure 4.4 Simply Supported Plate Load-Deflection Comparison for Elastic-Plastic Analysis

CHAPTER 5

ELASTIC ANALYSIS OF RHS T-JOINT

5.1 Introduction

The T-joint finite element model developed and previously described in Chapters 2 and 3 has been applied to a typical connection illustrated in figure 2.1 with the computer program developed in section 3.4 for the elastic range of loading. The punching shear stiffness C and rotational rigidity J are calculated and compared with the FDM results obtained by Mansour (7), the FEM results obtained by Shehata (25) and some experimental results that are available in the literature. In addition, a study of the effect of the coefficients of the boundary springs and the rounded corners of the RHS chord on the behaviour of the T-joint is presented in this chapter. Another important aspect to be discussed is the effect of mesh size on the joint characteristics. Finally, the length of the plate that is sufficient for analyzing an RHS T-joint will be considered.

5.2 Applications

Figure 2.3 shows the top flange plate of an RHS T-joint treated as a thin plate with rigid body displacement δ and rotation ϕ under the inclusion. The joint is thus subjected to an axial load P and applied moment M through the branch member. The punching shear

and rotational stiffnesses are

$$C = \frac{P}{\delta} \quad , \qquad J = \frac{M}{\phi} \tag{2.3.1}$$

a) Simply Supported Edge Case

A joint comprised of a 154.4 x 154.4 x 6.4 mm chord member with 101.6 x 101.6 mm inclusion was studied assuming all four edges are to be simply supported. Only one quarter of the plate was analyzed due to summetry. Two mesh sizes were considered (3 x 9 and 9 x 18 element meshes). The finite element grid for the first mesh together with the imposed kinematic boundary condition is shown in figure 5.1. The plate thickness within the branch inclusion was taken as one thousand times the RHS thickness to represent a relatively much larger stiffness for rigid plate action. Line loading as described earlier (equations 3.3.39 and 3.3.40) was employed in the analysis to simulate bending or axial forces imposed by the branch member. The punching shear C and rotational stiffness J are calculated for the given joint and tabulated in Table 5.2.1 and compared with the results by Mansour (9). As can be observed, increasing the number of elements is accompanied by a significant increase of both the C and J values. Thus, a finer mesh gives a stiffer model commensurate with the actual behaviour. In comparison with Mansour's simply supported finite difference results, his C value lies between the values obtained for the coarse and fine meshes of the FEM. For the two-mesh configurations indicated, his J value is higher than both values obtained by the FEM. Nonetheless, the results for the finer mesh do appear to be reasonable.

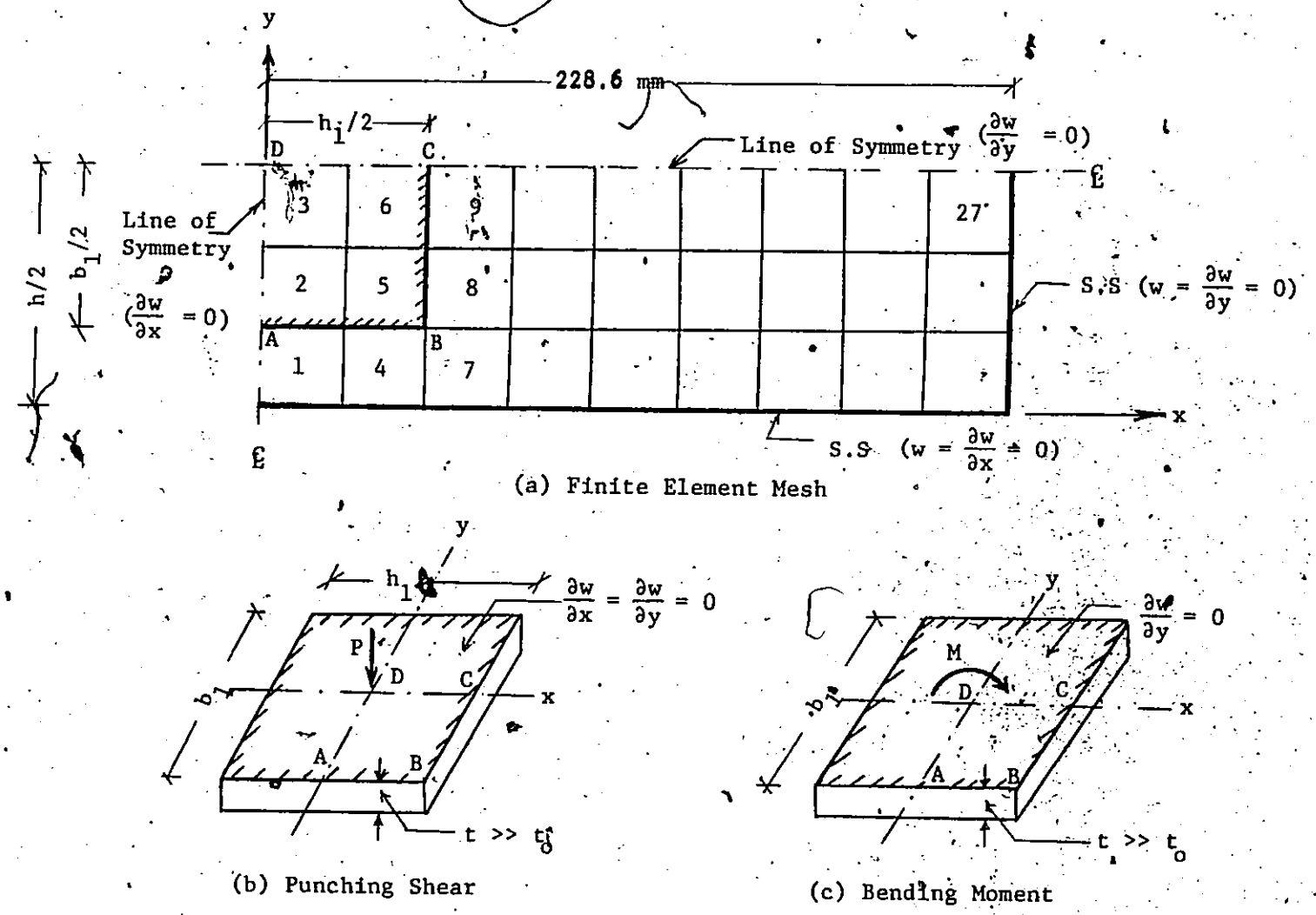

Figure 5.1 Finite Element Grid for 154.4 x 154.4 x 6.4 mm Chord and 101.6 x 101.6 mm Inclusion with S.S Edges

The following are the reasons for this discrepancy.

1) We do not expect rotation to improve at the same rate as the displacements do with a finer mesh.

2) The nonconforming plate bending element seems to yield a more flexible model than the finite difference method does for rotational resistance.

Mesh mxn	C Value KN/mm	J Value KN-m/rad
3 x 9	90	257
9 x 18	138	294
F.D.M. (Mansour)	115	365

Table 5.2.1 Computed C and J Values for Different Mesh Sizes (Simply Supported Case)

b) Longitudinal Edges Elastically Supported

The finite element model was applied to 254 x 254 x 9.5 mm chord with 154.4 x 154.4 mm branch member, taking into account springs or elastic supports along the longitudinal edges. Figure 5.2 shows the dimensions, boundary conditions and finite element grid. Results obtained for the punching shear stiffness C and rotational stiffness J are compared with those obtained by Redwood (6). Both stiffnesses are compared with results of Shehata (25) in Table 5.2.2 for the same mesh size. Shehata in his analysis took into account

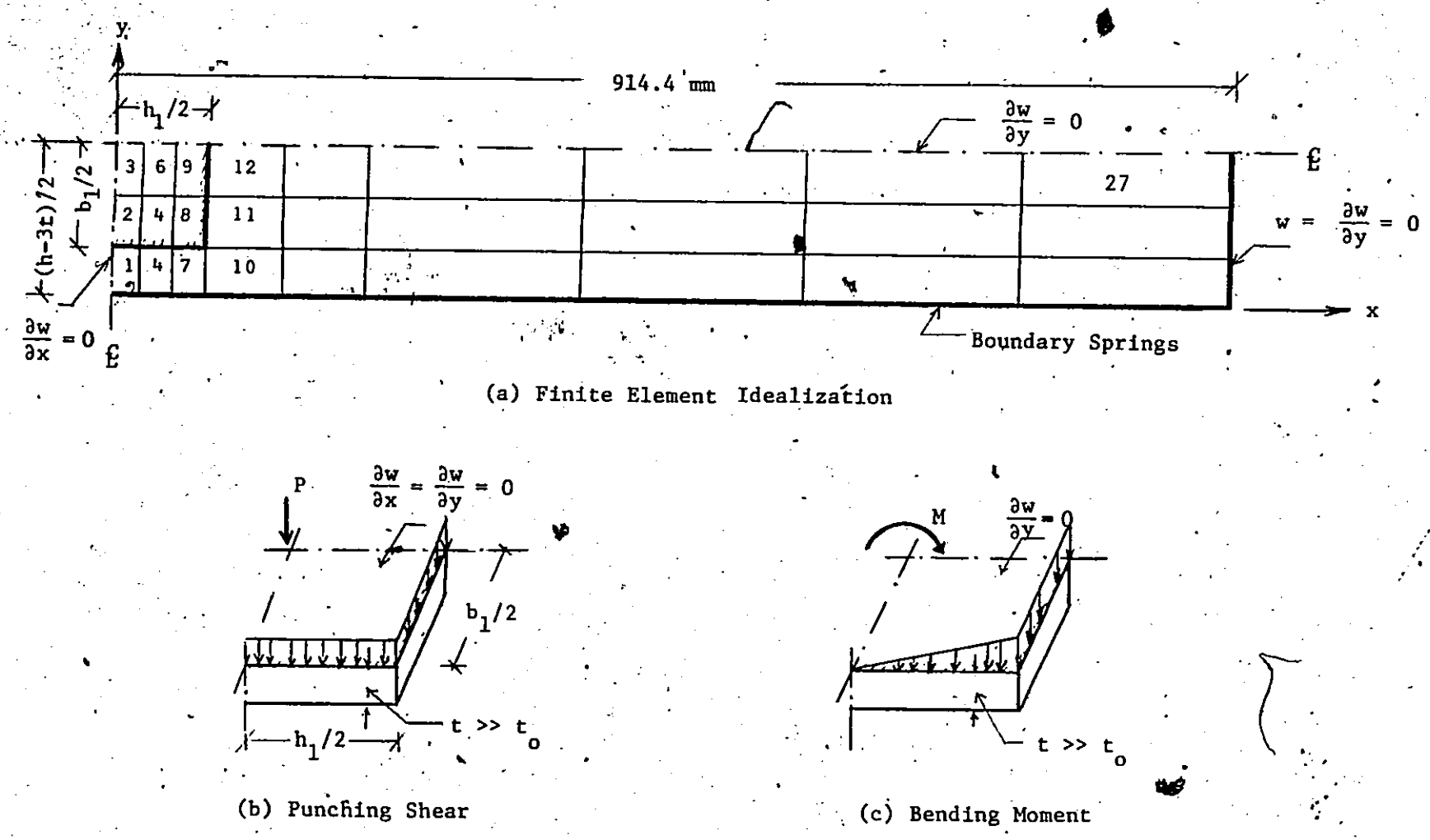

Figure 5.2 Finite Element Grid and Loads Under the Inclusion for 254 x 254 x 9.5 mm Chord with 154.4 x 154.4 mm Inclusion

the in plane action while the present work ignores this inplane action. In addition, he considered the corners of the RHS to be sharp while in this work the rounded corners were taken into account (see figure 2.3). The results obtained for C and J values in this study compare well with those in References (6) and (25).

The C and J values are also computed for the same joint with longitudinal edges simply supported in one case, and clamped for the other. The results shown in Table 5.2.2 indicate a larger increase in the punching shear stiffness C than the rotational stiffness J due to stiffer edge conditions, i.e. for clamped longitudinal edges, the boundary spring stiffness coefficients approach infinity.

Chord RHS 254 x 254 x 9.5 mm Branch 154.4 x 154.4 mm	C the KN/mm	C+the KN/mm	C**ex KN/mm	J the KN-m/rad	J+the KN-m/rad	J**exp KN-m/rad
Proper Joint	233	245	243	1333	1469	1390
S.S Longitudinal Edges	445	426	---	2079	2068	----
Clamped Longitudinal Edges	1630	1551	---	5898	5729	----

+ Shehata's results. ** Redwood's results.

Table 5.2.2 Axial and Rotational Stiffnesses for Top Plate with Edge Springs, Simply Supported Edges and Clamped Edges

5.3 Effect of the Stiffness of the Elastic Support

The importance of studying the effect of the stiffness of the elastic support is clear. Firstly, it indicates the degree of sensitivity of results with varying support moduli, and secondly

it shows a direct relationship between the rigidity of the connection and the stiffness of the support. Hence, two extreme limits for rigidity can be considered, i.e., when the two longitudinal edges are fixed or free. Of course, the actual joint lies between these two extremes. Figure 5.3 shows the effect of both vertical spring constant k_v, the rotational spring constant k_r, and the influence of the coupled spring constant k_{vr}, on the punching shear and rotational stiffnesses C and J of the joint in figure 5.2. The spring constant matrix for this joint is given by equation 2.2.4. As can be observed, the vertical spring constant k_v is the major constant that affects both J and C. Tending k_v to zero, yields a very weak joint of almost no stiffness, while forcing k_r, k_{vr} to be zero gives values of J and C about 0.8 the values for the simply supported case. The joint without spring coupling ($k_{vr} = 0$) has values of J and C higher than the S.S case. Including coupling of springs (actual joint) decreases the J and C values to about 0.6 of the values with no coupling. Therefore, coupled spring constants produce a more flexible joint.

5.4 Rounded Corner Effect

The assumption of assuming sharp corners for the chord member tends to increase the stiffnesses of the springs somewhat (figure 2.3) and accordingly, increases the rotational and punching shear stiffness of the joint. It is apparent from figure 5.4 that the C and J values for the sharp corner case are about 1.2 those of rounded corners. However, the actual joint has rounded corners and it should not be approx-

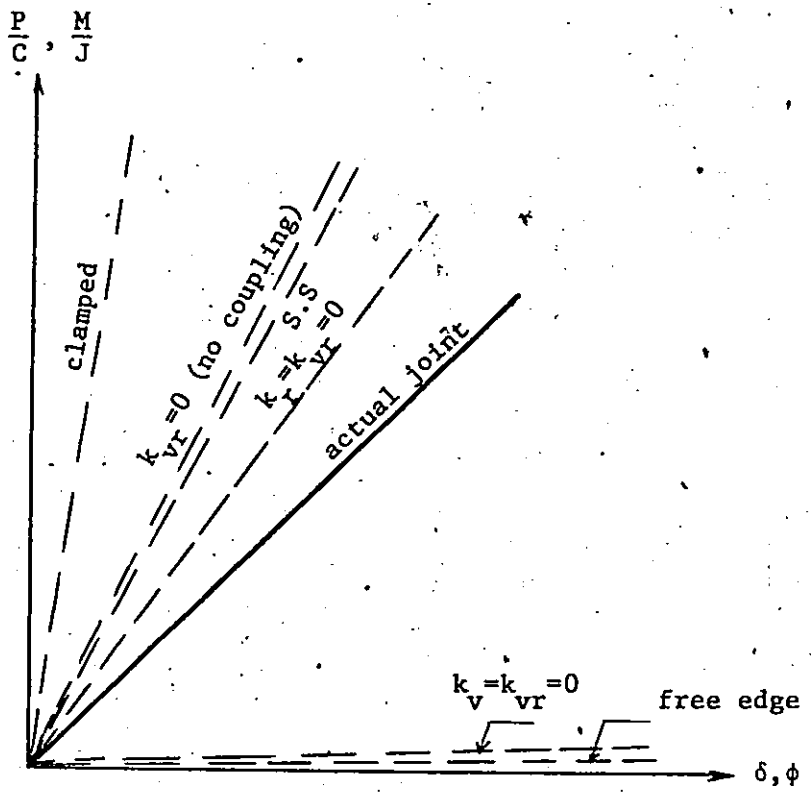

Figure 5.3 Effect of different edge conditions on the J and C values (154.4 x 154.4 mm branch to 254 x 254 x 9.5 mm chord)

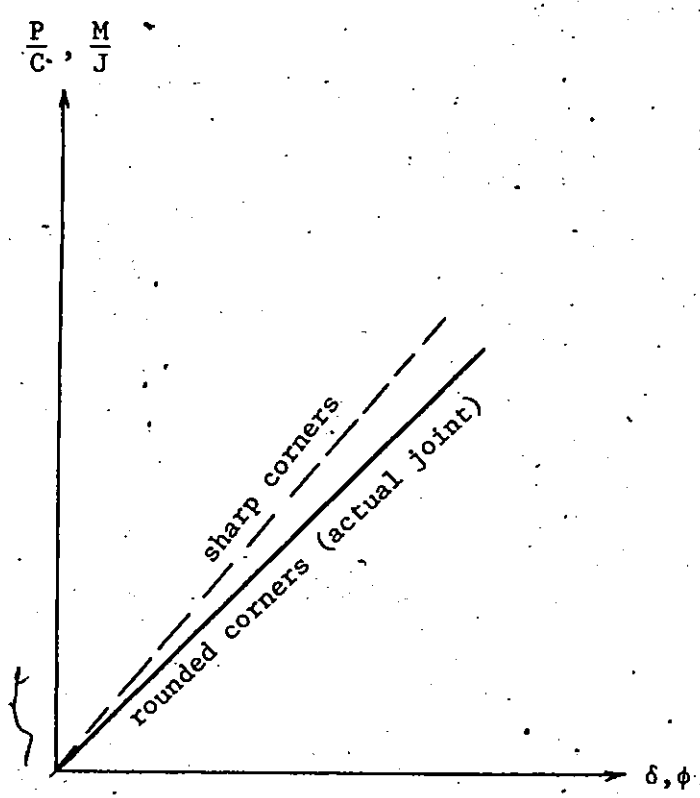

Figure 5.4 Effect of corner condition on the C and J values (154.4 x 154.4 mm branch to 254 x 254 x 9.5 mm chord)

imated by sharp corners.

5.5 Mesh Size Effect

Increasing the number of elements, especially between the edge of inclusion and the longitudinal edge of the plate, will improve the results significantly. Table 5.5.1 gives the values of C and J for two finite element meshes for the joint in figure 5.2. The finer mesh with 80 elements is shown in figure 5.5. It is to be noted that using a finer mesh yields a stiffer joint. A characteristic of the nonconforming rectangular plate bending elements is that an increased number for a given domain will result in a better representation of the behaviour of the actual structure. Also, it is to be observed that the finer mesh gives results that are in a very good agreement with Redwood's (6) experimental results.

Mesh Size	Number of Nodes	C KN/mm	J KN-m/rad
3 x 9	40	233	1333
4 x 20	105	247	1390
experimental results (Redwood)	---	243	1390

Table 5.5.1 Axial and Rotational Stiffness for Different Meshes (254 x 254 x 9.5 mm Chord with 154.4 x 154.4 mm Branch)

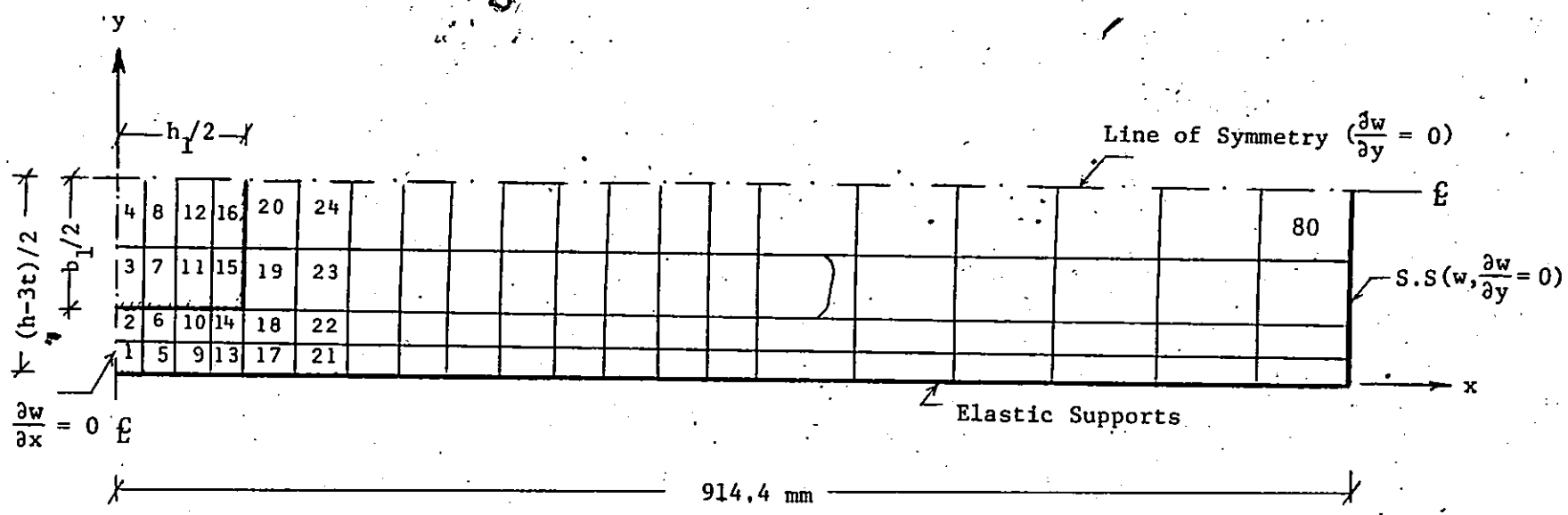

Figure 5.5 80-Element Mesh for 254 x 254 x 9.5 mm Chord with 154.4 x 154.4 mm Branch Member

5.6 Length of the Plate

From the viewpoint of a theoretical study, the length of the plate must be infinite. On the other hand, the plate should be one truss panel in length. From a numerical solution point of view, a more restricted plate length is necessary. However, it has been observed from the computer outputs obtained for the joint indicated in figure 5.5, that the deflections and the stresses at a distance of 381 mm from the inclusion, (i.e. length of the plate ≈ 4 times its width), tend to be negligible. Consequently, end effects could be ignored if the plate length is greater than four times its witdh. This justifies the assumed simple supports used at the far ends.

5.7 Conclusion

The linear elastic model of the RHS T-joint developed in Chapter 2 has been successfully applied to the single chord connection under branch member axial load and bending moment. The finite element formulation utilizing rectangular nonconforming plate elements and edges with springs (derived in Chapter 3) is, as expected, very versatile. The computer program that has been developed predicts punching shear and rotational stiffnesses of RHS T-joint that appear to be reasonable based on a comparison with some experimental and theoretical results. It is the purpose of the next chapter to extend the elastic model to include the elastic-plastic analysis of the RHS T-joint.

CHAPTER 6

ELASTIC PLASTIC ANALYSIS OF T-JOINTS

6.1 Introduction

In this chapter, the theoretical model developed in chapter 2 for the RHS T-joint with the top chord flange treated as a thin plate resting on coupled springs along its longitudinal edges and simply supported on the other two edges, is applied to a single chord connection beyond elastic limit. The connection is subjected to web axial force or bending moment.

The finite element elastic-plastic computer program developed in Chapter 4 has been used to study the effect of tangent modulus E_T, width ratio λ, haunch size λ_1, and the chord thickness t on the joint behaviour. The results are thus presented in the form of M-ϕ or P-δ diagrams in non-dimensional form.

A method for evaluating the ultimate load and moment carrying capacity of the RHS T-joint is also given, and compared with those obtained by Mouty (10) which is based on the upper bound yield line theorem.

6.2 Details of the Joints

The chord member size used throughout this work is 254 x 254 x 9.5 mm, with an assumed outside corner radius, = 1.5 t = 14.3 mm. The top flange plate dimensions become 7.2 h = 1828.8 mm long and h-t-2r = 225.4 mm wide. Only one quarter of the plate needs to be analyzed due to symmetry. The mesh used, with 80 elements, is shown in figure 5.5. Computer runs were made in which the relative sizes of elements around the inclusion were maintained the same for different values of λ, λ_1 and t.

The effective stress-effective strain curve for the steel was assumed to be elastic-linearly strain hardening with $E_T = 0.025$ E and yield stress $\bar{\sigma}_o = 344.75$ MPa.

The criterion for calculating the ultimate loads and moments is based on a maximum deflection δ of the top flange plate not to exceed twenty-five times the yield deflection δ_y (i.e. $\delta/\delta_y \nless 25$), otherwise, plastic collapse, described in section 4.3, indicated before deflection reaches that value.

6.3 T-Joint Analysis

In the analysis of the T-joint it is assumed that the top flange plate within the inclusion undergoes only rigid body type translation δ or rotation ϕ. The load transfer from the branch to the chord member is assumed to occur along the branch member edges as a line load. Figure 2.5 shows typical axial and moment transfer systems and rigid body type displacements of the part of the plate within the inclusion.

6.4 The Upper Bound Theorem and Ultimate Moment and Load

Mouty (10) used yield line plasticity theory to obtain an upper bound estimate for the ultimate moment and load that can be carried by an RHS T-joint. This theorem is deducible from the work principles for elastic-perfectly plastic materials, and is based on minimization of the virtual work expression for an assumed mechanism of failure.

The following two formulae for the RHS T-joint ultimate moment and axial load, are given by Mouty (10)

$$M^*_{ult} = t^2 \bar{\sigma}_o \frac{h_1}{2}\left[\frac{\frac{2h_1}{h-t}}{\frac{1-b_1}{h-t}} + \frac{h-t}{h_1} + 4\sqrt{\frac{1}{1-\frac{b_1}{h-t}}}\right] \qquad (6.4.1)$$

$$P^*_{ult} = t^2 \bar{\sigma}_o \left[\frac{\frac{2h_1}{h-t}}{\frac{1-b_1}{h-t}} + 4\sqrt{\frac{1}{1-\frac{b_1}{h-t}}}\right] \qquad (6.4.2)$$

where $\bar{\sigma}_o$ is the yield stress of steel used. Figure 6.1 shows the dimensions and the two mechanisms of failure used in Mouty's equations 6.4.1 and 6.4.2.

6.5 T-Joint Under Applied Moment

(a) Effect of Tangent Modulus E_T

A series of different values of E_T was used to study the effect of the characteristic stress-strain curve of steel on joint behaviour and strength under applied moment. The results are shown in figure 6.2 for the 154 x 154 mm to 254 x 254 x 9.5 mm joint described in Section

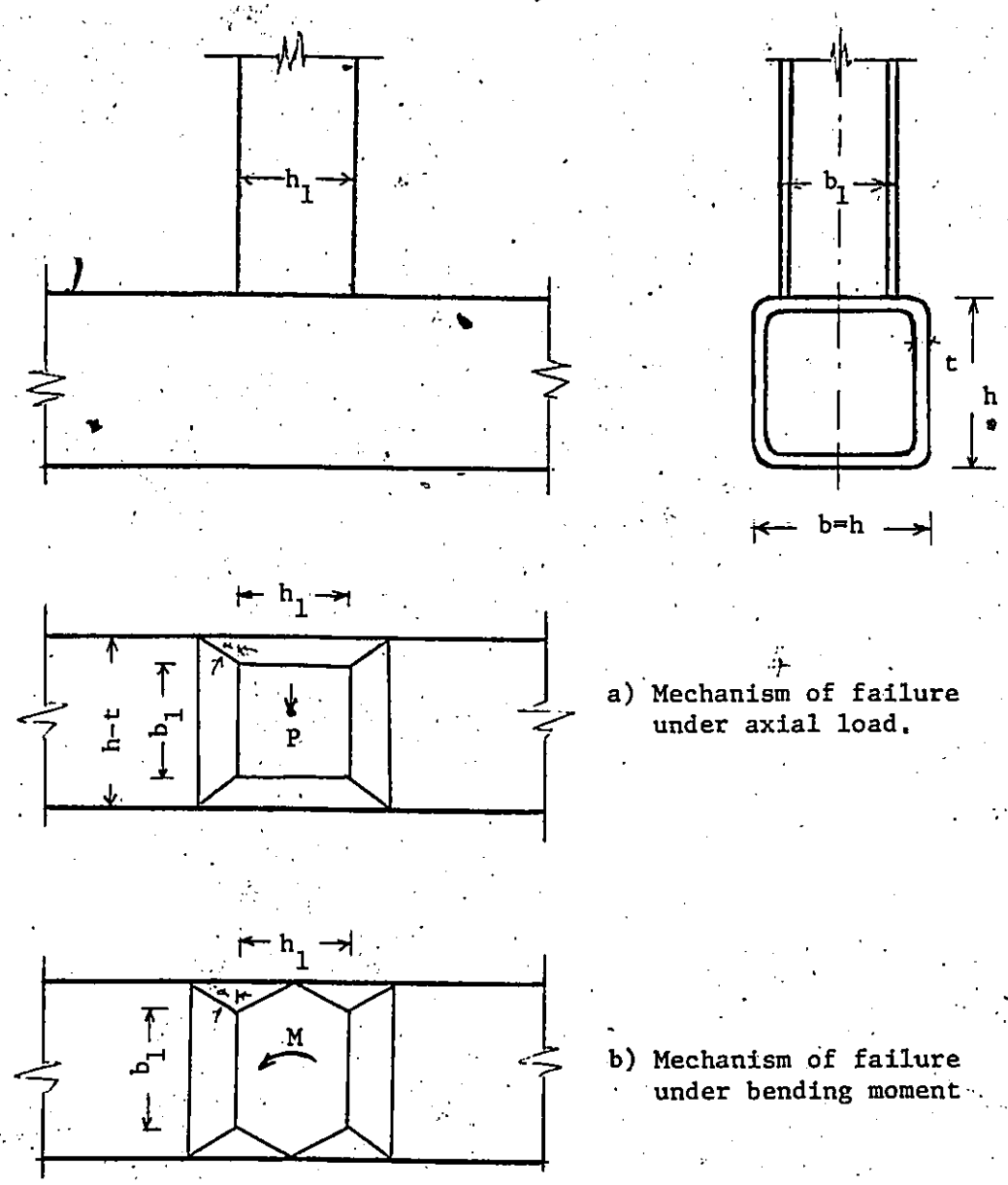

a) Mechanism of failure under axial load.

b) Mechanism of failure under bending moment

Figure 6.1 Details of the T-joint Dimensions and Mechanisms of Failure used in Mouty's Formulae .

6.2. Four values of E_T/E were investigated = 0, 0.01, 0.025 and 0.1. One can observe from the figure that the slope of the curve of E_T = 0.1E, in the inelastic range, is considerably steeper than the other cases of E_T. As expected, the slope of the curve reduces with smaller values of E_T. For the case of E_T = 0.0, the curve becomes quite flat which is characteristic of elastic-perfectly plastic material. The curve was terminated at $\phi/\phi_y \simeq 15$ ($M/M_y \simeq 4.5$), with the computer message that $\overline{\Delta\varepsilon}^p$ is negative, thus indicating plastic collapse. This condition did not arise with other cases. For E_T = 0.01 E, the curve becomes fairly flat before ϕ/ϕ_y reaches the predicted failure criterion of $\phi/\phi_y \leq 25$. When E_T increases to 0.025 E the curve crosses Mouty's ultimate moment line at $\phi/\phi_y \simeq 25$. Thus, for lower degrees of strain hardening, the joint tends to behave in a manner similar to that of perfect plastic material with ultimate moments between that obtained by yield line theory (10) and the elastic-plastic case. On the other hand, a higher value of tangent modulus will produce a $M_{ult} > M_{ult}^*$ by Mouty. Thus, when E_T = 0.1 E the finite element solution gives a value of M_{ult} equal to 1.37 that of Mouty. However, increasing the number of elements, as indicated in Section 5.5, would give rise to a slightly stiffer joint, which is expected for a strain hardening material.

(b) <u>Width Ratio λ</u>

The effect of λ on the joint behaviour under applied moment was examined for E_T = 0.025 E and is shown in figure 6.3 for different values of $\lambda = b_1/b$. The properties of the T-joint used earlier

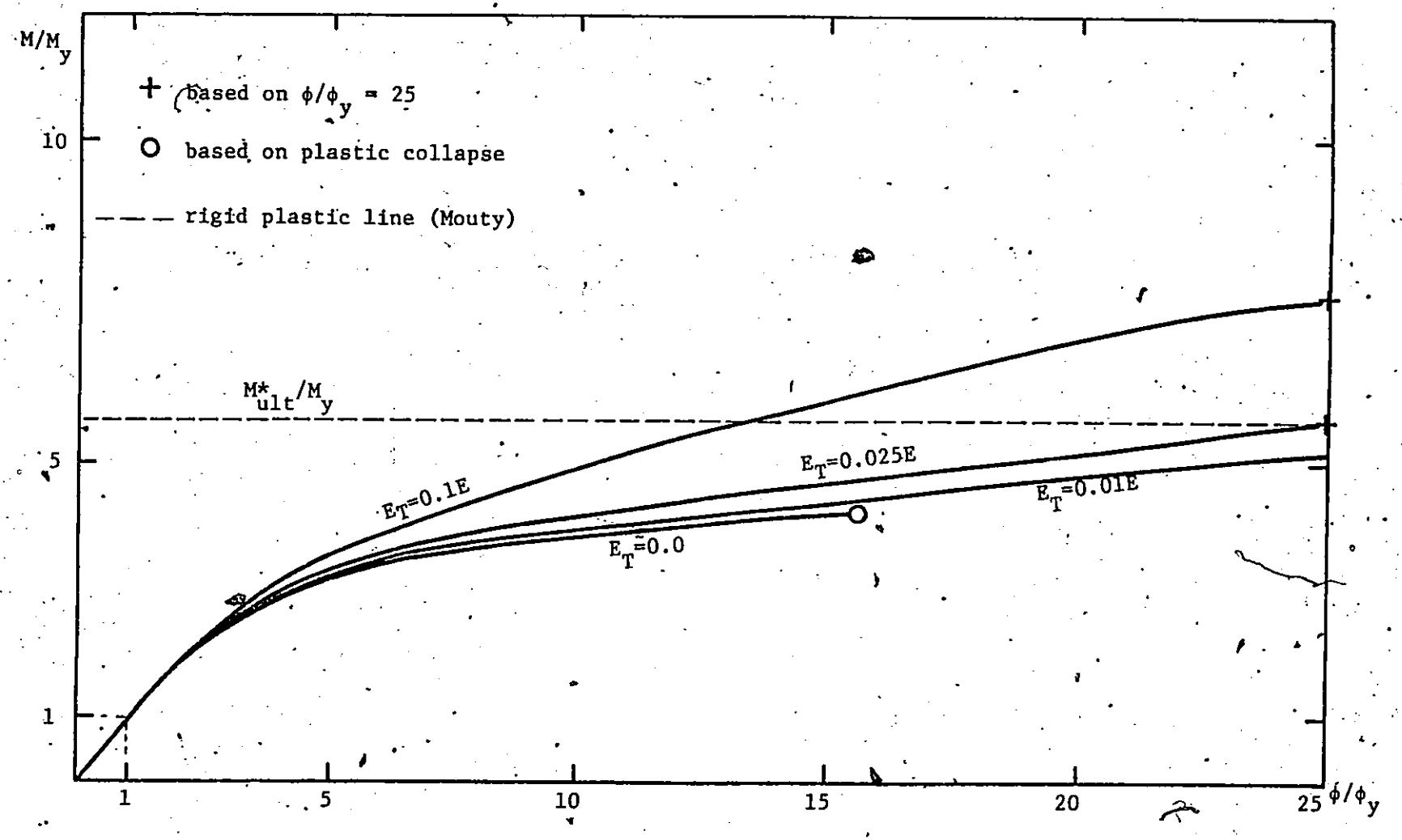

Figure 6.2 M-φ Curve for Different Values of Tangent Modulus E_T. (254 x 254 x 9.5 mm Chord to 154.4 x 154.4 mm Branch)

in this work, the 154.4 x 154.4 mm branch mated to 254 x 254 x 9.5 mm chord, will be denoted by subscript o and will serve as a baseline for comparisons with other connections. The yield moment M_{y_o} for $\lambda_o = 0.6$ is about 1.2 M_y for λ equal to 0.4. A similar increase in M_y occurs when the case $\lambda = 0.8$ is compared with that of λ_o ($\sim$ 1.5 times). However, the J value is more sensitive. For example, when $\lambda = 0.8$, J is almost four times that for which = 0.4. Thus, λ values have a considerable effect on joint behaviour in the elastic range.

In the inelastic range of loading, the joints loose stiffness but at different rates. The $\lambda = 0.4$ joint is observed to be very weak compared with the other two cases. In fact, for prescribed ϕ, the actual resisting moment with $\lambda = 0.8$ tends to be about 2 times that for $\lambda = 0.4$. Concerning the predicted values of ultimate moments that can be resisted by the joints, the joint with λ_o as indicated in section 6.5a has virtually the same value of M_{ult} at $\phi/\phi_y = 25$ as that given by the upper bound theorem. For $\lambda = 0.4$ the curve becomes quite flat when the deformation reaches the limit of $\phi/\phi_y = 25$, i.e. giving the same ultimate moment obtained from limit analysis. When λ increases to 0.8 the ultimate moment at the assumed criterion is almost 0.8 the value given by Mouty (10). However, the curve intersects the limit curve by Mouty at $\phi/\phi_y \simeq 40$.

For design purposes, a safety factor of about 1.65 should be used. Thus, an allowable branch moment that is limited by chord bending will be obtained by multiplying its ultimate moment by 1/1.65. A comparison between the yield moments and both the ultimate and working

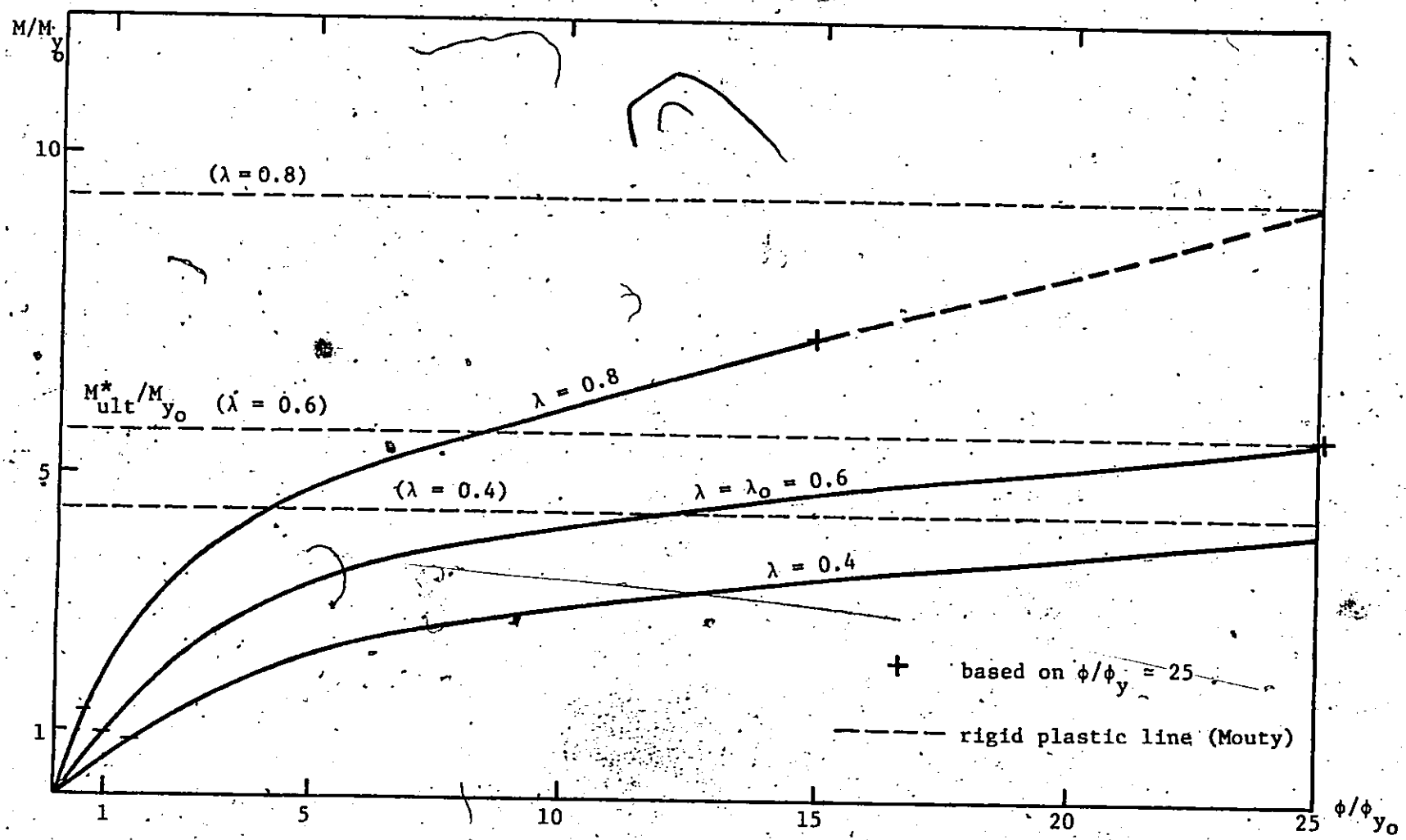

Figure 6.3 M-ϕ Curve for Various λ Values (254 x 254 x 9.5 mm Chord and E_T = 0.025E)

moments is given in Table 6.5.1 for different values of λ. The results in the table indicate that the ultimate moment is higher than 5.5 times the yield moment and hence an allowable working moment will be about 3.35 times the yield moment. This indicates the necessity of undertaking an elasto-plastic type of analysis to arrive at allowable moments. The yield moment will be far too conservative to be used in design.

λ	M_{ult} KN·m	M_{ult}/M_y	$M_{working}/M_{yield}$	J KN·m/rad
0.8	33.90	5.59	3.35	3020
0.6	27.12	5.64	3.41	1390
0.4	21.47	5.46	3.28	790

Table 6.5.1 Moment Values and Comparisons, and Rotational Stiffnesses for Different λ (254 x 254 x 9.5 mm Chord and E_T = 0.025 E).

Table 6.5.1 gives also the J values for different λ values.

(c) Chord Thickness Effect

Experiments (5) have shown that the chord thickness t, has a great effect on the joint behavibur, especially for the unreinforced joint with λ < 1.

In the present study when t increases the spring constants increase accordingly since they are functions of the dimensions of the chord. The width of the chord top plate is reduced from the nominal chord width b = h to h-3t. Figure 6.4 shows the M-φ curves with

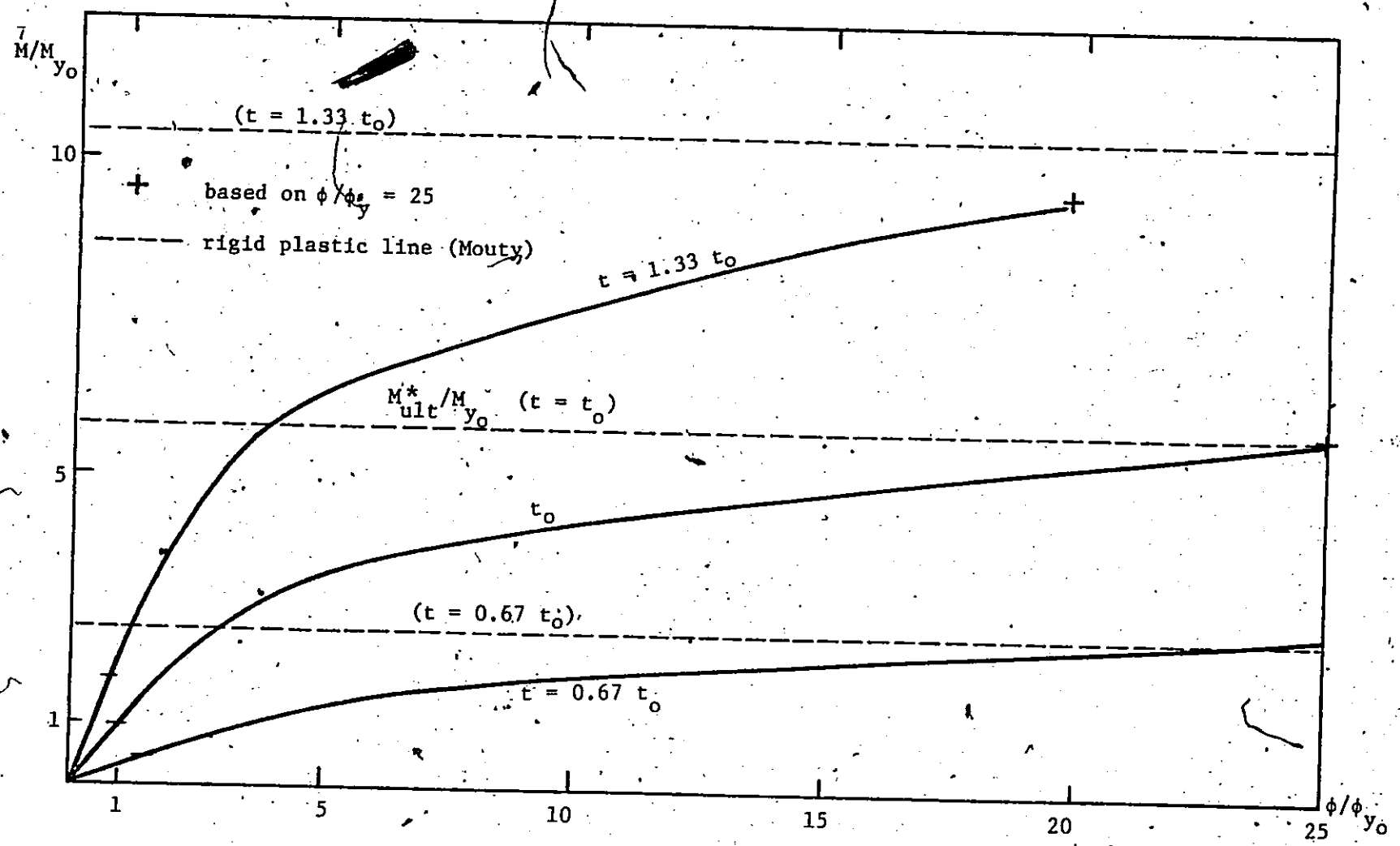

Figure 6.4 M-ϕ Curve for Different Chord Thicknesses (254 x 254 mm Chord to 154.4 x 154.4 mm Branch and E_T = 0.025 E)

respect to the case of $t = t_o = 9.5$ mm for the nominal 254 x 254 mm chord with 154.4 x 154.4 mm inclusion. The profound effect of chord thickness t on joint behaviour whether in the elastic range of loading (to affect J) or in the inelastic domain, is to be noted. The J value for $t = 0.67\ t_o$ decreases to $0.33\ J_o$. For the joint with $t = 1.33\ t_o$, the J value increases to twice J_o. The ultimate moments obtained from this analysis for $t = 0.67\ t_o$ is almost 1.1 times the limit analysis values. However, the behaviour of this joint is very flexible and the curve becomes very flat and crosses Mouty's rigid plastic line at $\phi/\phi_y \approx 15$. When t increases to $1.33\ t_o$, the predicted ultimate moment is about 0.92 the limit analysis moment by Mouty. The curve for this case gives the same value as Mouty at $\phi/\phi_y \approx 30$.

The predicted ultimate moments together with the ratios of the ultimate and working moments to the yield moments are given in Table 6.5.2 for different chord thicknesses. Again, the ultimate moment is higher than 5.5 times the yield moment and an estimate of the working moment is about 3.4 times the yield moment of the joint concerned. Table 6.5.2 gives also the J value for these joints.

t mm	M_{ult} KN-m	M_{ult}/M_{yield}	$M_{working}/M_{yield}$	J KN-m/rad
12.7	45.20	5.52	3.3	3057
9.5	27.12	5.64	3.4	1390
6.4	13.22	5.82	3.5	432

Table 6.5.2 Moment Values and Comparisons, and Rotational Stiffnesses for Different Chord Thicknesses (254 x 254 mm Chord with 154 x 154 mm Branch and $E_T = 0.025\ E$)

6.6 T-Joint Under Punching Shear

A similar parametric study was undertaken for the T-joint in punching shear when subjected to an axial force from the branch member. For eccentric loads, i.e. both moment and axial force exist (as in real joint problems), a combined analysis using the results obtained in this section and the previous one can be used in the elastic range of loading only. However, the finite element computer program developed for the elastic-plastic analysis of RHS T-joints is capable of accommodating any loading, whether eccentrically applied or not. The same joints used in Section 6.5 are analyzed here.

(a) Effect of Tangent Modulus E_T

The same values of the strain hardening constant E_T that were used to predict M-ϕ relationships were also employed to assess joint behaviour under axial load. Figure 6.5 shows P-δ curves for different E_T values, in a nondimensional form. One can observe that the curve for E_T = 0.1 E is again steeper than the curves for other values of E_T. The joint becomes more flexible for reduced E_T. For all values of E_T, the computer terminated the program after the plastic region extended sufficiently that elastic unloading occurred. This phenomenon is analogous to the unloading of plastic hinges in multistory frames that are loaded near ultimate loading. This plastic limit occurred when the displacement was about 4.7 mm or about one-half of the chord thickness, and with $\delta/\delta_y \doteq 14$. In this case, the load levels for the different values of E_T, highest obtainable by the

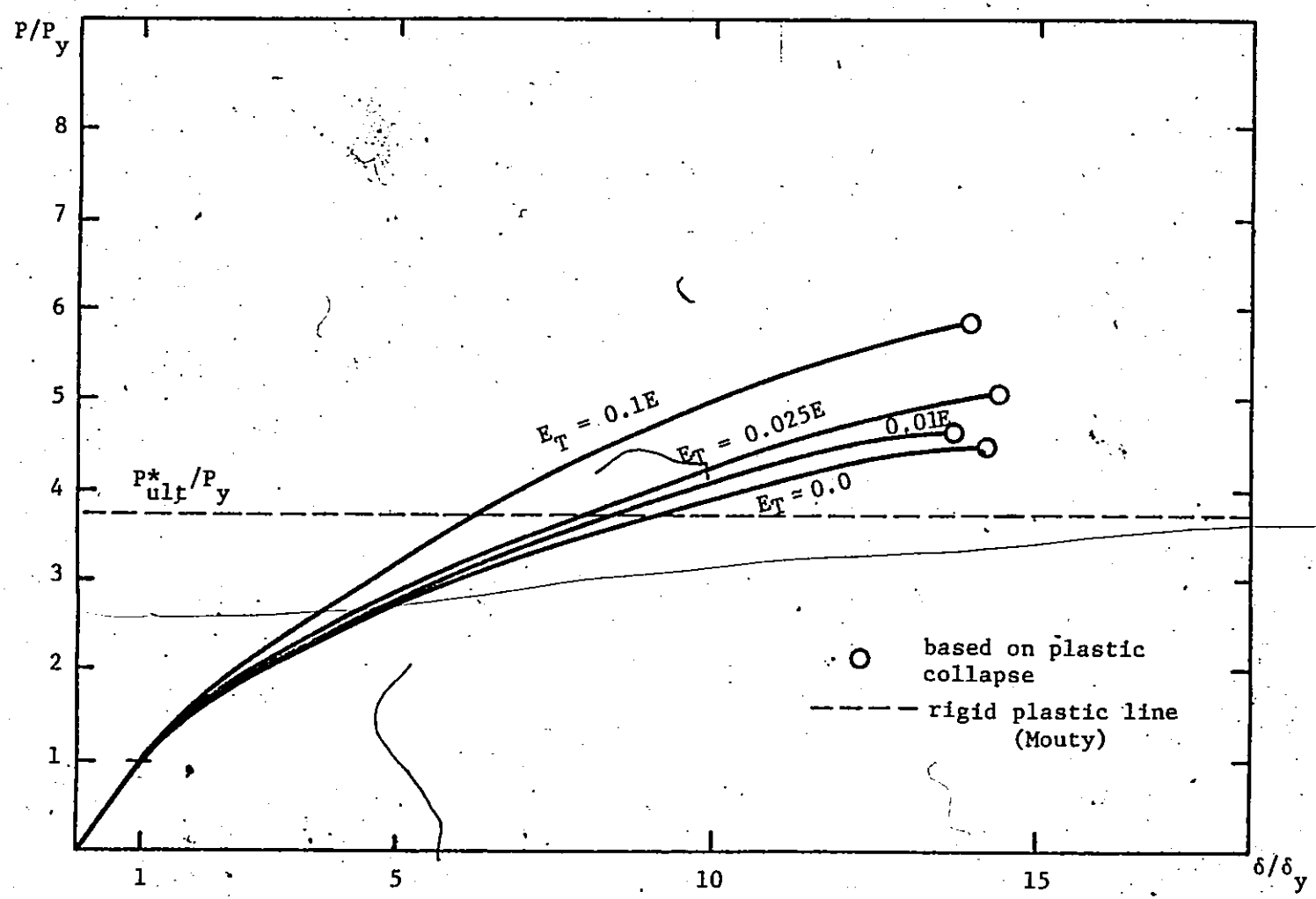

Figure 6.5 P-δ Curve for Different Tangent Modulus E_T (254 x 254 x 9.5 mm Chord to 154.4 x 154.4 mm Branch)

program, are higher than the values given by Mouty (indicated in figure 6.5). Furthermore, his predictions of ultimate loads for the T-joints are generally lower than experimental values. He suggested that a displacement-to-width ratio of $\delta/b \approx 1\%$ may be regarded as a failure point. Table 6.6.1 gives a comparison between the ultimate loads for different E_T according to the program's limit (P_{ult}) and those at $\delta/b = 1\%$ (P'_{ult}), and the ratio between these two values of ultimate loads and the value calculated using Mouty's formula given by equation 6.4.2 (P^*_{ult}).

E_T	P_{ult} KN	P'_{ult} KN	P_{ult}/P^*_{ult}	P'_{ult}/P^*_{ult}
0.1 E	469.26	435.90	1.53	1.29
0.25 E	415.18	304.69	1.35	0.99
0.01 E	381.86	293.57	1.24	0.95
≈0.0	365.85	282.45	1.19	0.92

Table 6.6.1 Comparison Between Different Predictions of Ultimate Loads (254 x 254 x 9.5 mm Chord with 154.4 x 154.4 mm Branch)

As can be seen from the table, the ultimate loads calculated at plastic collapse vary from 1.53 to 1.24 times the values obtained from the yield line theory, when E_T varies from 0.1 E to 0.01 E. For $E_T = 0.0$, (i.e. perfect plastic material) the finite element result is about 1.19 the limit result for the same material. Comparing the two limits predicted by Mouty (10), the results of P_{ult} at $\delta/b \approx 1\%$ (P'_{ult}) vary from 1.29 to 0.92 times the values calculated from limit analysis for different E_T values.

(b) Width Ratio λ

The finite element program developed has been used again to establish the effect of the width ratio λ on joint behaviour in punching shear. The results are plotted in figure 6.6 for the same chord 254 x 254 x 9.5 mm indicated in Section 6.2 and with different λ values. The Plots are in the form of P-δ curves in a nondimensional form with respect to $\lambda = \lambda_o = 0.6$. The slope of the curves in the elastic region which represents joint punching shear stiffness C, increase considerably with an increase in λ. The elastic C value for $\lambda = 0.4$ is about one eighth its value at $\lambda = 0.8$, which indicates that the joint with $\lambda = 0.4$, again, is a very weak one. In the inelastic range of loading, the effect of width ratio λ on joint stiffness cannot be neglected. As shown in figure 6.6 the slope of the curve is much steeper for $\lambda = 0.8$ than for the other two cases. Thus, the joint becomes more flexible when λ is progressively reduced from 0.8 to 0.6, then to 0.4. With respect to ultimate load prediction, the curve for $\lambda = 0.4$ becomes quite flat at $\delta/\delta_y \simeq 12$ and a displacement of about 0.6 the chord thickness which gives a ratio of P_{ult}/P_y of 1.1 times the value obtained by limit analysis. When λ increases to 0.6, the plastic collapse indicated at $\delta/\delta_y \simeq 14$ and a displacement of the order of half the chord thickness t is obtained with a value of P_{ult} about 35% higher than Mouty's results. For $\lambda = 0.8$ the ultimate load calculated at $\delta/\delta_y \simeq 25$ is about 1.25 the value of the yield line theory, and corresponds to a displacement of approximately 0.5 the chord thickness t. This may be an indication of considering the ultimate load to be the load that causes a maximum

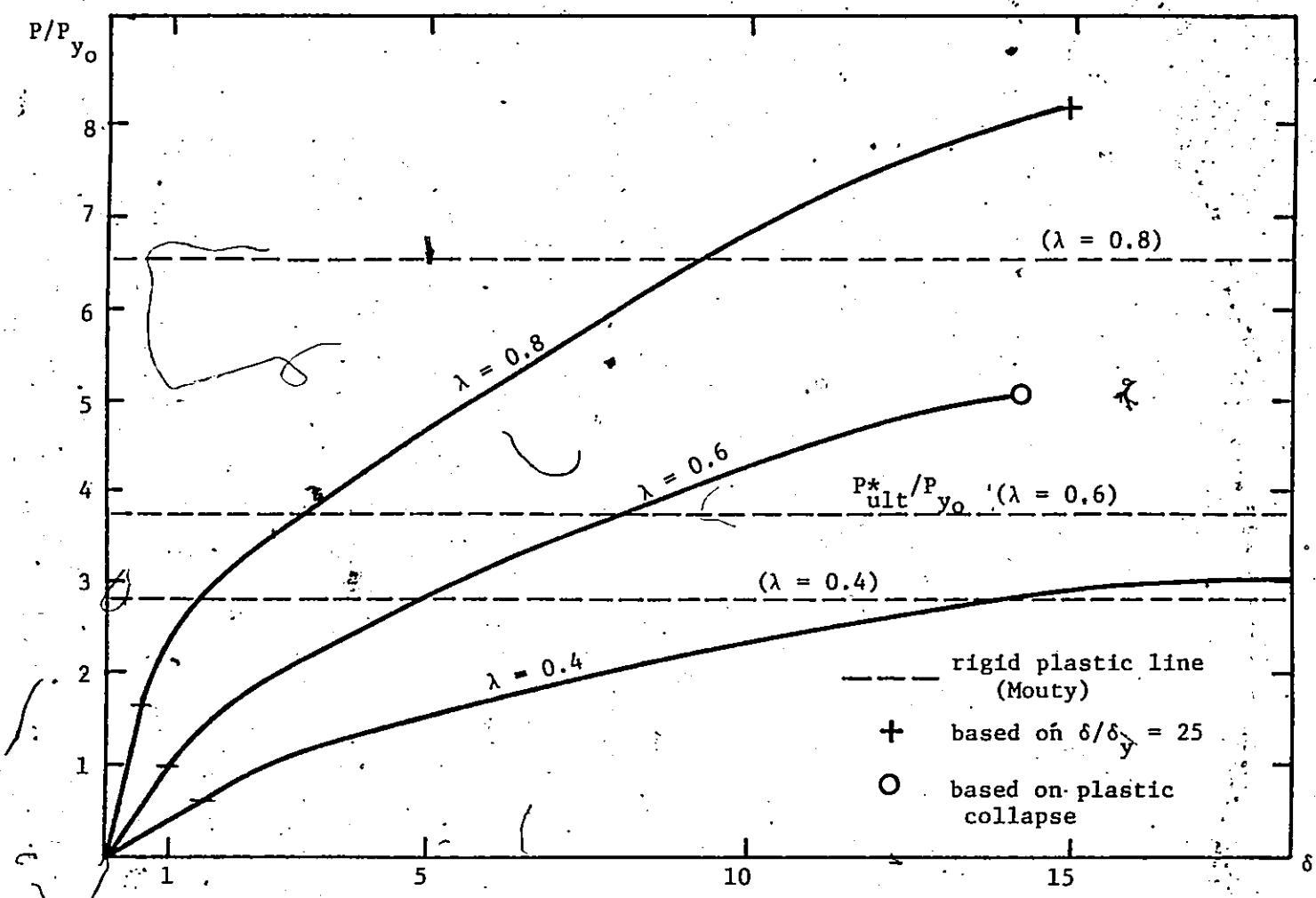

Figure 6.6 P-δ Curve for Different λ Values (254 x 254 x 9.5 mm Chord and E_T = 0.025E)

deflection of one-half the chord thickness.

Table 6.6.2 provides a comparison between different methods to predict the ultimate load carrying capacity of the RHS T-joint.

λ	P_{ult} KN	P'_{ult} KN	P_{ult}/P^*_{ult}	P'_{ult}/P^*_{ult}
0.8	667.20	480.38	1.25	0.9
0.6	415.18	304.69	1.35	0.99
0.4	253.54	164.58	1.1	0.7

Note: P_{ult} is based on program limits, P'_{ult} is based on $\delta/b = 1\%$
P^*_{ult} is based on Monty's formula

Table 6.6.2 Comparison of Different Predictions of Ultimate Loads for Different λ's (254 x 254 x 9.5 mm Chord and $E_T = 0.025$ E)

As can be seen from the table, the validity of assuming the ultimate load to be the load that causes a maximum deflection-to-width ratio $\delta/b = 1\%$, becomes questionable when λ reduces to 0.4. Hence, it should be noted that this criterion could only be used for a prescribed range of λ.

The ultimate loads obtained at the program limits are of the order of 1.1 to 1.35 times those given by Mouty. However, present results are based on steel with $E_T = 0.025$ E, while the limit analysis assumes the material to be perfectly plastic.

For design purposes, an estimate of the allowable or working load of the RHS T-joint can be obtained again from the ultimate loads by multiplying them by the factor 1/1.65. Table 6.6.3 gives the

predicted values of working loads obtained in this study, together with the ratios of both the ultimate and working loads to the yield load. It can be seen from the table that the ultimate load is about 5.0 times the yield loads and an estimate of the working load to be about 3.0 times the yield load appear to be quite reasonable in design. Table 6.6.3 provides also the C values for different λ.

λ	$P_{working}$ KN	P_{ult}/P_{yield}	$P_{working}/P_{yield}$	C KN/mm
0.8	404.36	4.93	2.96	742
0.6	251.62	5.07	3.04	247
0.4	153.66	4.49	2.70	101

Table 6.6.3 Load Values and Comparisons, and Punching Shear Stiffnesses for Different λ (254 x 254 x 9.5 mm Chord and E_T = 0.025 E)

(c) Chord Thickness Effect

As was discussed for branch moment applied to the chord, the chord thickness t was found to have a very significant effect on joint behaviour for the joint subjected to branch axial load P. Corresponding P-δ curves are thus plotted, as indicated in figure 6.7, in a non-dimensional form with respect to the joint with $t = t_o$ = 9.5 mm forming a base line for assessing relative strength and stiffness of the other joints. The trend of the curves is similar to those obtained for the joint under applied moment. Generally speaking, the variation in the elastic joint stiffness is very large with a relatively small variation

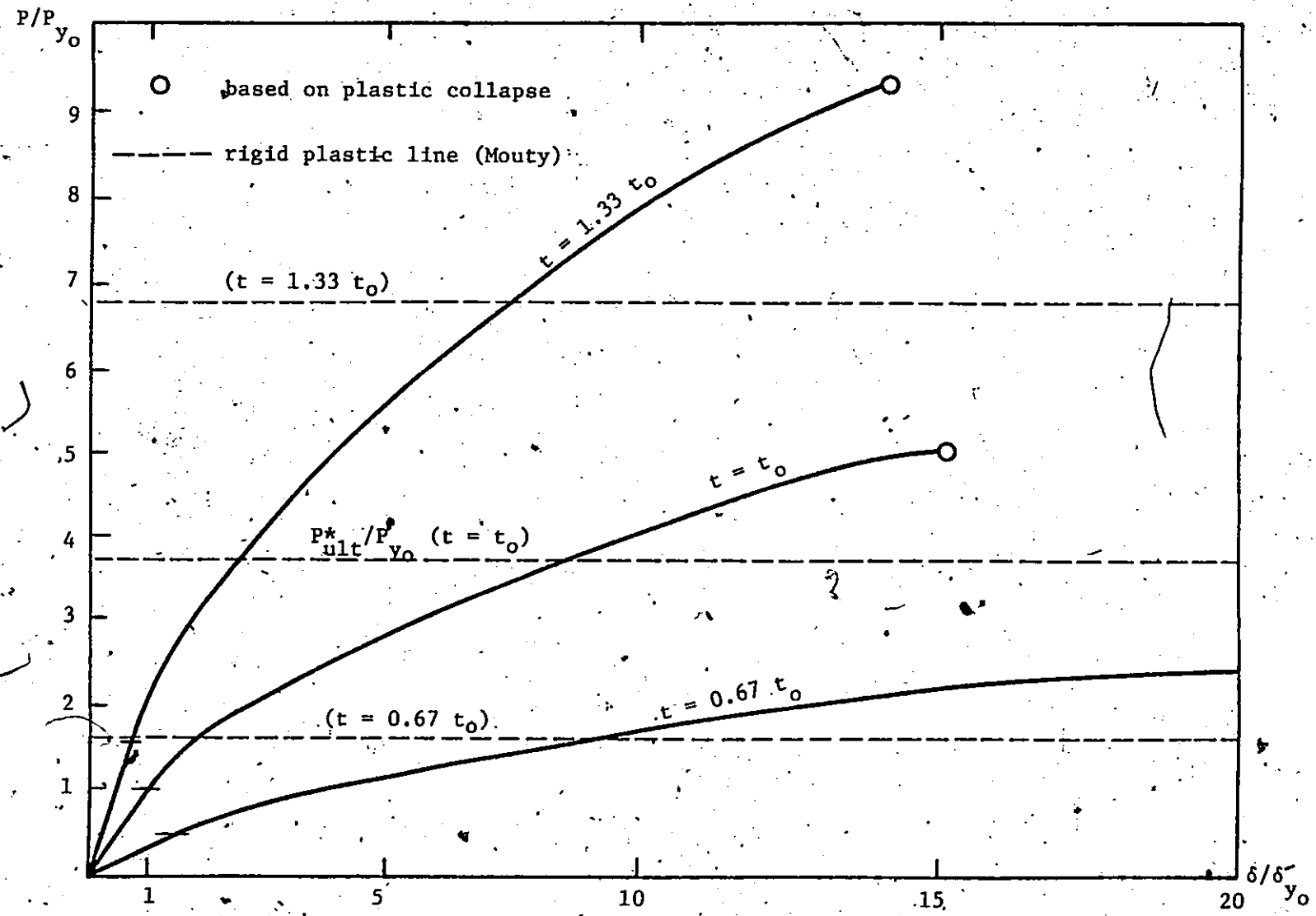

Figure 6.7 P-δ for Different Chord Thicknesses (254 x 254 mm Chord to 154.4 x 154.4 mm Branch and E_T = 0.025 E)

in the chord thickness. For example, the elastic C value for $t = 0.67\ t_o$ is about one-third the value for the joint with $t = t_o$. Also, the slope of the P-δ curve in the inelastic region is much steeper for the latter case at a given deflection. When t increases from t_o to $1.33\ t_o$, the effect in the elastic region is not as great, but nonetheless reflects a much stiffer joint in the inelastic range of loading.

In accordance with the criterion of predicting the ultimate load carrying capacity, the values obtained at the point of plastic collapse for $t = t_o$ and $t = 1.33\ t_o$, are almost 1.4 those obtained from limit analysis. This criterion was indicated at $\delta/\delta_y \approx 17$ and at a displacement $\approx 0.5\ t_o$ for the former joint, and 0.4 t for the latter one, indicating again that perhaps a failure or limit criterion may be considered at a maximum deflection that is equivalent to about half the chord thickness. When t is reduced to $0.67\ t_o$, the P-δ curve is very flexible; no plastic unloading was indicated, and the curve becomes quite flat at $\delta/\delta_y \approx 12$ giving a value of ultimate load that is equal to 1.6 the value obtained from limit analysis. However, these higher values are expected since the steel used has a strain hardening modulus $E_T = 0.025\ E$. Mouty's limit analysis neglected strain hardening.

Table 6.6.4 gives a comparison between different approaches for obtaining the ultimate load that can be carried by a given joint. The ultimate loads calculated at $\delta/b = 1\%$ (P'_{ult}) are almost the same as given by limit analysis (P^*_{ult}).

t mm	P_{ult} KN	P'_{ult} KN	P_{ult}/P^*_{ult}	P'_{ult}/P^*_{ult}
12.7	773.42	584.91	1.39	1.05
9.5	415.18	302.46	1.35	0.99
6.4	215.42	126.77	1.6	0.94

Note: P_{ult} based on Program Limits, P'_{ult} based on $\delta/b = 1\%$. P^*_{ult} based on Mouty's formula.

Table 6.6.4 Comparison Between Different Predictions of Ultimate Load (254 x 254 mm Chord with 154.4 x 154.4 mm Branch and $E_T = 0.025$ E)

For design purposes, Table 6.6.5 gives the predicted values of working load (= 1/1.65 times ultimate loads) and the ratios of the ultimate and working loads to the yield loads for different chord thicknesses together with the corresponding elastic C values. Again, the ultimate loads are higher than 5.0 times the yield ones and an estimation of the working load is found to be about 3.2 times the yield load.

t mms	$P_{working}$ KN	P_{ult}/P_{yield}	$P_{working}/P_{yield}$	C KN/mm
12.7	468.74	5.65	3.39	501
9.5	251.62	5.07	3.04	247
6.4	130.56	5.26	3.16	82

Table 6.6.5 Load Values and Comparisons, and Punching Shear Stiffnesses for Different t. (254 x 254 mm Chord with 154.4 x 154.4 mm Branch and $E_T = 0.025$ E)

6.7 Haunch Connection

6.7.1 Introduction

Experiments and theoretical analyses performed on the unreinforced T-joints indicate that these joint types are weak in transmitting branch member forces to the chord, especially for $\lambda < 1$. Consequently, one of the possible ways to improve the rigidity of the joint is by increasing the thickness of the chord member. In this instance, yield stresses may be reached in the branch member before the occurrence of the joint failure. On the other hand, this may produce an uneconomical design due to an excessively heavy chord wall thickness. Therefore, some form of joint reinforcement is essential for most applications. Korol et al (5) tested a variety of reinforced joint types, some of which were shown to be structurally superior to others. One such type is the haunch type of connection as shown in figure 1.2. In this type, a considerable improvement in the joint stiffness was obtained experimentally (5). It is the purpose of this section to present a theoretical analysis of this joint in the elastic-plastic stage of loading and discuss its behaviour when the joint is subjected to either applied moment or axial force.

6.7.2 The Analysis

In this case, the branch member together with the connected haunches are presumed to represent a rigid inclusion. The top flange plate of the chord within this inclusion is presumed to

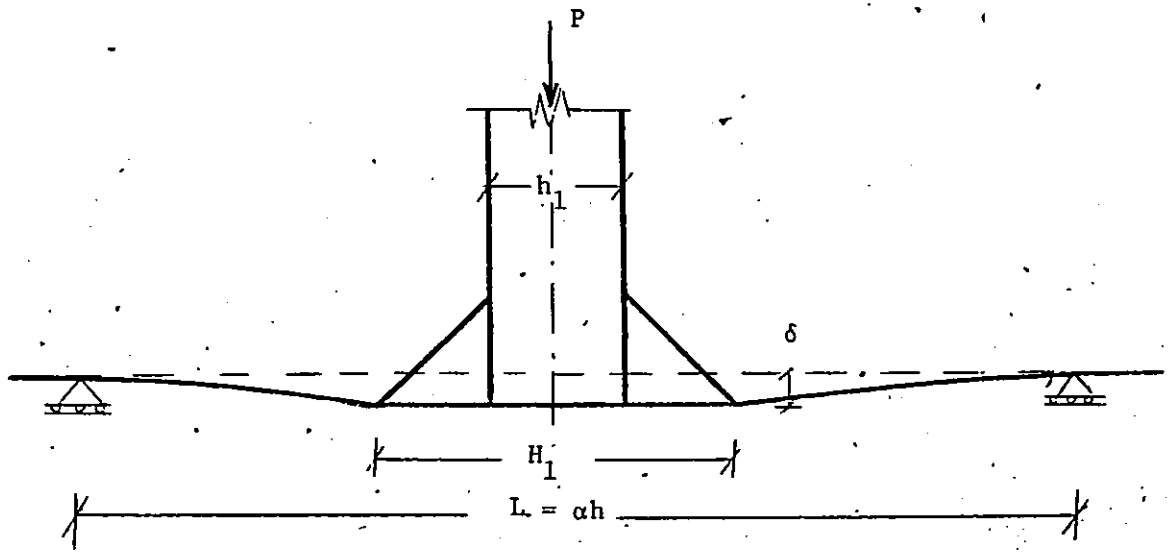

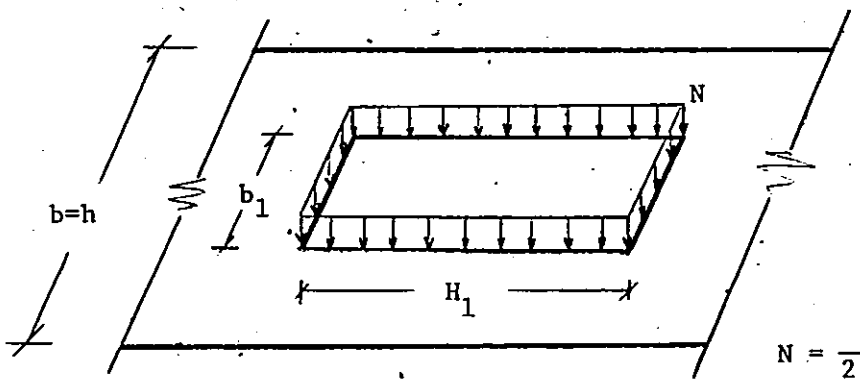

$$N = \frac{P}{2(b_1 + H_1)}$$

Figure 6.8a Branch Axial Load Transfer for the Haunch ($\alpha = 7.2$)

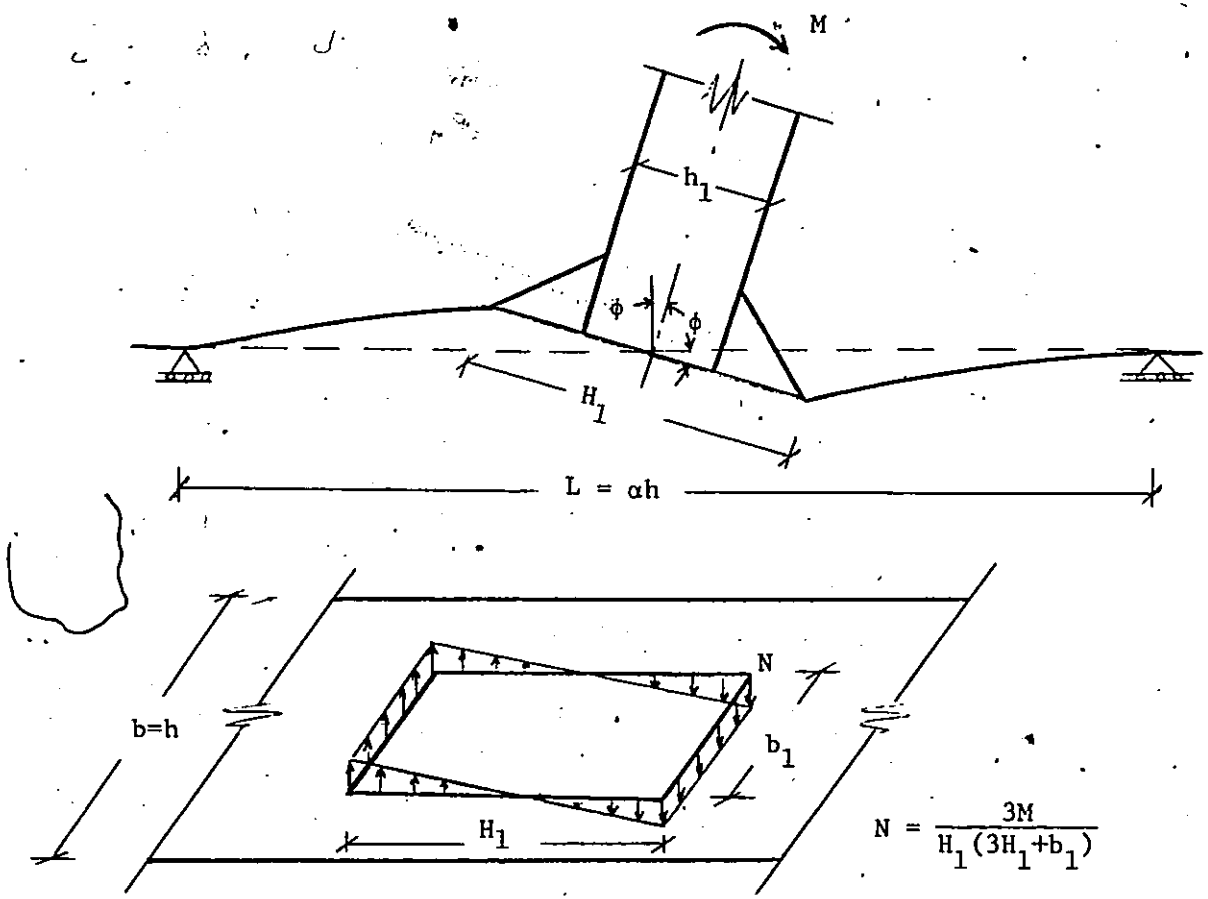

Figure 6.8 b Branch Moment Transfer for the Haunch (α = 7.2)

undergo only rigid body type translation δ or rotation ϕ. The load transfer from the branch to the chord member is assumed to occur along the perimeter of the inclusion as a line load and distributed linearly in accordance with the load transfer system presented earlier. The distribution of axial load and moment with associated rigid body type displacements of the flange plate are sketched in figure 6.8.

6.7.3 Joint Under Applied Moment

Three different haunch connections were analyzed with the aid of the computer program described earlier. The results are plotted in the form of M-ϕ curves, for the 254 x 254 x 9.5 mm chord to 154.4 x 154.4 mm branch and $E_T = 0.025 \cdot E$, and are shown in figure 6.9. The slope of the M-ϕ curve in the elastic region, i.e. the joint flexural rigidity J, increases significantly with an increase of λ_1 (= H_1/h_1). Using $\lambda_1 = 1.5$ increases J by more than 200% from value when $\lambda_1 = 1.0$ (i.e. unreinforced joint). Comparing the case when $\lambda_1 = 2.0$ with the unreinforced connection, one observes a J value of the former almost four times the value of the latter. As expected, in the inelastic range of loading the joint behaviour becomes stiffer when using the haunch reinforcement in comparison with the unreinforced joint ($\lambda_1 = 1.0$). Increasing the size of the haunch makes the joint stiffer under applied moment. The correlation between the ultimate moments obtained in the present analysis at $\delta/\delta_y \approx 25$ and those given by Mouty (10) is fairly good as indicated in figure 6.9.

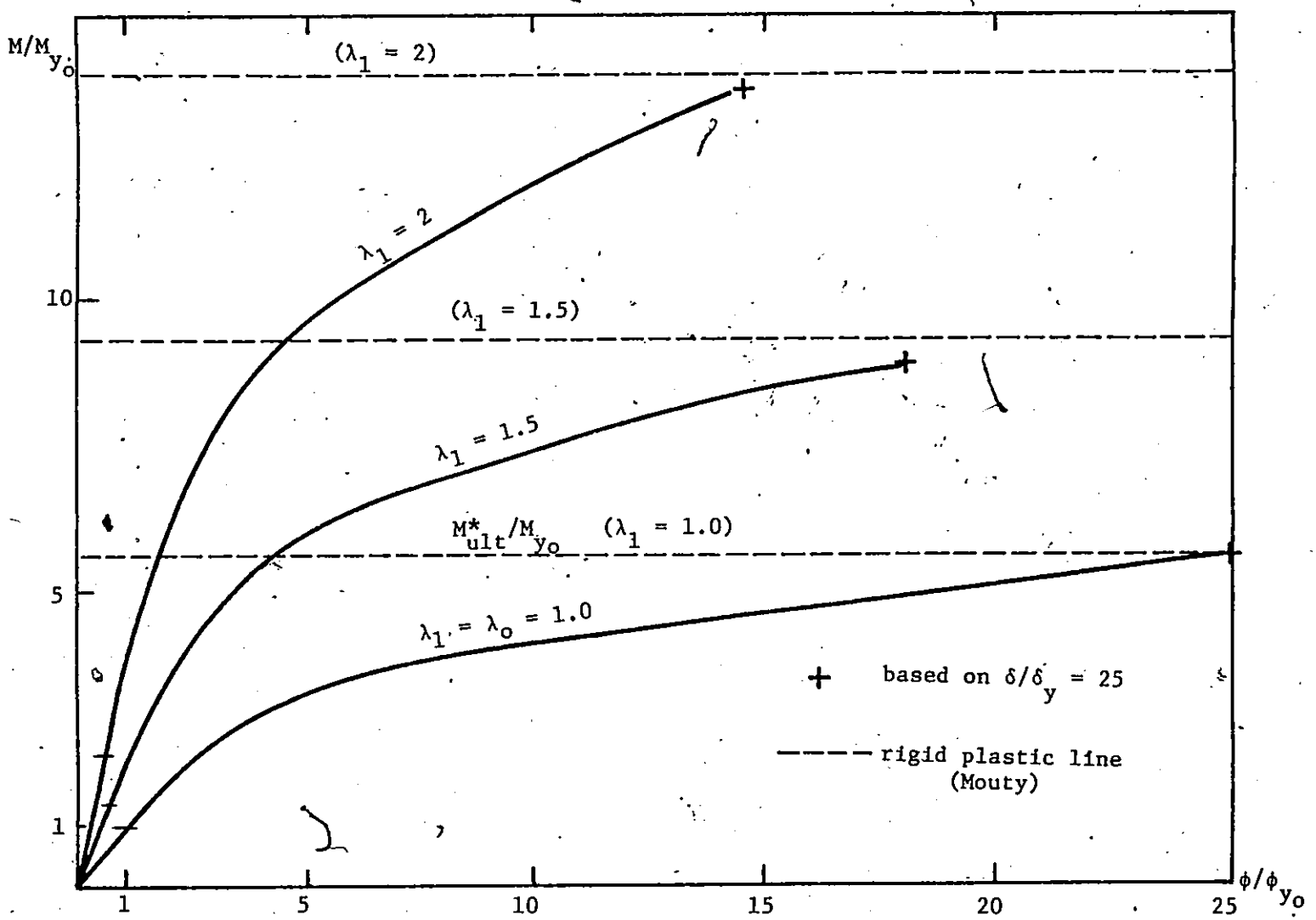

Figure 6.9 M-ϕ Curve for Various $\lambda 1$ Values (254 x 254 x 9.5 mm Chord with 154.4 x 154.4 mm Branch and E_T = 0.025 E)

The working moments of the given joint for different λ_1 values were calculated from the ultimate moments obtained and are compared with the yield moments in Table 6.7.1. Again, all values of the M_{ult} are higher than 5.7 times the M_{yield} and an estimation of the working moment of ≈ 3.5 times the yield moment is obtained.

λ_1	M_{ult} KN·m	M_{ult}/M_{yield}	$M_{working}/M_{yield}$	J KN·m/rad
2.0	65.54	6.14	3.68	5198
1.5	43.05	5.84	3.5	2938
1.0	27.12	5.69	3.4	1390

Table 6.7.1 Moment Values and Comparisons, and Rotational Stiffness of Different λ_1 Values (254 x 254 x 9.5 mm Chord to 154.4 x 154.4 mm Branch and $E_T = 0.025\,E$)

Table 6.7.1 provides also the corresponding J value for each joint. It can be observed that the haunch connection is much stiffer than the unreinforced joint for the same value of λ and t.

6.7.4 Joint Under Punching Shear

A similar study on the haunched type T-joint discussed in section 6.7.3 is presented here when the joint is subjected to an

axial force on the perimeter of the inclusion. The same joints that were used to predict M-ϕ relationships were also employed here. Figure 6.10 shows the P-δ curves for different λ_1 values in a nondimensional form with respect to the joint with $\lambda_1 = 1$. The sensitivity of the C value with λ_1 is significant, but not as great as in the case of the J value. Using a haunch size $\lambda_1 = 1.5$ increased the C value to about 1.32 the case with no haunch reinforcement. When λ_1 increased to 2.0, the C value increased by a factor of 1.65. Hence, it would appear that a joint with haunch reinforcing supplies a considerable increase in rigidity and is, therefore, capable of developing the full axial force in the branch member if properly designed. One can observe that the displacements δ at yield are the same for the three values of λ_1 studied in figure 6.10. In the inelastic range of loading, the final displacements at the program limit (plastic collapse) are also the same for all values of λ_1. This result may indicate that reinforcing the joint by using haunches may not affect the displacement values at the perimeter of the rigid inclusion. However, yield values and ultimate loads are significantly affected. It is to be noted that the values of ultimate loads obtained from the program limit are 35 to 60% higher than Mouty's rigid plastic loads as indicated in Table 6.7.2. The relatively large difference is likely due in part to the assumption of neglecting the strain hardening of the steel in the yield line method, while a value of $E_T = 0.025$ E has been used herein. Comparing the

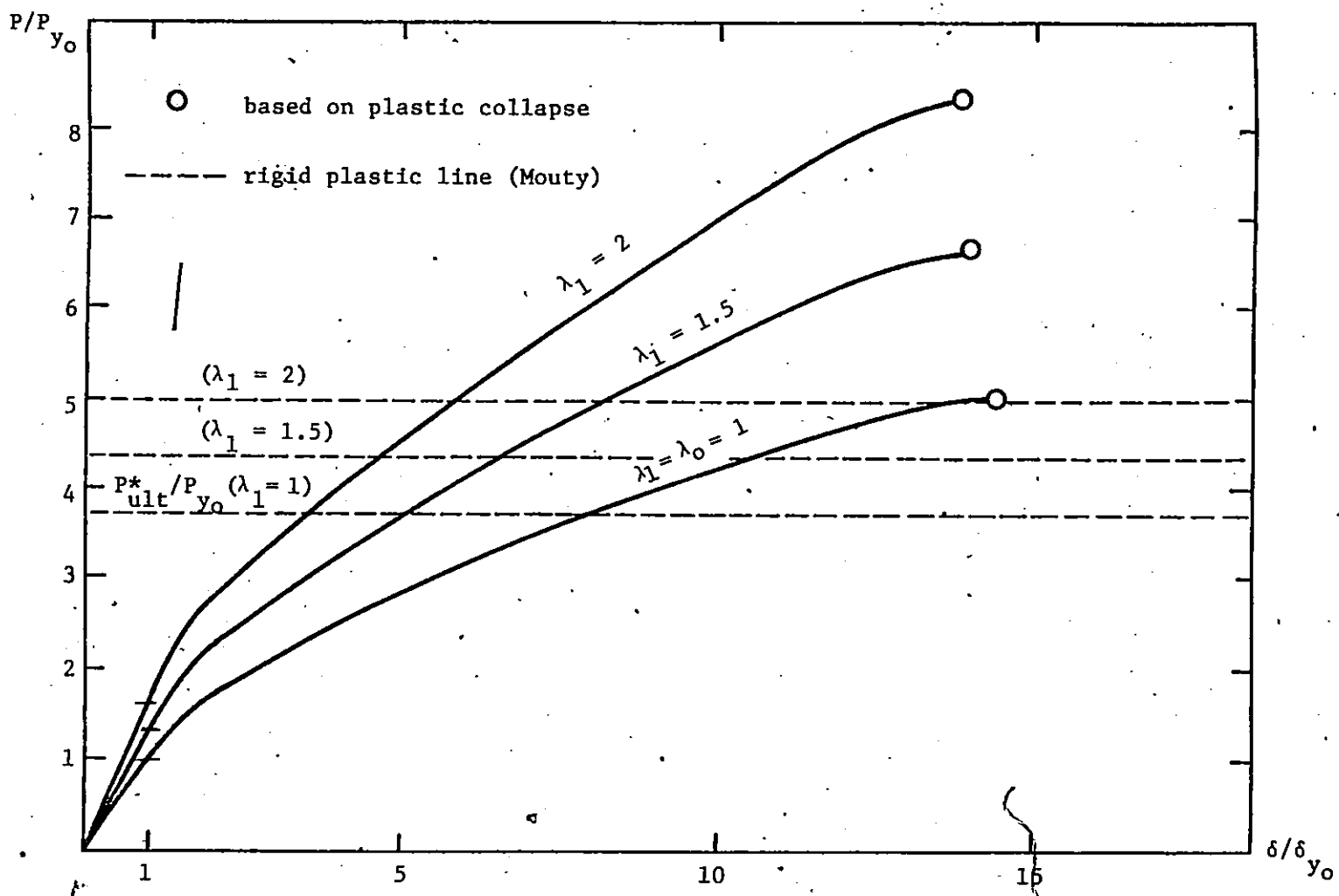

Figure 6.10 P-δ Curves for Different λ_1 (254 x 254 x 9.5 mm Chord with 154.4 x 154.4 mm Branch and $E_T = 0.025\,E$)

ultimate loads obtained at $\delta/b = 1\%$ (P'_{ult}) with those obtained from limit analysis, it is observed that the correlation is fairly good.

Also, the final displacement at the point of plastic collapse is 4.7 mm which is equivalent to one-half of the chord thickness, t.

λ_1	P_{ult} KN	P'_{ult} KN	P_{ult}/P^*_{ult}	P'_{ult}/P^*_{ult}
2.0	684.50	489.28	1.60	1.19
1.5	547.19	391.42	1.50	1.09
1.0	415.18	304.69	1.35	0.99

Note: P_{ult} is based on the program limits, P^*_{ult} is Mouty's value.

Table 6.7.2 Comparison Between Different Predictions of Ultimate Loads for Different Haunch Sizes (254 x 254 x 9.5 mm Chord to 154.4 x 154.4 mm Branch and $E_T = 0.025$ E)

Concerning working loads, Table 6.7.3 gives their estimated values based on the ultimate loads. Ultimate-to-yield load ratios for different values of λ_1 are also given. An estimation of the working load of about 3 times the yield load is thus obtained. The corresponding values of C are also given in the same table.

λ_1	$P_{working}$ KN	P_{ult}/P_{yield}	$P_{working}/P_{yield}$	C KN/mm
2.0	410.68	5.05	3.03	6999
1.5	328.31	5.04	3.03	5595
1.0	249.09	5.07	3.04	4245

Table 6.7.3 Load Values and Comparisons and Punching Shear Stiffnesses for Different Haunch Size λ_1 (254 x 254 x 9.5 mm Chord to 154.4 x 154.4 mm Branch and $E_T = 0.025$ E)

The higher values obtained for ultimate loads in almost all cases may have been caused:

(i) Because only one iteration is performed for each load increment, some drifting is expected. Nonetheless, the small value of load increment used ($0.1\ P_{yield}$) may reduce this drifting.

(ii) All values of ultimate loads obtained herein are for steel with strain hardening modulus $E_T = 0.025\ E$.

(iii) The use of nonconforming elements may give rise to a stiffer model. Hence, higher ultimate loads are produced.

CHAPTER 7

CONCLUSIONS

An analytical model for the single chord RHS T-joint has been presented. The top chord flange is treated as a thin plate subjected to transverse bending and punching shear. The remaining section (two vertical webs and the bottom flange) provides the edge restraints for the top plate. This restraint is accomplished through using coupled translational and rotational springs along the longitudinal edges.

A computer program using nonconforming rectangular plate bending finite elements was developed and twenty-seven integration points were used to predict the elastic strain hardening behaviour of the RHS T-joints by using a bi-linear stress-strain curve for steel ($E_T = 0.025\ E$). The loads were applied in an incremental manner until total rotations (for branch bending) or total displacements (branch punching shear) reached a value of about twenty-five times the corresponding elastic limits. Calculations were terminated when unloading was indicated.

In the analysis, a rigid inclusion is utilized to transmit the branch forces to the chord. Hence, a typical beam-column type of stress distribution has been assumed at the connection loading to a symmetric load distribution at the inclusion for branch axial force and an antisymmetric loading for the branch moment. Because of symmetry and antisymmetry, one quarter of the plate was used in the analysis performed in this work.

The sensitivity of the joint stiffnesses to various geometric parameters, i.e. width ratio λ, haunch size ratio λ_1 and chord thickness t together with different degrees of strain hardening (E_T/E) for the entire range of loading is examined.

From the analysis performed on various T-joints, the following conclusions are deduced.

(1) The single chord T-joints can be analyzed successfully by using only one quarter of the plate and a finite element grid of 4 elements across with 20 elements in the longitudinal direction. Twenty-seven integration points per element used herein appear to be very reasonable for predicting the inelastic behaviour.

(2) The program predicts punching shear and rotational stiffnesses of RHS T-joints that are within a few percent of experimental and theoretical results determined by other researchers (6,7,25).

(3) The ultimate branch axial loads or moments obtained in almost all cases were found to be higher than 5 times the corresponding yield load or moment. An estimation of the working load or moment (= 1/1.65 times the ultimate load or moment) of about 3.35 the corresponding yield values is thus obtained. This result indicates the necessity of undertaking an elastic-plastic type of analysis to arrive at allowable load or moment of an RHS T-joint. The load or moment at which initial yielding begins is far too conservative a criterion for design purposes.

(4) The ultimate moments obtained in this study for different joint

geometries and low but nonzero E_T/E compare well with those given by Mouty (10). In fact, higher values were expected since the study herein employed a strain hardening modulus of E_T = 0.025 E while Mouty's rigid plastic analysis implicitly assumes a value of zero.

On the other hand, ultimate punching shear loads using the standard $E_T/E = 0.025$ ratio were higher than those of Mouty as expected, by about 30 to 60%, for almost all combinations of λ λ_1 and t examined. One of the reasons for high ultimate loads may be due to drifting during the inelastic analysis as the incremental method used here does not check equilibrium after every load increment. However, it is reasonable to expect that using a small load increment (0.1 P_{yield} as used in the analysis) would prevent any considerable drifting. Also, it is quite possible that the nonconforming plate bending elements rendered a more flexible model under branch moments and thus yielded more comparable ultimate moments to Mouty's values.

(5) The unreinforced joints with small λ (= 0.4), as expected, are very weak in resisting moment and branch punching shear. Hence, for $\lambda \leq 0.4$ the joint is too flexible to be considered for practical applications, unless some form of reinforcing is provided. It was found that, by doubling λ from 0.4 to 0.8, the strength increases by about 160% for branch axial loading and about 60% for branch moment for a 254 x 254 x 9.5 mm chord. Thus λ appears to be a very important parameter for both the

joint strength and stiffness.

(6) Based on the analysis presented herein and El Zanaty's experimental results (4), providing a haunch around the T-joint is an excellent way of strengthening and stiffening. A significant gain in joint stiffness, ultimate and working loads and moments is achieved even for small λ_1 (≈ 2).

(7) The chord thickness t is also a very important parameter affecting joint behaviour, stiffness and capacity for an unreinforced joint with $\lambda < 1$. The chords of joints having small thickness-to-width ratio of the connecting plate tend to be overly flexible both for moment and punching shear. For example, a reduction in thickness by 50% had the effect of reducing C by 84% and J by 86% for a 254 x 254 mm chord and a 154.4 x 154.4 mm branch. The ultimate branch axial load and moment were also significantly reduced by 72% and 70% respectively.

(8) In most of the analysis the calculations were terminated at a displacement of the magnitude of t/2 and before δ/δ_y reached the maximum allowable value of 25. This happened after the plastic region extended sufficiently and some elastic unloading occurred. Hence, a criterion for calculating ultimate load may be regarded as the load or moment that causes maximum displacement of the magnitude of half the chord thickness.

(9) With the aid of the computer program developed in this study, it is possible to analyze any joint size in the elasto-plastic range and to obtain the corresponding working load or moment provided

that a reasonably large number of elements are used around the inclusion. Unfortunately, computer storage limitations on the CDC 6400 at McMaster University and cost have prevented a more extensive study.

Based on this investigation, some suggestions for further research are proposed, as follows:

(a) Experimental work appears to be needed, particularly for strain measurements, in order to confirm the results of the theoretical studies and to assist in making recommendations for design of the single chord T-joints.

(b) It would be useful to include the effect of in-plane actions in the plate bending element. This might give a better representation of the actual behaviour of the top flange plate of the chord member. In fact, the coupled edge springs will also cause coupling of in-plane and bending actions.

(c) It would be more appropriate, in modelling the joint, to include an inelastic frame analysis of the chord member cross section excluding the top flange plate. In this case, the spring constants would be calculated according to the elastic-plastic behaviour of the entire rectangular hollow section rather than according to the stress state of the flange plate done.

APPENDIX A.

A Closed Form of the Transformation Matrix [T]

The constants a_1 to a_{12} appearing in Equation 3.3.1 can be evaluated by writing the twelve simultaneous equations linking the values of w and its slopes at the nodes when the co-ordinates take up their appropriate values. For instance (figure 3.1)

$$w_i = a_1 + a_2 x_i + a_3 y_i + a_4 x_i^2 + \text{etc.}$$

$$w_{xi} = a_2 + 2 a_4 x_i + \text{etc.}$$

$$w_{yi} = a_3 + \text{etc.}$$

where i = i, 2, 3, 4, and

$$x_1 = x_4 = 0 \qquad y_1 = y_2 = 0$$

$$x_2 = x_3 = a \qquad y_3 = y_4 = b$$

Listing all twelve equations, we can write, in matrix form:

$$
\begin{Bmatrix} w_{x1} \\ w_{y1} \\ w_1 \\ w_{x2} \\ w_{y2} \\ w_2 \\ w_{x3} \\ w_{y3} \\ w_3 \\ w_{x4} \\ w_{y4} \\ w_4 \end{Bmatrix}
=
\begin{bmatrix}
0 & 0 & 1 & 0 & 0 & 0 & 0 & 0 & 0 & 0 & 0 & 0 \\
1 & 0 & 0 & 0 & 0 & 0 & 0 & 0 & 0 & 0 & 0 & 0 \\
0 & 1 & 0 & 0 & 0 & 0 & 0 & 0 & 0 & 0 & 0 & 0 \\
a & 0 & 1 & 0 & 0 & a^2 & 0 & 0 & a^3 & 0 & 0 & 0 \\
1 & 0 & 0 & 0 & 0 & 2a & 0 & 0 & 3a^2 & 0 & 0 & 0 \\
0 & 1 & 0 & a & 0 & 0 & a^2 & 0 & 0 & a^3 & 0 & 0 \\
a & b & 1 & ab & b^2 & a^2 & a^2b & ab^2 & a^3 & a^3b & ab^3 & b^3 \\
1 & 0 & 0 & b & 0 & 2a & 2ab & b^2 & 3a^2 & 3a^2b & b^3 & 0 \\
0 & 1 & 0 & a & 2b & 0 & a^2 & 2ab & 0 & a^3 & 3ab & 3b^2 \\
0 & b & 1 & 0 & b^2 & 0 & 0 & 0 & 0 & 0 & 0 & b^3 \\
1 & 0 & 0 & b & 0 & 0 & 0 & b^2 & 0 & 0 & b^3 & 0 \\
0 & 1 & 0 & 0 & 2b & 0 & 0 & 0 & 0 & 0 & 0 & 3b^2
\end{bmatrix}
\begin{Bmatrix} a_1 \\ a_2 \\ a_3 \\ a_4 \\ a_5 \\ a_6 \\ a_7 \\ a_8 \\ a_9 \\ a_{10} \\ a_{11} \\ a_{12} \end{Bmatrix}
$$

or $\{w^e\} = [T]\{A\}$

where [T] is a twelve-by-twelve matrix depending on nodal co-ordinates and {A} is a vector of the twelve unknown constants. Inverting we have

$$\{A\} = [T]^{-1}\{w^e\}$$

This inversion can be carried out by the computer, or, can be formed

algebraically. A closed form of $[T]^{-1}$ is given below:

$$[T]^{-1} = \begin{bmatrix} 0 & 0 & 1 & 0 & 0 & 0 & 0 & 0 & 0 & 0 & 0 & 0 \\ a & 0 & 0 & 0 & 0 & 0 & 0 & 0 & 0 & 0 & 0 & 0 \\ 0 & b & 0 & 0 & 0 & 0 & 0 & 0 & 0 & 0 & 0 & 0 \\ -2a & 0 & -3 & -a & 0 & 3 & 0 & 0 & 0 & 0 & 0 & 0 \\ -a & -b & -1 & 0 & b & 1 & 0 & 0 & -1 & a & 0 & 1 \\ 0 & -2b & -3 & 0 & 0 & 0 & 0 & 0 & 0 & 0 & -b & 3 \\ a & 0 & 2 & a & 0 & -2 & 0 & 0 & 0 & 0 & 0 & 0 \\ 2a & 0 & 3 & a & 0 & -3 & -a & 0 & 3 & -2a & 0 & -3 \\ 0 & 2b & 3 & 0 & -2b & -3 & 0 & -b & 3 & 0 & b & -3 \\ 0 & b & 2 & 0 & 0 & 0 & 0 & 0 & 0 & 0 & b & -2 \\ -a & 0 & -2 & -a & 0 & 2 & -a & 0 & -2 & -a & 0 & 2 \\ 0 & -b & -2 & 0 & b & 2 & 0 & b & -2 & 0 & -b & 2 \end{bmatrix}$$

APPENDIX B

A Closed Form of the Strain Matrix [B]

The strain matrix [B] relates nodal displacements to strains, where (equation 3.3.9)

$$\{\varepsilon\} = \begin{Bmatrix} \varepsilon_x \\ \varepsilon_y \\ \gamma_{xy} \end{Bmatrix} = \begin{Bmatrix} -z \dfrac{\partial^2 w}{\partial x^2} \\ -z \dfrac{\partial^2 w}{\partial y^2} \\ -2z \dfrac{\partial^2 w}{\partial x \partial y} \end{Bmatrix} = \begin{Bmatrix} -z \dfrac{\partial^2 N}{\partial x^2} \\ -z \dfrac{\partial^2 N}{\partial y^2} \\ -2z \dfrac{\partial^2 N}{\partial x \partial y} \end{Bmatrix} \{w^e\} = [B]\{w^e\} \tag{3.3.9}$$

where {N} is the shape function given by equation 3.3.6 from equation 3.3.9

$$\underset{3x12}{[B]} = \begin{Bmatrix} -z \dfrac{\partial^2 w}{\partial x^2} \\ -z \dfrac{\partial^2 w}{\partial y^2} \\ -2z \dfrac{\partial^2 w}{\partial x \partial y} \end{Bmatrix}_{3x12}$$

where

$$
\underset{1\times 12}{\left\langle -z \frac{\partial^2 w}{\partial x^2} \right\rangle} = \begin{Bmatrix} -\frac{t}{4a}(3\xi-1)(1-\eta)\zeta \\ 0.0 \\ -\frac{3t}{2a^2}\xi(1-\eta)\zeta \\ -\frac{t}{4a}(3\xi+1)(1-\eta)\zeta \\ 0.0 \\ \frac{3t}{2a^2}\xi(1-\eta)\zeta \\ -\frac{t}{4a}(3\xi+1)(1+\eta)\zeta \\ 0.0 \\ \frac{3t}{2a^2}\xi(1+\eta)\zeta \\ -\frac{t}{4a}(3\xi-1)(1+\eta)\zeta \\ 0.0 \\ -\frac{3t}{2a^2}\xi(1+\eta)\zeta \end{Bmatrix}^T_{12\times 1}
$$

$$
\underset{1\times 12}{\left\langle -z\,\frac{\partial^2 w}{\partial y^2}\right\rangle} = \underset{12\times 1}{\begin{Bmatrix} 0.0 \\ -\frac{t}{4b}(1-\xi)(3\eta-1)\zeta \\ -\frac{3t}{2b^2}(1-\xi)\eta\zeta \\ 0.0 \\ -\frac{t}{4b}(1+\xi)(3\eta-1)\zeta \\ -\frac{3t}{2b^2}(1+\xi)\eta\zeta \\ 0.0 \\ -\frac{t}{4b}(1+\xi)(3\eta+1)\zeta \\ \frac{3t}{2b^2}(1+\xi)\eta\zeta \\ 0.0 \\ -\frac{t}{4b}(1-\xi)(3\eta+1)\zeta \\ -\frac{3t}{2b^2}(1-\xi)\eta\zeta \end{Bmatrix}^T}
$$

$$\text{and} \quad \left\langle -2z \frac{\partial^2 w}{\partial x \partial y} \right\rangle_{1\times 12} = \begin{Bmatrix} -\frac{t}{4b}(1-\xi)(1+3\xi)\zeta \\ -\frac{t}{4a}(1-\eta)(1+3\eta)\zeta \\ -\frac{t}{2ab}(4-3\xi^2-3\eta^2)\zeta \\ -\frac{t}{4b}(1+\xi)(1-3\xi)\zeta \\ \frac{t}{4a}(1-\eta)(1+3\eta)\zeta \\ \frac{t}{2ab}(4-3\xi^2-3\eta^2)\zeta \\ \frac{t}{4b}(1+\xi)(1-3\xi)\zeta \\ \frac{t}{4a}(1+\eta)(1-3\eta)\zeta \\ -\frac{t}{2ab}(4-3\xi^2-3\eta^2)\zeta \\ \frac{t}{4b}(1-\xi)(1+3\xi)\zeta \\ -\frac{t}{4a}(1+\eta)(1-3\eta)\zeta \\ \frac{t}{2ab}(4-3\xi^2-3\eta^2)\zeta \end{Bmatrix}_{12\times 1}^{T}$$

APPENDIX C

```
      PROGRAM TST(INPUT,OUTPUT,TAPE5=INPUT,TAPE6=OUTPUT,TAPE1,
     1TAPE8,TAPE9,TAPE10,TAPE11,TAPE7)
     1PP(378),XX(126),YY(126),IX(378),JX(378),CON(30),ICON(30),
     1PP(315),XX(105),YY(105),IX(315),JX(315),CON(30),ICON(30),
     2ICO(80,6),B(315),CC(315),B1(315),R(315),D(3,3),A(9999)
      WRITE(6,1)
    3 READ(5,2) NPROB,THICK
      READ(5,4) NEL,NNOD,NVAR,NNODEL
      READ(5,333) IL,ET,YL
      NVEL=NVAR*NNODEL
      NMAT=NNOD*NVAR
      CALL LAYOUT(XX,YY,ICO,IX,JX,NEL,NNOD,NVAR,NMAT,NNET,NNODEL)
      CALL BANDWH(ICO,JX,LJ,NEL,NVAR,LBAND,NNODEL,NMAT)
      NB3=LBAND+1
      NVA=NB3*NNET
      WRITE(6,5) NPROB,NNET,LBAND,NVA
      CALL PRESET(S,NVEL,NVEL)
      CALL PSET(CC,NNET)
      CALL PSET(PP,NMAT)
      CALL PSET(B,NNET)
      CALL PSET(A,NVA)
      READ(5,6) E,ANU,NCON
      WRITE(6,7) E,ANU,NCON
      IF(NCON.EQ.0) GO TO 13
      READ(5,14) (ICON(I),I=1,NCON)
      READ(5,15) (CON(I),I=1,NCON)
      WRITE(6,16) (ICON(I),I=1,NCON)
      WRITE(6,17) (CON(I),I=1,NCON)
   13 REWIND 1
      ILC=0
      SIGMAX=0.0
      XMAX=0.0
      YMAX=0.0
      ZMAX=0.0
      NEMAX=0
      IFLAG=0
  100 CONTINUE
      CALL PSET(FL,NVEL)
      IF(ILC.EQ.0) GO TO 1000
      IF(ILC.EQ.2) GO TO 31
      DO 50 I=1,NNET
   50 CC(I)=CC(I)+B(I)
      DO 51 I=1,NNET
   51 B1(I)=B(I)
      IF(ILC.EQ.1) GO TO 1000
   31    CALL EXPAND(PP,NMAT,  JX,NNOD,NVAR,CC)
 1000 REWIND 10
      REWIND 11
      CALL PSET(B,NNET)
      CALL PSET(A,NVA)
      IF(ILC.LE.2)GO TO 1111
      IF(IFLAG.EQ.0) GO TO 222
      IF(IFLAG.EQ.1) GO TO 322
  222 IFLAG=1
      GO TO 1111
  322 IFLAG=0
 1111 WRITE(6,225) IFLAG
  225 FORMAT(10X,"IFLAG",I7,//)
      DO 8 IEL=1,NEL
      DO 9 I=1,NNODEL
      ICOO=ICO(IEL,I)
      X(I)=XX(ICOO)
    9 Y(I)=YY(ICOO)
      AA=ABS(X(2)-X(1))
      BB=ABS(Y(4)-Y(1))
```

```
      IS=ICO(IEL,NNODEL+1)
      IB=ICO(IEL,NNODEL+2)
      DO 10 J=1,NNODEL
      J1=(J-1)*NVAR
      J2=NVAR*(ICO(IEL,J)-1)
      DO 10 I=1,NVAR
   10 LJ(I+J1)=JX(J2+I)
      IF(ILC.EQ.0) GO TO 52
      REWIND 9
      CALL STRESS2(E,ET,B1,U,LJ,IEL,NVEL,THICK,AA,BB,YL,
     1SIGMAX,IFLAG,ANU,SIGBND,S11B,S22B,S33B,NNET,ILC)
      REWIND 9
   52 CALL KMATRX(S,IEL,ILC,THICK,AA,BB,IS,E,ET,ANU)
      CALL BOUNDRY(S,AA,BB,IS,IB,SIGBND,YL,ILC,IEL,S11B,
     1S22B,S33B)
      IF(ILC.GT.0) GO TO 53
      CALL DLOAD(FL,AA,BB,IEL,IB,IS)
   53 CALL SETUP(A,B,S,FL,NVEL,LJ,NVAR,LBAND,IEL,NNET,
     1NVA)
    8 CONTINUE
      IF(ILC.GT.IL)GO TO 995
      IF(ILC.GT.0) GO TO 54
   55 IF(NCON.EQ.0) GO TO 11
      CALL PLACEZ(B,A,CON,ICON,NCON,NNET,LBAND)
   11 REWIND 7
      WRITE(7) (B(I),I=1,NNET)
      GO TO 56
   54 REWIND 8
      IF(ILC.EQ.1) GO TO 57
      GO TO 58
   57 FAC=YL/SIGMAX
      WRITE(6,60) FAC
   60 FORMAT(10X,"FAC=  ",F15.5,//)
      REWIND 7
      READ (7) (B(I),I=1,NNET)
      DO 59 I=1,NNET
      CC(I)=FAC*CC(I)
      B1(I)=FAC*B1(I)
   59 B(I)=FAC*B(I)
      REWIND 7
      WRITE(7) (B(I),I=1,NNET)
      WRITE(8) (B(I),I=1,NNET)
   58 CONTINUE
      IF(ILC.EQ.1) GO TO 75
      REWIND 8
      READ (8) (B(I),I=1,NNET)
   56 DET=1.E-10
      CALL BAND(A,B,NNET,NBJ,1,DET,NVA)
      IF(ILC.EQ.0) GO TO 611
  611 IF(DET.LE.0.0) GO TO 998
      WRITE(6,12) DET
      IF(ILC.EQ.0) WRITE(6,555)
      IF(ILC.GT.0) GO TO 75
          CALL EXPAND(PP,NMAT,  JX,NNOD,NVAR,B)
  555 FORMAT(10X,"FIRST TRIAL ELASTIC SOLUTION",//)
   75 WRITE(6,63)ILC
   63 FORMAT(10X,"ILC WAS",I10,//)
   12 FORMAT(10X,"DETERMINENT IS",E20.7,//)
      ILC=ILC+1
      IF(ILC.EQ.1) GO TO 100
      IF(ILC.GT.IL) GO TO 100
      REWIND 7
      REWIND 8
      READ (7) (PP(I),I=1,NNET)
      III=ILC-1
```

```
      FAC=0.05
      IF(ILC.GT.2) FAC=0.1
      IF(ILC.GT.12) FAC=0.2
      WRITE(6,717) FAC
  717 FORMAT(10X,"**FAC**",F10.7,//)
      DO 64 I=1,NNET
   64 PP(I)=FAC*PP(I)
      WRITE(8) (PP(I),I=1,NNET)
      IF(ILC.EQ.2) WRITE(6,666)
  666 FORMAT(10X,"START THE NONLINEAR PART",//)
      GO TO 100
  998 WRITE(6,997) DET
  995 WRITE(6,989)
  988 STOP
  989 FORMAT(//,4X,"*****END OF ANALYSIS***",//)
    1 FORMAT("1",10X,"***BEAM FINITE ELEMENT ANALYSIS****
     1",///)
    2 FORMAT(I5,F10.0)
    4 FORMAT(4I5)
    5 FORMAT(/,5X,"PROBLEM NO.",I5,10X,"TOTAL UNKNOWNS",
     1I5,//,5X,"BANDWIDTH",I5,10X,"MATRIX SIZE",I8,/)
  333 FORMAT(I5,2F10.0)
    6 FORMAT(E10.2,F10.0,I5)
    7 FORMAT(/,5X,"MODULUS OF ELASTICITY =",F15.1,10X,
     1"POISSONS RATIO="
     1,F8.4,//,5X,"NUMBER OF CONSTRAINTS =",I6,/)
   14 FORMAT(20I4)
   15 FORMAT(8F10.0)
   16 FORMAT(/,5X,"CONSTRAINTS ON DOF",8I10)
   17 FORMAT(/,5X,"CONSTR. VALUES ARE",8F10.4)
  996 FORMAT(//,5X,"*********M END *******1**",/)
  997 FORMAT(/,5X,"MATRIX IS NOT POSITIVE DEFINITE",5X,
     1"DET=",E20.8)
 2000 FORMAT(8F10.0)
      END
      SUBROUTINE CLOAD(FL)
      DIMENSION FL(1),W(4)
      READ(5,1) (W(I),I=1,4)
      DO 2 I=1,4
      NN=3*I
    2 FL(NN)=FL(NN)+W(I)
    1 FORMAT(4F10.0)
      RETURN
      END
      END
      SUBROUTINE SETUP(A,B,S,FL,NVEL,LJ,NVAR,LBAND,IEL,NNET,NVA)
      DIMENSION A(NVA),B(NNET),S(12,12),FL(12),LJ(12)
      DO 12 I=1,NVEL
      LJR=LJ(I)
      IF(LJR.EQ.0) GO TO 12
      B(LJR)=B(LJR)+FL(I)
      DO 11 J=I,NVEL
      LJC=LJ(J)
      IF(LJC.EQ.0)  GO TO 11
      IF(LJR-LJC) 9,10,10
   10 K=(LJC-1)*LBAND+LJR
      GO TO 13
    9 K=(LJR-1)*LBAND+LJC
   13 A(K)=A(K)+S(I,J)
   11 CONTINUE
   12 CONTINUE
      RETURN
      END
      SUBROUTINE BANDWH(ICO,JX,LJ,NE,NVAR,LBAND,NNOD,NMA)
      DIMENSION ICO(NE,6),JX(NMA),LJ(12)
```

```
      LBAND=0
      NV2=2*NVAR
      DO 3 I=1,NE
      DO 4 J=1,NVAR
      DO 4 K=1,NNOD
      K1=(K-1)*NVAR
      LJ(J+K1)=JX(NVAR*ICO(I,K)-NVAR+J)
    4 CONTINUE
      MAX=0
      MIN=1000
      NV3=NVAR*NNOD
      DO 8 J=1,NV3
      IF(LJ(J).EQ.0) GO TO 8
      IF(LJ(J)-MAX) 6,6,5
    5 MAX=LJ(J)
    6 IF(LJ(J)-MIN) 7,8,8
    7 MIN=LJ(J)
    8 CONTINUE
      NB1=MAX-MIN
      IF(NB1.GT.LBAND) LBAND=NB1
    3 CONTINUE
      RETURN
      END
      SUBROUTINE EXPAND(AMODE,NAM,    JX,NDS,NVAR,VV)
      DIMENSION VV(NAM),AMODE(NAM),JX(NAM)
      DO 5 I=1,NAM
      AMODE(I)=0.0
      IF(JX(I).EQ.0) GO TO 5
      AMODE(I)=VV(JX(I))
    5 CONTINUE
      WRITE(6,40)
      DO 10 I=1,NDS
      I2=NVAR*I
      I1=I2-NVAR+1
      WRITE(6,41) I,(AMODE(J),J=I1,I2)
   10 CONTINUE
   40 FORMAT(///,5X,"NODE",8X,"THETA-X",9X,"THETA-Y",9X,"DISPLACEMENT",
     1/)
   41 FORMAT(I7,8X,E12.6,5X,E12.6,5X,E12.6)
      RETURN
      END
      SUBROUTINE PLACEZ(PP,C,CON,ICON,NCON,NN,LBAND)
      DIMENSION C(1),CON(1),PP(1),ICON(1)
      DO 18 I=1,NCON
      I1=ICON(I)
      I2=LBAND*(I1-1)+I1
      LC1=I1-LBAND
      IF(LC1.LE.0) LC1=1
      LC2=I1+LBAND
      IF(LC2.GT.NN) LC2=NN
      DO 17 J=LC1,LC2
      IF(I1-J) 9,10,10
   10 IJ=LBAND*(J-1)+I1
      GO TO 16
    9 IJ=LBAND*(I1-1)+J
   16 PP(J)=PP(J)-C(IJ)*CON(I)
   17 C(IJ)=0.D0
   18 CONTINUE
      DO 25 I=1,NCON
      I1=ICON(I)
      I2=LBAND*(I1-1)+I1
      C(I2)=1.E08
      PP(I1)=1.E08*CON(I)
   25 CONTINUE
      RETURN
```

```
      END
      SUBROUTINE BAND(A,B,N,M,LT,DET,NVA)
      DIMENSION A(NVA),B(N)
      MM=M-1
      NM=N*M
      NM1=NM-MM
      IF (LT.NE.1) GO TO 55
      MP=M+1
      KK=2
      FAC=DET
      A(1)=1./SQRT(A(1))
      BIGL=A(1)
      SML=A(1)
      A(2)=A(2)*A(1)
      A(MP)=1./SQRT(A(MP)-A(2)*A(2))
      IF(A(MP).GT.BIGL)BIGL=A(MP)
      IF(A(MP).LT.SML)SML=A(MP)
      MP=MP+M
      DO 62 J=MP,NM1,M
      JP=J-MM
      MZC=0
      IF(KK.GE.M) GO TO 1
      KK=KK+1
      II=1
      JC=1
      GO TO 2
1     KK=KK+M
      II=KK-MM
      JC=KK-MM
2     DO 65 I=KK,JP,MM
      IF(A(I).EQ.0.)GO TO 64
      GO TO 65
64    JC=JC+M
65    MZC=MZC+1
      ASUM1=0.
      GO TO 61
55    MMZC=MM*MZC
      II=II+MZC
      KM=KK+MMZC
      A(KM)=A(KM)*A(JC)
      IF(KM.GE.JP)GO TO 6
      KJ=KM+MM
      DO 5 I=KJ,JP,MM
      ASUM2=0.
      IM=I-MM
      II=II+1
      KI=II+MMZC
      DO 7 K=KM,IM,MM
      ASUM2=ASUM2+A(KI)*A(K)
7     KI=KI+MM
5     A(I)=(A(I)-ASUM2)*A(KI)
6     CONTINUE
      ASUM1=0.
      DO 4 K=KM,JP,MM
4     ASUM1=ASUM1+A(K)*A(K)
61    S=A(J)-ASUM1
      IF(S.LT.0.)DET=S
      IF(S.EQ.0.)DET=0.
      IF(S.GT.0.)GO TO 63
      NROW=(J+MM)/M
      WRITE(6,99) NROW
99    FORMAT(35H0ERROR CONDITION ENCOUNTERED IN ROW,I6)
      RETURN
63    A(J)=1./SQRT(S)
      IF(A(J).GT.BIGL)BIGL=A(J)
```

```
      IF(A(J).LT.SML)SML=A(J)
62    CONTINUE
      IF(SML.LE.FAC*BIGL)GO TO 54
      GO TO 53
54    DET=0.
      RETURN
53    DET=SML/BIGL
55    B(1)=B(1)*A(1)
      KK=1
      K1=1
      J=1
      DO 8 L=2,N
      BSUM1=0.
      L1=L-1
      J=J+M
      IF(KK.GE.M)GO TO 12
      KK=KK+1
      GO TO 13
12    KK=KK+M
      K1=K1+1
13    JK=KK
      DO 9 K=K1,L1
      BSUM1=BSUM1+A(JK)*B(K)
      JK=JK+MM
9     CONTINUE
8     B(L)=(B(L)-BSUM1)*A(J)
      B(N)=B(N)*A(NM1)
      NMM=NM1
      NN=N-1
      ND=N
      DO 10 L=1,NN
      BSUM2=0.
      NL=N-L
      NL1=N-L+1
      NMM=NMM-M
      NJ1=NMM
      IF(L.GE.M)ND=ND-1
      DO 11 K=NL1,ND
      NJ1=NJ1+1
      BSUM2=BSUM2+A(NJ1)*B(K)
11    CONTINUE
10    B(NL)=(B(NL)-BSUM2)*A(NMM)
      RETURN
      END
      SUBROUTINE PSET(A,M)
      DIMENSION A(M)
      DO 1 I=1,M
    1 A(I)=0.00
      RETURN
      END
      SUBROUTINE PRESET(A,M,N)
      DIMENSION A(M,N)
      DO 1 I=1,M
      DO 2 J=1,N
    2 A(I,J)=0.0
    1 CONTINUE
      RETURN
      END
      SUBROUTINE BMATRIX(ZDXX,ZDYY,ZDXY,B)
      DIMENSION ZDXX(12),ZDYY(12),ZDXY(12),B(3,12)
      DO 1 I=1,12
      B(1,I)=ZDXX(I)
      B(2,I)=ZDYY(I)
    1 B(3,I)=ZDXY(I)
      RETURN
```

```
      END
      SUBROUTINE MULT1(X,Y,S,Z,M1,M2,M3)
C
C     MULTIPLIES THE MATRICES  Y (TRANSPOSE) * X * Y
C
      DIMENSION X(3,3),Y(3,12),Z(3,12),S(12,12)
      DO 1 I=1,M1
      DO 2 K=1,M2
      XX=0.D0
      DO 3 J=1,M1
    3 XX=XX+X(I,J)*Y(J,K)
    2 Z(I,K)=XX
    1 CONTINUE
      DO 4 I=1,M2
      DO 5 K=I,M2
      XX=0.D0
      DO 6 J=1,M1
    6 XX=XX+Y(J,I)*Z(J,K)
      S(I,K)=XX
    5 S(K,I)=XX
    4 CONTINUE
      RETURN
      END
      SUBROUTINE SHAPE(S,T,U,ZDXX,ZDYY,ZDXY,H,A,B)
*   THIS SUBROUTINE CALCULATES THE 3 ROWS OF THE STRAIN MATRIX (B)
      DIMENSION ZDXX(12),ZDYY(12),ZDXY(12)
      C=1.0-T
      D=1.0+T
      E=3.0*S-1.0
      F=3.0*S+1.0
      G=1.0-S
      R=1.0+S
      P=3.0*T-1.0
      Q=3.0*T+1.0
      ZDXX(1)=-C*E*H*U/(4.0*A)
      ZDXX(2)=0.0
      ZDXX(3)=-3.0*S*C*H*U/(2.0*A*A)
      ZDXX(4)=-C*F*H*U/(4.0*A)
      ZDXX(5)=0.0
      ZDXX(6)=-ZDXX(3)
      ZDXX(7)=-D*F*H*U/(4.0*A)
      ZDXX(8)=0.0
      ZDXX(9)=3.0*S*D*H*U/(2.0*A*A)
      ZDXX(10)=-D*E*H*U/(4.0*A)
      ZDXX(11)=0.0
      ZDXX(12)=-ZDXX(9)
      ZDYY(1)=0.0
      ZDYY(2)=-G*P*H*U/(4.0*B)
      ZDYY(3)=-3.0*T*G*H*U/(2.0*B*B)
      ZDYY(4)=0.0
      ZDYY(5)=-R*P*H*U/(4.0*B)
      ZDYY(6)=-3.0*R*T*H*U/(2.0*B*B)
      ZDYY(7)=0.0
      ZDYY(8)=-R*Q*H*U/(4.0*B)
      ZDYY(9)=-ZDYY(6)
      ZDYY(10)=0.0
      ZDYY(11)=-G*Q*H*U/(4.0*B)
      ZDYY(12)=-ZDYY(3)
      ZDXY(1)=-G*F*H*U/(4.0*B)
      ZDXY(2)=-C*Q*H*U/(4.0*A)
      ZDXY(3)=-(4.0-3.0*S*S-3.0*T*T)*H*U/(2.0*A*B)
      ZDXY(4)=R*E*H*U/(4.0*B)
      ZDXY(5)=-ZDXY(2)
      ZDXY(6)=-ZDXY(3)
      ZDXY(7)=-ZDXY(4)
```

```
      ZDXY(8)=-D*P*H*U/(4.0*A)
      ZDXY(9)=  ZDXY(3)
      ZDXY(10)=-ZDXY(1)
      ZDXY(11)=-ZDXY(8)
      ZDXY(12)=-ZDXY(3)
      RETURN
      END
      SUBROUTINE DMATRX(IFL,TXX,TYY,TXY,EFT,ANU,E,ET,D)
*  ELASTIC OR ELASTO-PLASTIC MATRIX (D)
      DIMENSION D(3,3)
      CALL PRESET(D,3,3)
      IF(IFL)4,3,4
    3 AD=E/(1.0-ANU*ANU)
      D(1,1)=AD
      D(2,1)=AD*ANU
      D(1,2)  =D(2,1)
      D(2,2)=AD
      D(3,3)=AD*(1.0-ANU)/2.0
      RETURN
    4 TXX1=(2.0*TXX-TYY)/3.0
      TYY1=(2.0*TYY-TXX)/3.0
      H1=E*ET/(E-ET)
      P=(2.0*H1/(9.0*E))*EFT*EFT+TXY*TXY/(1.0+ANU)
      R=TXX1**2+2.0*ANU*TXX1*TYY1+TYY1**2
      Q=R+2.0*(1.0-ANU**2)*P
      D(1,1)=TYY1**2+2.0*P
      D(2,1)=-TXX1*TYY1+2.0*ANU*P
      D(3,1)=-(TXX1+ANU*TYY1)*TXY/(1.0+ANU)
      D(2,2)=TXX1**2+2.0*P
      D(3,2)=-(TYY1+ANU*TXX1)*TXY/(1.0+ANU)
      D(3,3)=(R/(2.0*(1.0+ANU)))+(2.0*H1*(1.0-ANU)*EFT**2/(9.0*E))
      DO 9 I=1,3
      DO 10 J=1,3
   10 D(I,J)=D(J,I)
    9 CONTINUE
      DO 11 I=1,3
      DO 12 J=1,3
   12 D(I,J)=(E/Q)*D(I,J)
   11 CONTINUE
      RETURN
      END
      SUBROUTINE MDMATRX(TXX,TYY,TXY,EFT,ANU,E,ET,D)
*  ELASTO-PLASTIC MATRIX (D) FOR POINTS JUST PERIOR TO YIELD
      DIMENSION D(3,3),A(3,3),B(3,3)
      CALL PRESET(D,3,3)
      CALL PRESET(A,3,3)
      CALL PRESET(B,3,3)
      AD=0.9*E/(1.0-ANU*ANU)
      A(1,1)=AD
      A(2,1)=AD*ANU
      A(1,2)  =A(2,1)
      A(2,2)=AD
      A(3,3)=AD*(1.0-ANU)/2.0
      TXX1=(2.0*TXX-TYY)/3.0
      TYY1=(2.0*TYY-TXX)/3.0
      H1=E*ET/(E-ET)
      P=(2.0*H1/(9.0*E))*EFT*EFT+TXY*TXY/(1.0+ANU)
      R=TXX1**2+2.0*ANU*TXX1*TYY1+TYY1**2
      Q=R+2.0*(1.0-ANU**2)*P
      B(1,1)=TYY1**2+2.0*P
      B(2,1)=-TXX1*TYY1+2.0*ANU*P
      B(3,1)=-(TXX1+ANU*TYY1)*TXY/(1.0+ANU)
      B(2,2)=TXX1**2+2.0*P
      B(3,2)=-(TYY1+ANU*TXX1)*TXY/(1.0+ANU)
      B(3,3)=(R/(2.0*(1.0+ANU)))+(2.0*H1*(1.0-ANU)*EFT**2/(9.0*E))
```

```
      DO 9 I=1,3
      DO 10 J=1,3
   10 B(I,J)=B(J,I)
    9 CONTINUE
      DO 11 I=1,3
      DO 12 J=1,3
   12 B(I,J)=(E/Q)*B(I,J)*0.1
   11 CONTINUE
      DO 13 I=1,3
      DO 14 J=1,3
   14 D(I,J)=A(I,J)+B(I,J)
   13 CONTINUE
      RETURN
      END
      SUBROUTINE DABLU(F,G,C,E,ET,D,W)
*  CALCULATES THE W MATRIX RELATING DILTA EPSPP TO STRAIN INCREMENTS
      DIMENSION D(3,3),W(1,3)
      H1=E*ET/(E-ET)
      AB=F*D(1,1)+G*D(2,1)
      BC=F*D(1,2)+G*D(2,2)
      HH=C*D(3,3)
      AE=F*AB+G*BC+C*HH
      AC=H1+AE
      W(1,1)=AB/AC
      W(1,2)=BC/AC
      W(1,3)=HH/AC
      RETURN
      END
      SUBROUTINE KMATRX(ST,IEL,ILC,H,AA,BB,IS,E,ET,ANU)
      DIMENSION ST(12,12),      D(3,3),ZDXX(12),ZDYY(12),ZDXY(12),
     1W(3),XI(3),AK(12,12),C(3,12),B(3,12)
      DATA W/0.55555555555556,0.88888888888889,0.55555555555556/
      DATA XI/-0.774596669241 48,0.0,0.774596669241 48/
      IF(IS.EQ.0) GO TO 1000
      CALL PRESET(ST,12,12)
      CALL PRESET(B,3,12)
      IF(ILC.GT.1) GO TO 24
      TXX=0.0
      TYY=0.0
      TXY=0.0
      EFT=0.0
      IFL=0
   24 DO 26 I=1,3
      DO 27 J=1,3
      DO 28 K=1,3
      S=XI(I)
      T=XI(J)
      U=XI(K)
      H=0.375
      IF(IS.EQ.9) H=1000.0
      CALL SHAPE(S,T,U,ZDXX,ZDYY,ZDXY,H,AA,BB)
      CALL BMATRIX(ZDXX,ZDYY,ZDXY,B)
      CALL PRESET(D,3,3)
      IF(ILC.LT.2) GO TO 55
      READ(9) IFL,TXX,TYY,TXY,EFT
      IF(IFL.EQ.2) GO TO 56
   55 CALL DMATRX(IFL,TXX,TYY,TXY,EFT,ANU,E,ET,D)
      IF(IFL.NE.2) GO TO 57
   56 CALL MDMATRX(TXX,TYY,TXY,EFT,ANU,E,ET,D)
   57 CALL MULT1(D,B,AK,C,3,12,3)
      DET=4*AA*BB/8.0
      DO 3 M=1,12
      DO 4 L=1,12
    4 ST(M,L)=ST(M,L)+(W(I)*W(J)*W(K)*AK(M,L)*DET)
    3 CONTINUE
```

```
   29 CONTINUE
   27 CONTINUE
   26 CONTINUE
 1000 RETURN
      END
      SUBROUTINE STRESS2(E,ET,B,U,LJ,IEL,NVEL,H,AA,BB,YL,
     1SIGMAX,IFLAG,ANU,SIGBND,S11B,S22B,S33B,NNE,ILC)
      DIMENSION D(3,3),ZDXX(12),ZDYY(12),ZDXY(12),XI(3),W(1,3),
     1U(12),LJ(12),B(NNE),BBB(3,12)
      DATA XI/-0.7745966692414B,0.0,0.7745966692414B/
      H1=E*ET/(E-ET)
      DO 2 J=1,NVEL
      IKK=LJ(J)
      IF(IKK)3,4,3
    4 U(J)=0.0
      GO TO 2
    3 U(J)=B(IKK)
    2 CONTINUE
      CALL PRESET(D,3,3)
      AD=E/(1.0-ANU*ANU)
      D(1,1)=AD
      D(2,1)=AD*ANU
      D(1,2) =D(2,1)
      D(2,2)=AD
      D(3,3)=AD*(1.0-ANU)/2.0
      S11B=0.0
      S22B=0.0
      S33B=0.0
      SIGBND=0.0
      DO 26 I=1,3
      DO 27 J=1,3
      DO 28 K=1,3
      CALL PRESET(BBB,3,12)
      S=XI(I)
      T=XI(J)
      UU=XI(K)
      H=0.375
      CALL SHAPE(S,T,UU,ZDXX,ZDYY,ZDXY,H,AA,BB)
      CALLBMATRIX(ZDXX,ZDYY,ZDXY,BBB)
      EXX=0.0
      EYY=0.0
      EXY=0.0
      DO 8 JK=1,12
      EXX=EXX+BBB(1,JK)*U(JK)
      EYY=EYY+BBB(2,JK)*U(JK)
      EXY=EXY+BBB(3,JK)*U(JK)
    8 CONTINUE
      IF(ILC.GT.2) GO TO 77
      IFL=0
      IF(ILC.LE.2) GO TO 56
   77 IF(IFLAG.EQ.1) READ(10) IFL,TX2,TY2,TXY2,EFT2
      IF(IFLAG.EQ.0) READ(11) IFL,TX2,TY2,TXY2,EFT2
      IF(EFT2.LT.YL) GO TO 98
      TXX2=(2.0*TX2-TY2)/3.0
      TYY2=(2.0*TY2-TX2)/3.0
      F=3.0*TXX2/(2.0*EFT2)
      G=3.0*TYY2/(2.0*EFT2)
      C=3.0*TXY2/EFT2
      CALL DABLU(F,G,C,E,ET,D,W)
      EPSPP=EXX*W(1,1)+EYY*W(1,2)+EYY*W(1,3)
      EPS=EPSPP
      IF(EPSPP.LT.0.0) WRITE(6,19) IEL,S,T,UU,EPSPP
      IF(EPSPP) 98,98,6
    6 EXXP=F*EPSPP
      EYYP=G*EPSPP
```

```
      EXYP=C*EPSPP
      GO TO 59
   56 TX2=0.0
      TY2=0.0
      TXY2=0.0
   98 EXXP=0.0
      EYYP=0.0
      EXYP=0.0
      EPSPP=0.0
   59 DSIGX=(EXX-EXXP)*D(1,1)+(EYY-EYYP)*D(2,1)
      DSIGY=(EXX-EXXP)*D(2,1)+(EYY-EYYP)*D(2,2)
      DSIGXY=(EXY-EXYP)*D(3,3)
      TXX=TX2+DSIGX
      TYY=TY2+DSIGY
      TXY=TXY2+DSIGXY
      EFT=SQRT(TXX**2+TYY**2+3.0*TXY**2-TXX*TYY)
      IF(ILC.LE.2) GO TO 88
      IF(EFT2.GT.YL)EFT=EFT2+H1*EPSPP
   88 IF(ILC.EQ.1) GO TO 99
      IF(EFT.LE.0.9*YL)IFL=0
      IF(EFT.GT.0.9*YL) IFL=2
      IF(EFT.GT.YL) IFL=1
      IF(ILC.LE.2) GO TO 10
      IF(EFT2.LT.YL) GO TO 10
      IF(EPS   .LT.0.0) IFL=0
   10 WRITE(9) IFL,TXX,TYY,TXY,EFT
      IF(IFLAG.EQ.0) WRITE(10) IFL,TXX,TYY,TXY,EFT
      IF(IFLAG.EQ.1) WRITE(11) IFL,TXX,TYY,TXY,EFT
   99 IF(EFT.GE.SIGMAX) SIGMAX=EFT
      IF(EFT.GE.SIGMAX) NEMAX=IEL
      IF(EFT.GE.SIGMAX) XMAX=S
      IF(EFT.GE.SIGMAX) YMAX=T
      IF(EFT.GE.SIGMAX) ZMAX=UU
      IF(EFT.GE.SIGBND) SIGBND=EFT
      IF(I.EQ.1.AND.J.EQ.1.AND.K.EQ.1) S11B=EFT
      IF(I.EQ.1.AND.J.EQ.2.AND.K.EQ.1) S22B=EFT
      IF(I.EQ.1.AND.J.EQ.3.AND.K.EQ.1) S33B=EFT
   28 CONTINUE
   27 CONTINUE
   26 CONTINUE
      WRITE(6,16) IEL,SIGBND
   16 FORMAT(10X,"ELEMENT NO.",I10,10X,"STRESSED UP TO ",F15.5,/)
   19 FORMAT(5X,"FOR ELEMENT NO",I10,5X,"AT S=",F10.5,5X,"AND T=",
     2F10.5,5X,"AND U=",F10.5,5X,"-VE PLASTIC STRAIN IS",F15.5,//)
      RETURN
      END
      SUBROUTINE DLOAD(FL,AA,BB,IEL,IB,IS)
*  THIS SUBROUTINE TAKES CARE OF CONSISTANT LINE LOAD
      DIMENSION FL(12)
      CALL PSET(FL,12)
      IF(IS.EQ.0) GO TO1000
      IF(IB.NE.3) RETURN
      READ(5,1) W1,W2,W4
      WRITE(6,2) IEL,W1,W2,W4
      FL(1)=W1*AA**2/12.0
      FL(2)=+W4*BB**2/12.0
      FL(3)=W1*AA/2.0+W4*BB/2.0
      FL(4)=-W1*AA**2/12.0
      FL(5)=-W2*BB**2/12.0
      FL(6)=W1*AA/2.0+W2*BB/2.0
      FL(8)=W2*BB**2/12.0
      FL(9)=W2*BB/2.0
      FL(11)=-W4*BB**2/12.0
      FL(12)=W4*BB/2.0
    2 FORMAT(/,5X,"LINE.LOAD ON ELEM. NO.",I5,5X,"W1",
```

```
     2F10.5,5X,"W2",F10.5,5X,"W4",F10.5,/)
    1 FORMAT(3F10.0)
 1000 RETURN
      END
      SUBROUTINE TRANS (T,A,B)
      DIMENSION T(12,12)
      CALL PRESET (T,12,12)
      T(1,3)=1.0
      T(2,1)=A
      T(3,2)=B
      T(4,1)=-2.0*A
      T(4,3)=-3.0
      T(4,4)=-A
      T(4,6)=3.0
      T(5,1)=-T(2,1)
      T(5,2)=-T(3,2)
      T(5,3)=-1.0
      T(5,5)=T(3,2)
      T(5,6)=1.0
      T(5,9)=-1.0
      T(5,10)=T(2,1)
      T(5,12)=1.0
      T(6,2)=-2.0*B
      T(6,3)=-3.0
      T(6,11)=-T(3,2)
      T(6,12)=3.0
      T(7,1)=T(2,1)
      T(7,3)=2.0
      T(7,4)=A
      T(7,6)=-2.0
      T(8,1)=-T(4,1)
      T(8,3)=3.0
      T(8,4)=T(2,1)
      T(8,6)=-3.0
      T(8,7)=T(5,1)
      T(8,9)=3.0
      T(8,10)=T(4,1)
      T(8,12)=-3.0
      T(9,2)=-T(6,2)
      T(9,3)=3.0
      T(9,5)=T(6,2)
      T(9,6)=-3.0
      T(9,8)=-T(3,2)
      T(9,9)=3.0
      T(9,11)=T(3,2)
      T(9,12)=-3.0
      T(10,2)=T(3,2)
      T(10,3)=2.0
      T(10,11)=T(3,2)
      T(10,12)=-2.0
      T(11,1)=T(5,1)
      T(11,3)=-2.0
      T(11,4)=T(5,1)
      T(11,6)=2.0
      T(11,7)=T(2,1)
      T(11,9)=-2.0
      T(11,10)=T(2,1)
      T(11,12)=2.0
      T(12,2)=T(5,2)
      T(12,3)=-2.0
      T(12,5)=T(3,2)
      T(12,6)=2.0
      T(12,8)=T(3,2)
      T(12,9)=-2.0
      T(12,11)=T(5,2)
```

```
      T(12,12)=2.0
      RETURN
      END
      SUBROUTINE MULT(Q,T,Z)
      DIMENSION Q(12,12),T(12,12),Z(12,12)
      CALL PRESET(Z,12,12)
      DO 1 I=1,12
      DO 2 J=1,12
      X=0.0
      DO 3 K=1,12
    3 X=X+Q(I,K)*T(K,J)
    2 Z(I,J)=X
    1 CONTINUE
      DO4 I=1,12
      DO 5 J=I,12
      X=0.0
      DO 6 K=1,12
    6 X=X+T(K,I)*Z(K,J)
      Q(I,J)=X
    5 Q(J,I)=Q(I,J)
    4 CONTINUE
      RETURN
      END
      SUBROUTINE BOUNDRY(S,AA,BB,IS,IB,SIGRND,YL,ILC,IEL,S11B,S22B,
     1S33B)
*  CALCULATES THE CONTRIBUTION TO THE STIFFNESS MATRIX DUE TO SPRINGS
      DIMENSION M(12),N(12),T(12,12),Q(12,12),Z(12,12),S(12,12)
      DATA M/0,1,0,2,0,0,3,2,1,0,3,1/
      DATA N/0,0,1,0,1,2,0,1,2,3,1,3/
      CALL PRESET(Q,12,12)
      IF(IB.EQ.4) GOTO 12
      RETURN
   12 CALL PRESET(Q,12,12)
      CALL TRANS(T,AA,BB)
      WRITE(6,86) S11B,S22B,S33B
   86 FORMAT(/,5X,"S11B= ",F15.5,5X,"S22B= ",F15.5,5X,"S33B= ",
     2F15.5,/)
      IF(ILC.LT.2) GO TO 28
      IF(S11B.GE.YL.OR .S22B.GE.YL.OR .S33B.GE.YL) GO TO 25
   28 XKZ=377.31067
      XKN=126.79564
      XKS=-175.23076
      GO TO 26
   25 XKZ=35.256498
      XKN=11.95239
      XKS=-28.05611
   26 Y=0.1E-20
      WRITE(6,9)
      WRITE(6,11) IE,XKZ,XKN,XKS
      DO 3I=1,12
      DO 4 J=I,12
      NIJ=N(I)+N(J)
      MIJ=M(I)+M(J)
      Q(I,J)=AA*XKZ*Y**NIJ/(MIJ+1)+Q(I,J)
      Q(I,J)=Q(I,J)+AA*XKS*NIJ *Y**(NIJ-1)/((MIJ+1)*BB)
      Q(I,J)=Q(I,J)+AA*N(I)*N(J)*XKN*Y**(NIJ-2)/((MIJ+1)*BB**2)
    4 Q(J,I)=Q(I,J)
    3 CONTINUE
   10 CALL MULT(Q,T,Z)
      DO 7 I=1,12
      DO 8 J=I,12
      S(I,J)=S(I,J)+Q(I,J)
    8 S(J,I)=S(I,J)
    7 CONTINUE
    9 FORMAT(/,15X,"IE",15X,"XKZ",15X,"XKN",15X,"XKS",/)
```

```
11 FORMAT(10X,I3,5X,F15.7,5X,F15.7,5X,F15.7)
   RETURN
   END
   SUBROUTINE LAYOUT(X,Y,ICO,IX,JX,NE,NN,NVAR,NMAT,NDEG,NNODEL)
   DIMENSION X(NN),Y(NN),ICO(NE,6),IX(NMAT),JX(NMAT)
   NNN=NNODEL+2
   WRITE(6,41) NE,NN,NVAR,NNODEL
   WRITE(6,42)
   DO 10 I=1,NN
   I2=NVAR*I
   I1=I2-NVAR+1
   READ(5,43) X(I),Y(I),(IX(J),J=I1,I2)
   WRITE(6,44) I,X(I),Y(I),(IX(J),J=I1,I2)
10 CONTINUE
   WRITE(6,47)
   DO 11 I=1,NE
   READ(5,45) (ICO(I,J),J=1,NNN)
11 WRITE(6,46) I,(ICO(I,J),J=1,NNN)
   NDEG=0
   DO 12 I=1,NMAT
   IF(IX(I)) 1,2,3
 3 IF(IX(I)-1) 80,80,81
81 NDEG=NDEG+IX(I)
   GO TO 82
80 NDEG=NDEG+1
82 JX(I)=NDEG
   GO TO 12
 1 NDEG=NDEG+IX(I)+1
   JX(I)=NDEG
   GO TO 12
 2 JX(I)=0
12 CONTINUE
41 FORMAT(//,4X,"TOTAL NO. OF ELEMENTS ",
  1I5,5X,"NO. OF NODES",I5,5X,"VARIABLES PER NODE",
  2I5,3X,"NO.OF NODES PER ELEM.",I5,/)
42 FORMAT(/,4X,"NODE",6X," X-CORD",6X,"Y-CORD",7X,
42 FORMAT(/,4X,"NODE",6X," X-CORD",6X,"Y-CORD",7X,"WX",3X,"WY",3X,
  1"WX",3X,"WY",3X,"W",/)
43 FORMAT(2F10.0,3I3)
44 FORMAT(1X,I5,5X,F10.6,2X,F10.6,5X,6I4)
45 FORMAT(16I3)
46 FORMAT(5X,I5,6X,4I4,2X,2I5)
47 FORMAT(/,5X,"ELEMENT",7X,"NODE NUMBERS","   IS","   IB",//)
   RETURN
```

REFERENCES

(1) Jubb, J. E. and Redwood, R. G., "Design of Joints to Box Sections". The Institution of Structural Engineers, Conference on Industrial Building and the Structural Engineer, (May 1966).

(2) Brady, F. J., "An Experimental Investigation of Unequal Width HSS Moment Connections for Vierendeel Trusses". Project Report, McMaster University, (1974).

(3) Mee, B. L., "The Structural Behaviour of Joints in Rectangular Hollow Section". Ph.D. Thesis, University of Sheffield, (1969).

(4) El-Zanaty, M., "Vierendeel Trusses with Hollow Structural Sections". M. Eng. Thesis, McMaster University, (1976).

(5) Korol, R. M., El-Zanaty, M. and Brady, F. J., "Unequal Width Connections of Square Hollow Sections in Vierendeel Trusses". Canadian Journal of Civil Engineering, Vol. 4, No. 2, pp. 190-201, (1977).

(6) Redwood, R. G., "The Behaviour of Joints Between Rectangular Hollow Structural Members". Civil Engineering and Public Works Review, Vol. 60, No. 711, pp. 1463-1469, (1965).

(7) Korol, R. M. and Mansour, M., "Theoretical Analysis of Haunch-Reinforced T-Joints". Journal of the Structural Div. ASCE. Tech. Note 105 (STB), pp. 1717-1721, (1979).

(8) Blockley, D. I. and Eastwood, W., "Elastic Behaviour of Joint Between Structural Hollow Sections". The Engineer, July 5, pp. 22-25, (1968).

(9) Mansour, M., "Theoretical Analysis of T-Joints in Hollow Structural Sections". M. Eng. Thesis, McMaster University, (1977).

(10) Mouty, J., "Theoretical Prediction of Welded Joint Strength". International Symposium on Hollow Structural Sections, Toronto Symposium, (May 1977).

(11) Timoshenko, S. P. and Woinowsky-Krieger, S., "Theory of Plates and Shells". McGraw-Hill Book Company (1959).

(12) Szilard, R., "Theory and Analysis of Plates, Classical and Numerical Methods". Prentice-Hall, Inc. Englewood Cliffs, New Jersey, (1974).

(13) Cook, R. D., "Concepts and Applications of Finite Element Analysis". John Wiley, Sons, Inc., (1974).

(14) Derai, C. S., Abel, J. F., "Introduction to the Finite Element Method". Van Nostrand Reinhold Company, (1972).

(15) Zienkiewicz, O. C., "The Finite Element Method". McGraw Hill Book Company, (1977).

(16) Bazeley, G. P., Cheung, Y. K., Irons, B. M., Zienkiewicz, O. C., "Triangular Elements in Plate Bending-Conforming and Non-Conforming Solutions". WPAFBl Conf. pp. 547-576.

(17) Irons, B. M., Zienkiewicz, O. C., and Oliveira, E. R., "Comments on the Paper: Theoretical Foundations of Finite Element Method". IJSOST, Vol. 6, No. 5, pp. 695-697(1970).

(18) Irons, B. M., and Razzaque, A., "Introduction of Shear Deformations into Thin Plate Displacement Formulation". AIAAJ, Vol. 11, No. 10, pp. 1438-1439, (1973).

(19) Melosh, R. J., "Basis for Derivation of Matrices of the Direct Stiffness Method". AIAAJ Vol. 1, No. 7, pp. 1631-1637, (1963).

(20) Clough, R., and Tocher, J., "Finite Element Stiffness Matrices for Analysis of Plate Bending". Proc. Conf. Matrix Method in Struc. Mech., Air Force Inst. of Technol. Wright Patterson Air Force Base, Ohio, U.S.A., (1965).

(21) Mirza, F., "Finite Element Method and Basic Finite Element Computer Programs". Graduate Course Notes, McMaster University, Civil Eng. Department, (1979-1980).

(22) Kopal, Z., "Numerical Analysis". John Wiley & Sons, New York, (1955).

(23) Irons, B. M., "Engineering Applications of Numerical Integration is Stiffness Method". AIAAJ, Vol. 4, No. 11, pp. 2035-2037, (1966).

(24) Stroud, A. H. and Secrest, D., "Gaussian Quadrature Formulas". Prentice-Hall, Englewood Cliffs, 1966.

(25) Shehata, A. A., "Modelling of Double Chord Rectangular Hollow Section T-Joint by Finite Element Method". Department of Civil Engineering, McMaster University, (1980).

(26) Stanton, E. L., "A Discrete Element Stress and Displacement Analysis of Elastoplastic Plates". AIAA Journal, Vol. 8, No. 7, pp. 1245-1251, (1970).

(27) Yamada, Y. and Yoshimura, N., "Plastic Stress Strain Matrix and its Application for the Solution of Elastic-Plastic Problems by the Finite Element Method". Int. J. Mech. Sci., Vol. 10, pp. 343-354, (1968).

(28) Wegmuller, A. W., "Elastic-Plastic Finite Element Analysis of Plates". Ingenieur-Archiv. 44 pp. 63-77, (1975).

(29) Marcal, P. V., "A Stiffness Method for Elastic-Plastic Problems". Int. J. Mech. Sci., Vol. 7, pp. 229-238, (1969).

(30) Marcal, P. V., King, I. P., "Elastic-Plastic Analysis of Two-Dimensional Stress System by the Finite Element Method". Int. J. Mech. Sci., Vol. 9, pp. 143-155, (1967).

(31) Illyushin, A. A., "Plasticity". Eyrolles, (1956).

(32) Green, A. E., Naghdi, P. M., "Some Remarks on Elastic-Plastic Deformations at Finite Strains". Int. J. Engng. Sci., 9, pp. 1219-1229, (1971).

(33) Green, A. E., Naghdi, P. M., "A general Theory of an Elastic-Plastic Continuum". Arch. Rational Mech. Anal., 18, pp. 251-281, (1965).

(34) Gadala, M. S., Kokainish, M. A., "Nonlinear Finite Element Programming System". McMaster University, Metalworking Research & Design Group, Research No. 139, August 1979.

(35) Tillerson, J. R., Stricklin, J. A., and Haisler, W. E., "Numerical Methods for the Solution of Nonlinear Problems in Structural Analysis". ASME Meeting (1973), Edited by R. E. Haitung, 67-101.

(36) Stricklin, J. A., Haisler, W. E., and Von Riesemann, W. A., "Computation and Solution Procedures for Nonlinear Analysis by Combined Finite Element-Finite Difference Methods". Comp. St., Vol. 2, Nos. 516, pp. 955-974, (1972).